

**EFFECT OF AGING HEAT TREATMENTS ON Ni₅₂Ti₄₈ SHAPE
MEMORY ALLOY**

A Thesis

by

ERHAN AKIN

Submitted to the Office of Graduate Studies of
Texas A&M University
in partial fulfillment of the requirements for the degree of

MASTER OF SCIENCE

August 2010

Major Subject: Mechanical Engineering

**EFFECT OF AGING HEAT TREATMENTS ON Ni₅₂Ti₄₈ SHAPE
MEMORY ALLOY**

A Thesis

by

ERHAN AKIN

Submitted to the Office of Graduate Studies of
Texas A&M University
in partial fulfillment of the requirements for the degree of

MASTER OF SCIENCE

Approved by:

Chair of Committee,
Committee Members,
Head of Department,

Ibrahim Karaman
Xinghang Zhang
Rashid K. Abu Al-Rub
Dennis L. O'Neal

August 2010

Major Subject: Mechanical Engineering

ABSTRACT

Effect of Aging Heat Treatments on Ni₅₂Ti₄₈ Shape Memory Alloy.

(August 2010)

Erhan Akin, B.S., Kocaeli University, Turkey

Chair of Advisory Committee: Dr. Ibrahim Karaman

Ni-rich NiTi shape memory alloys (SMAs) are capable of attaining a wide range of transformation temperatures depending on the heat treatment conditions and superior thermo-mechanical cycling stability, which are desired for repeated solid-state actuation. High Ni-content Ni-rich SMAs have very low transformation temperatures in a solutionized condition due to the high Ni-content of the matrix. Slow cooling (furnace-cooling) from solutionizing temperature and additional aging heat treatments result in the formation of Ni-rich precipitates such as Ni₄Ti₃, Ni₃Ti₂ and Ni₃Ti and increase transformation temperatures above ambient by depleting excess Ni from the matrix. However, the precipitates do not undergo a martensitic phase transformation and they decrease the transformation strain by reducing the volume fraction of the material capable of transforming. Meanwhile, recent preliminary work shows that Ni₃Ti precipitates dominate fatigue failure.

The objectives of the present study are: (1) to eliminate Ni₃Ti but still have Ni₄Ti₃ precipitates, which are responsible for the dimensional stability and increase transformation temperatures, (2) to investigate the effect of heat treatments on the transformation strain, and (3) to select single variant Ni₄Ti₃ precipitates through constrained aging for the formation of oriented internal stress and eventually obtain two-way shape memory effect (TWSME) and enhanced dimensional stability. Based on these objectives, the effect of aging heat treatment on transformation temperatures, microstructural evolution, and shape memory behavior were investigated for a Ni₅₂Ti₄₈ shape memory alloy (SMA) by using differential scanning calorimetry (DSC), optical microscopy, scanning electron microscopy (SEM), and thermo-mechanical testing, including isobaric heating-cooling experiments under various stress levels.

It was observed that solutionizing at 900°C for 24 hours eliminated Ni₃Ti type precipitates, but additional aging heat treatments are needed to form Ni₄Ti₃ precipitates to increase transformation temperatures. Furnace-cooling and additional aging heat treatment results in the multi-stage martensitic transformation due to chemical and stress inhomogeneities in the microstructure. Aging of the controlled furnace-cooled material at 400°C for 48 hours resulted in the highest transformation temperatures among all processing conditions investigated due to the combination of Ni₃Ti precipitates and 27 % volume fraction of the Ni₄Ti₃ precipitates, which led to the depletion of Ni from the transforming matrix. However, since overaging results in losing coherency of the precipitates, dimensional stability during isobaric thermal cycling was negatively impacted.

To
My Parents and Brother

ACKNOWLEDGEMENTS

I am sincerely thankful to my advisor, Prof. Ibrahim Karaman, whose support, guidance and encouragement from the beginning to the end enabled me to understand the subject and complete this work.

I also thank Prof. Xinghang Zhang and Prof. Rashid K. Abu Al-Rub for serving on my committee and sharing their valuable and helpful comments.

I am also thankful to Prof. Yuriy Chumlyakov for our discussions and his comments improving my knowledge on this subject.

I am grateful to Prof. Ray Guilemette for his work on the microstructural analysis part of the study.

Special thanks to my officemates, Kadri Can Atli and Fatmata Barrie, for their precious help on the experiments and valuable discussions. I also thank my other officemates, Ebubekir Dogan, Cengiz Yegin, Fevzi Ozaydin, Nevin Ozdemir, James Monroe, Ji Ma and Ruxian Zhu. I am also grateful to Dr. Benat Kockar for her comments on some parts of the study. Special thanks to Ebubekir Dogan and Cengiz Yegin for working together on the Turkish Student Association and also being a brother to me.

I thank my roommate, Onur Cetin, for his kindness and quietness, being sometimes boring. We not only shared our food and goods, but also shared life during my stay at Texas A&M University about 2 years.

I thank Emin Akarcay, Erdinc Basbolat, Erhan Delen, Erkan Atalmis, Esra Turan, Murat Demiray, Mucahit Aydin, Neslihan & Kubilay Dagtoros, Okan Bulut, Ozgur Aydogmus and Oznur Gulhan. We came to the USA together and helped each other to overcome the difficulties of adaptation to a new culture.

I am also thankful to Turkish Petroleum International Company (TPIC) employees for the financial support and encouragement that enabled me to come and do my master's at Texas A&M University in the U.S.A.

Especially, I am thankful to my family for their patience and inspiration. They have handled a lot of difficulties to educate and make me ready to overcome the difficulties of my future life.

TABLE OF CONTENTS

	Page
ABSTRACT.....	iii
DEDICATION.....	v
ACKNOWLEDGEMENTS.....	vi
TABLE OF CONTENTS.....	vii
LIST OF FIGURES.....	ix
LIST OF TABLES.....	xiv
CHAPTER	
I INTRODUCTION.....	1
1.1 History and Background on Shape Memory Alloys.....	1
1.2 Ni-rich NiTi Shape Memory Alloys.....	5
1.3 Motivation.....	8
1.4 Objectives.....	9
1.5 Approaches.....	10
II EXPERIMENTAL PROCEDURE.....	11
2.1 Sample Preparation.....	11
2.2 Determination of Aging Heat Treatment Conditions.....	12
2.3 Isobaric Cooling-Heating Experiments.....	15
2.4 Isothermal Loading-Unloading Experiments.....	17
2.5 Optical, Scanning and Transmission Electron Microscopy.....	17
2.6 Differential Scanning Calorimetry.....	18
2.7 X-ray Diffraction.....	18
2.8 Microhardness.....	18
III EFFECT OF AGING HEAT TREATMENTS ON THE SHAPE MEMORY CHARACTERISTICS OF FURNACE-COOLED Ni ₅₂ Ti ₄₈ SMA.....	19
3.1 Differential Scanning Calorimetry Experiments.....	19
3.2 Microstructural Evolution.....	25
3.3 Isobaric Cooling-Heating Experiments.....	36
3.4 Summary.....	45
IV EFFECTS OF CONSTRAINED AND UNCONSTRAINED AGING ON THE SHAPE MEMORY CHARACTERISTICS OF Ni ₅₂ Ti ₄₈ SMA.....	47

	Page
CHAPTER	
4.1 Differential Scanning Calorimetry Experiments.....	47
4.2 Microstructural Evolution.....	49
4.3 Isobaric Cooling-Heating Experiments.....	52
4.4 Isothermal Loading-Unloading Experiments.....	58
4.5 Texture Analysis.....	60
4.6 Summary.....	63
V ELIMINATION OF Ni ₃ Ti PRECIPITATES.....	64
5.1 Influence of Ni ₃ Ti Precipitates.....	64
5.2 Solutionizing (at 900°C for 1 hr).....	65
5.3 Solutionizing (at 900°C for 24 hrs).....	66
5.4 The Effects of Aging Heat Treatments to Solutionized Materials.....	68
VI CONCLUSION AND FUTURE RECOMMENDATION.....	70
6.1 Conclusion.....	70
6.2 Future Recommendation.....	71
REFERENCES.....	72
VITA.....	75

LIST OF FIGURES

		Page
Figure 1.1	Schematic representation of Gibbs Free Energy vs. temperature curves for both parent and martensitic phases, and their relation to martensitic transformation.....	2
Figure 1.2	Schematic representation of stress and temperature ranges for SME and PE behavior and critical stress for slip which is (A) for high critical stress and (B) for low critical stress.....	4
Figure 1.3	Time-temperature-transformation reaction diagram describing precipitation behavior of Ni ₅₂ Ti ₄₈ SMA.....	6
Figure 1.4	M _s temperature as a function of mole-fraction of Ni for binary NiTi alloys. Different symbols represent data from different authors. The solid line is obtained by thermodynamic calculations.....	7
Figure 2.1	A schematic illustration of the tension sample dimensions.....	11
Figure 2.2	Time-temperature-vickers microhardness relationship for Ni ₅₂ Ti ₄₈ materials furnace-cooled and aged at different temperatures (350°C-600°C) for different aging times (30 mins.-48 hrs).....	13
Figure 2.3	Time-temperature-martensite finish temperatures (M _f) relationship for Ni ₅₂ Ti ₄₈ materials furnace-cooled and aged at different temperatures (350°C-600°C) for different aging times (30 mins.-48 hrs).....	13
Figure 2.4	Servo hydraulic MTS load frame used for thermo-mechanical testing.....	15
Figure 2.5	High temperature extensometer used to measure axial strain.....	16
Figure 2.6	A schematic of strain vs. temperature response of a SMA showing how to determine the transformation temperatures, transformation thermal hysteresis, and the recovered transformation (ϵ_{rec}) and irrecoverable (ϵ_{irr}) strain values.....	17
Figure 3.1	DSC response of the furnace-cooled Ni ₅₂ Ti ₄₈ aged at 450°C for 5 hrs exhibiting multi-stage transformation.....	20
Figure 3.2	DSC response of the furnace-cooled Ni ₅₂ Ti ₄₈	21

	Page	
Figure 3.3	DSC responses showing the effect of aging at 400°C and 450°C for 30 mins., 1, 5, 24 and 48 hrs on the transformation temperatures of the furnace-cooled Ni ₅₂ Ti ₄₈ samples during; (a) cooling and (b) heating.....	22
Figure 3.4	The change in transformation temperatures for the furnace-cooled Ni ₅₂ Ti ₄₈ aged at; (a) 400°C and (b) 450°C, for different aging times..	24
Figure 3.5	a) Optical micrograph, and b) SEM image of the furnace cooled Ni ₅₂ Ti ₄₈ and chemical compositions of the matrix and precipitates obtained by EDS analysis.....	26
Figure 3.6	SEM images of (a) furnace-cooled and (b) furnace-cooled and aged at 400°C for 48 hrs Ni ₅₂ Ti ₄₈	27
Figure 3.7	SEM image of the sample furnace-cooled and aged at 450°C for 48 hrs.....	28
Figure 3.8	Bright and dark-field TEM images of the sample furnace-cooled and aged at 400°C for 48 hrs at room temperature showing the big Ni ₄ Ti ₃ precipitates and microstructure in details.....	31
Figure 3.9	(a) Bright, (b) and (c) dark-field TEM images, and (d) electron pattern obtaining from image (c) of the material furnace-cooled and aged at 400°C for 48 hrs showing big and small Ni ₄ Ti ₃ precipitates and R-phase regions.....	33
Figure 3.10	Partial cooling-heating experiments of the material furnace-cooled and aged at 400°C for 48 hrs.....	34
Figure 3.11	SEM images of the furnace-cooled and aged Ni ₅₂ Ti ₄₈ at 450°C for; (a) 30 mins. and (b) 48 hrs.....	35
Figure 3.12	Schematic illustration of growth of Ni ₄ Ti ₃ precipitates having different size after long aging times. Solid lines represent precipitate sizes before aging treatment; dashed lines represent precipitate sizes after long aging times. Large and intermediate precipitates coarsen at the expense of small precipitates after long aging times.....	36
Figure 3.13	Strain vs. temperature response of the furnace-cooled Ni ₅₂ Ti ₄₈ ; (a) before and (b) after aging at 400°C for 48 hrs under various constant stress levels during isobaric cooling-heating experiments.....	37
Figure 3.14	Comparison of strain vs. temperature curves of the furnace-cooled	

	Page
and aged Ni ₅₂ Ti ₄₈ under various constant stress levels: (a) 0 MPa, (b) 100 MPa, (c) 200 MPa and (d) 400 MPa.....	40
Figure 3.15 (a) Recovered transformation and (b) Irrecoverable strain responses of the furnace-cooled and aged Ni ₅₂ Ti ₄₈ as a function of constant tensile stress levels.....	42
Figure 3.16 Temperature hysteresis responses of the furnace-cooled and aged Ni ₅₂ Ti ₄₈ as a function of constant tensile stress levels.....	43
Figure 3.17 The effect of aging on the martensitic transformation start temperature, and stress induced martensitic transformation for the furnace-cooled and aged Ni ₅₂ Ti ₄₈	44
Figure 3.18 Martensitic transformation start temperatures of the furnace-cooled and aged at 400°C for 48 hrs sample from DSC and isobaric cooling-heating experiments under 0 MPa.....	45
Figure 4.1 Transformation temperatures of the as-received and aged at 450°C for 5 hrs and air-cooled materials under stress free condition.....	48
Figure 4.2 (a) Optical Microscopy, and SEM images of the as-received material showing; (b) lenticular precipitates, (c) matrix, gray and dark and (d) white precipitate compositions.....	50
Figure 4.3 SEM images of the matrix and different precipitates including their types obtained by WDS analysis for the material as-received, aged at 450°C for 5 hours, and air-cooled condition.....	51
Figure 4.4 Strain vs. temperature response of the as-received (hot-rolled) Ni ₅₂ Ti ₄₈ under various constant stress levels during isobaric heating-cooling experiments.....	52
Figure 4.5 Strain vs. temperature response of the as-received, aged at 450°C for 5 hours, and air-cooled Ni ₅₂ Ti ₄₈ under various constant stress levels during isobaric heating-cooling experiments.....	53
Figure 4.6 Strain vs. temperature response of the solutionized at 900°C for 1 hour, aged at 450°C for 5 hours, and air-cooled Ni ₅₂ Ti ₄₈ under various constant stress levels during isobaric heating-cooling experiments.....	54
Figure 4.7 Strain vs. temperature response of the as-received and aged at 450°C for 5 hours under 200 MPa Ni ₅₂ Ti ₄₈ under various constant stress	

	levels during isobaric heating-cooling experiments.....	55
Figure 4.8	(a) Recovered transformation and (b) irrecoverable strain responses of as-received, aged at 450°C for 5 hours, solutionized (at 900°C for 1 hour) and aged at 450°C for 5 hours, and as-received and aged at 450°C for 5 hours under 200 MPa Ni ₅₂ Ti ₄₈ samples as a function of constant tensile stress levels.....	56
Figure 4.9	Thermal hysteresis responses of the as-received, aged at 450°C for 5 hours, solutionized (at 900°C for 1 hour) and aged at 450°C for 5 hours, and as-received and aged at 450°C for 5 hours under 200 MPa Ni ₅₂ Ti ₄₈ samples as a function of constant tensile stress levels...	57
Figure 4.10	The effect of aging with or without stress on the martensitic transformation start temperatures for the as-received and solutionized material.....	58
Figure 4.11	Isothermal loading-unloading experiments of the as-received Ni ₅₂ Ti ₄₈ at different temperatures.....	59
Figure 4.12	Effect of temperature on the critical stress for stress-induced martensitic transformation of as-received Ni ₅₂ Ti ₄₈	60
Figure 4.13	Pole figures for the as-received material in the austenite state at room temperature.....	61
Figure 4.14	Strain vs. temperature response of the as-received Ni ₅₂ Ti ₄₈ under various constant stress levels during isobaric heating-cooling experiments. The rolling direction is parallel to the tension direction.	62
Figure 4.15	Recovered transformation and irrecoverable strain responses of the as-received Ni ₅₂ Ti ₄₈ samples, cut along different directions, as a function of constant tensile stress levels.....	63
Figure 5.1	Room temperature XRD result of the as-received sample; identification of B2 matrix, Ni ₄ Ti ₃ and Ni ₃ Ti precipitates.....	64
Figure 5.2	(a) Optical microscopy and (b) SEM images of the Ni ₅₂ Ti ₄₈ sample solutionized at 900°C for 1 hr.....	65
Figure 5.3	Room temperature XRD result of the Ni ₅₂ Ti ₄₈ sample solutionized at 900°C for 1 hr	66
Figure 5.4	SEM images of the sample solutionized at 900°C for 24 hrs at	

	Page
different magnifications.....	67
Figure 5.5 Room temperature XRD result of the sample solutionized at 900°C for 24 hrs.....	67
Figure 5.6 DSC responses showing the effect of aging heat treatment at 400, 500, 550 and 600°C for 3, 10 and 24 hrs to the transformation temperatures of the Ni ₅₂ Ti ₄₈ samples solutionized at 900°C for 24 hrs.....	69

LIST OF TABLES

	Page
Table 2.1 Solution and aging heat treatment conditions for polycrystalline Ni ₅₂ Ti ₄₈ samples. All samples are hot-rolled prior to these heat treatments. Cooling rates FC and WQ represent furnace-cooling for 12 hours and water-quenching, respectively.....	14

CHAPTER I

INTRODUCTION

1.1 History and Background on Shape Memory Alloys

Shape memory effect (SME) was first observed in a Au-47.5 at%Cd alloy in 1951 [1]. However, it was not used in an actual applications until it was found in a NiTi alloy in Naval Ordnance Laboratory in 1963 [2]. Since these alloys have the ability of remembering their original shape upon heating after deformation, they have wide range of usage such as pipe couplings, various actuators in electrical appliances, automobile applications, aerospace, and medical applications [3-4].

Shape memory alloys (SMAs) differ from classic metals and alloys due their unique properties like SME and pseudoelasticity (PE). Both SME and PE are related with a crystallographically reversible martensitic phase transformation. The martensitic transformation is a solid state diffusionless phase transformation having cooperative atomic movement (military motion) and shear-like deformation [3, 5]. In order to form a martensite variant, lattice invariant shear deformation is required that is generally provided through twinning, which is reversible in shape memory alloys and creates shape strain during the transformation between austenite (parent) and martensite phases. Martensitic transformation from parent phase occurs in four different ways; thermally induced, stress-induced, strain-induced [3, 5-6] and magnetic-field induced [7-8]. Generally, the high temperature phase (parent phase) has cubic structure and the low temperature phase (martensite) has a lower symmetry structure. When the material is cooled below a critical temperature, martensitic transformation starts with a shear like mechanism. Since the martensite has lower symmetry structure, the transformation occurs in different orientations which are called as lattice correspondence variants [3, 5, 9-10]. If the material is heated above a critical temperature, it returns to its original structure via reversible martensitic transformation.

This thesis follows the style and format of Acta Materialia.

Martensitic transformation is associated with the free energies of both parent and martensite phases as a function of temperature. Figure 1.1 helps better understand the thermodynamics of martensitic transformation. G^p and G^m are the Gibbs Free Energies of parent and martensite phases, respectively, and T_0 is the equilibrium temperature at which both phases have the same chemical energy. $\Delta G = G^m - G^p$ provides the driving force needed for nucleation of martensite from parent phase or vice versa. ΔT_s represent the supercooling temperature which is necessary to nucleate martensite during forward transformation, and superheating is necessary for the nucleation of parent phase during reverse transformation [3, 5].

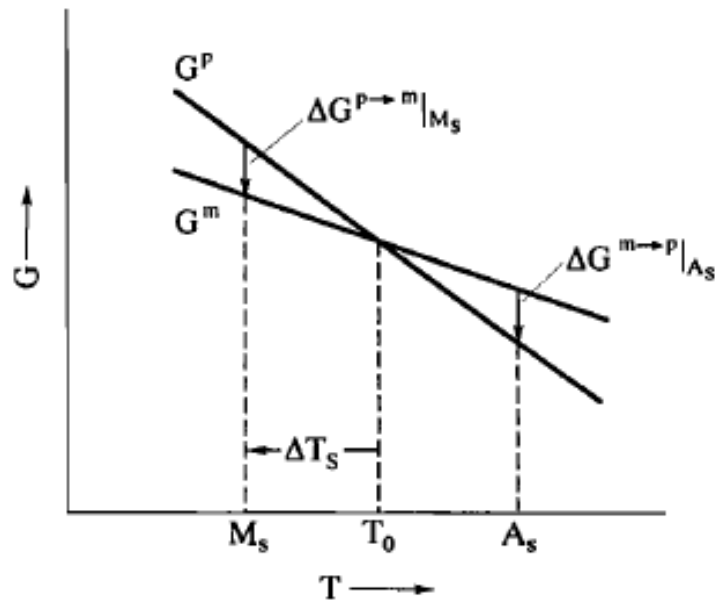


Figure 1.1 Schematic representation of Gibbs Free Energy vs. temperature curves for both parent and martensitic phases, and their relation to martensitic transformation [3, 5].

Martensitic transformation does not start and finish at the same temperature. Since elastic strain energy and lattice friction resists the growth of the martensite, additional driving force is needed to continue nucleation and it is provided by supercooling during forward transformation [3]. Due to the similar behavior, austenite start (A_s) and finish (A_f) temperatures are not the same.

SMAAs exhibit different behaviors (SME and PE) depending on testing temperature with respect to transformation temperatures and the condition of martensite and austenite phases. After deforming the material in martensite below austenite start temperature (A_s), if it is heated up above austenite finish temperature (A_f), it returns to its original shape. This phenomenon is called as shape memory effect (SME) [3, 5-6, 10-12]. Following this, even if the material is cooled below martensite finish temperature (M_f), it doesn't show any macroscopic shape change due to the self-accommodation of martensite variants. Therefore, this behavior is also known as one way shape memory effect.

There are different ways of triggering martensitic transformation as mentioned above. If the material is cooled below M_f temperature martensitic transformation is thermally induced and parent phase transforms to martensite. On the other hand, if a stress is applied to the same material in parent phase, martensite can also be formed and this type of martensite is called stress-induced martensite [3, 5-6, 10-11, 13-14]. In other words, mechanical energy is used as driving force to form martensite instead of thermal energy. Only single martensite variant, the one most favored by applied stress state, is formed. When the material is unloaded, the material transforms back to parent phase and retains its original shape. This phenomenon is called as pseudoelasticity (PE).

Since a shape memory alloy can exhibit both SME and PE, there is a correlation between these two behaviors, and stress and temperature. Figure 1.2 schematically shows stress-temperature relationship for SME and PE behaviors, critical stress for the onset of martensitic transformation, and critical stress for slip. M_s and M_f represent martensite start and finish temperatures, respectively, and A_s and A_f represent austenite start and finish temperatures. The material exhibits SME behavior below A_s and PE occurs above A_s but full recovery of PE shape change occurs above A_f . Meanwhile, if the critical stress for slip is about or lower than (B) in the figure, the material can not exhibit PE behavior. Critical stress for slip can be improved by using solution hardening, precipitation hardening and work hardening principles [3].

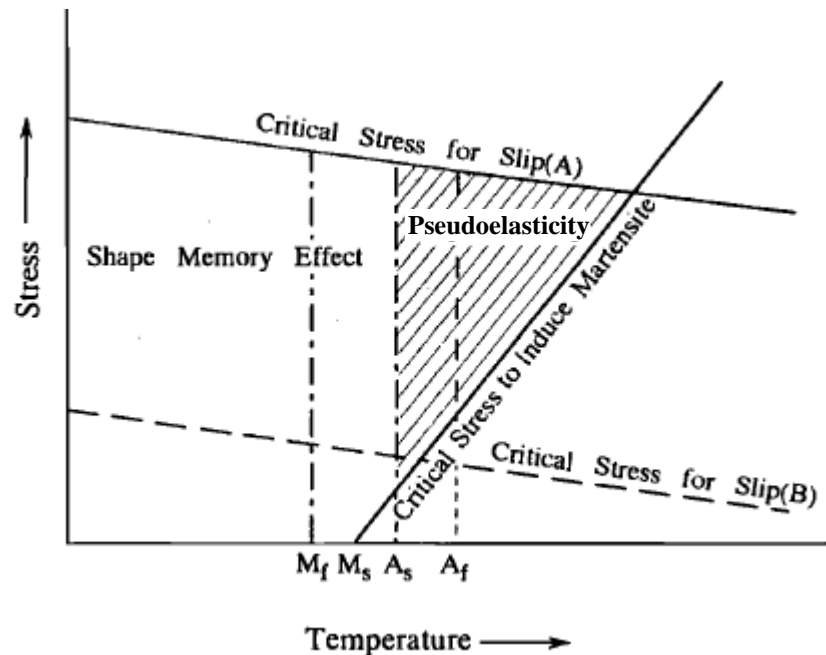


Figure 1.2 Schematic representation of stress and temperature ranges for SME and PE behavior and critical stress for slip which is (A) for high critical stress and (B) for low critical stress [3, 5-6].

Another important phenomenon is two way shape memory effect [3, 9-10, 15]. As explained previously, in one-way shape memory effect, the material just remembers the shape of higher temperature phase and there isn't any shape change when the material is cooled to martensitic phase. On the other hand, if directional internal stresses are created in parent phase, parent phase transforms to stress-induced martensite together with the associated shape change. Since directional internal stresses can activate a single variant of martensite, a spontaneous shape change occurs. There are certain thermo-mechanical treatments to obtain directional internal stress in the structure which eventually results in the two way-shape memory effect. Some of these treatments are plastic deformation of martensite, constrained aging, and thermal cycling [3].

Compared to other SMAs such as Cu-based and ferrous SMAs, NiTi based SMAs have unique properties such as low elastic anisotropy, high ductility, corrosion resistance, abrasion resistance, and high damping capacity, making them advantageous for applications [16]. In NiTi SMAs, thermo-elastic martensitic transformation occurs from a cubic B2 structured parent phase to a monoclinic B19' martensitic phase structure [3, 16].

Sometimes, there is another martensitic phase transformation prior to B2–B19' transformation that is B2–R transformation and occurs only under certain conditions such as: (1) addition of a third element such as Fe or Al to equiatomic NiTi alloys substitution to a few % Ni; (2) aging at intermediate temperatures (300°C - 500°C) of NiTi alloys due to precipitation of Ni₄Ti₃; (3) heat treatment after cold-working in NiTi alloys due to create rearranged dislocation structures [16]. R-phase has rhombohedral structure.

Large transformation strain levels can be obtained with B2 – B19' transformation. On the other hand, the transformation strain associated with the B2–R phase transformation is relatively smaller. Due to the R-phase transformation prior to B19', martensitic transformation occur in 2-stages, B2–R–B19', rather than B2–B19' [16]. Small transformation strain, cyclic stability and small hysteresis due to the R-phase transformation render these alloys and R-phase transformation desirable for some actuator applications.

1.2 Ni-rich NiTi Shape Memory Alloys

Shape memory characteristics of NiTi alloys are very sensitive to factors such as Ni content [3, 5, 15], heat treatments [3, 10, 17], thermo-mechanical processing [3, 18-19] and additional alloying [3, 5, 16, 20]. Aging heat treatments are effective methods to improve mechanical and shape memory properties of Ni-rich alloys. This is mostly due to the formation of coherent Ni₄Ti₃ precipitates which cause coherency stress fields in the microstructure influencing martensitic transformation characteristics, increasing transformation temperatures by depleting Ni-content of the matrix, and increasing critical stress for slip.

Ni-rich NiTi alloys, exceeding 50.5at.%Ni, are capable of a wide range of transformation temperatures, depending on aging heat treatments, and have superior thermo-mechanical cyclic stability compared to near-equiatomic NiTi alloys. They are particularly sensitive to intermediate aging temperatures from 300 to 500°C because coherent and semi coherent Ni₄Ti₃ precipitates can be formed which influence the shape memory properties [3, 16, 21-24].

Figure 1.3 shows the precipitation sequence for Ni₅₂Ti₄₈ SMA. Both Ni₄Ti₃ and Ni₃Ti₂ phases are metastable. Ni₃Ti is the equilibrium phase. Ni₄Ti₃ phase has

rhombohedral structure, and is very helpful in controlling the transformation temperatures by changing the matrix Ni content and improve shape memory properties by increasing critical stress for slip [3, 16, 22]. The composition of Ni_4Ti_3 precipitate was determined as $\text{Ni}_{14}\text{Ti}_{11}$ by Nishida and Honma [15] when it is first discovered, but it was correctly determined as Ni_4Ti_3 with further EDS analysis later [16]. Ni_4Ti_3 phase is coherent to the matrix at early stages at precipitation and create strain fields that lead to two-way shape memory effect [3, 16].

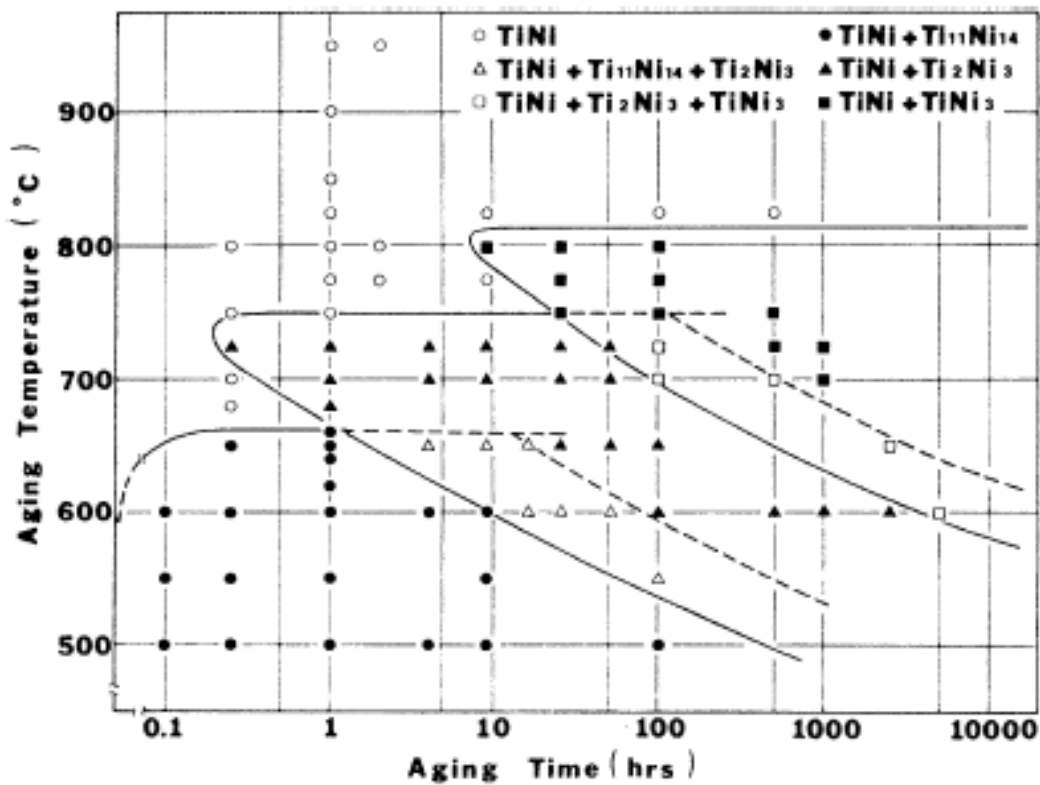


Figure 1.3 Time-temperature-transformation reaction diagram describing precipitation behavior of $\text{Ni}_{52}\text{Ti}_{48}$ SMA [21].

For low Ni content ($<50.5\text{at.}\%$) Ni-rich NiTi alloys, the nucleation rate is slow and precipitation process is affected by the grain boundaries. Since the precipitate nucleation rate is higher at grain boundaries than in the grain interiors, there is a heterogeneous precipitation. However, for high Ni content alloys, nucleation rates at

grain boundaries and grain interiors are similar, and the precipitation of Ni_4Ti_3 takes place homogeneously throughout the sample [16, 25].

Ni concentration is highly effective to transformation temperatures. Figure 1.4 shows the M_s temperature relationship with mole-fraction of Ni for binary NiTi alloys. Ni-rich NiTi alloys, having high Ni-content, have very low B2–B19' martensitic transformation temperatures in solutionized condition due to the high Ni-content. However, transformation temperatures are adjustable in these alloys via additional aging treatment due to formation of Ni-rich precipitates and depletion of Ni-content of the matrix.

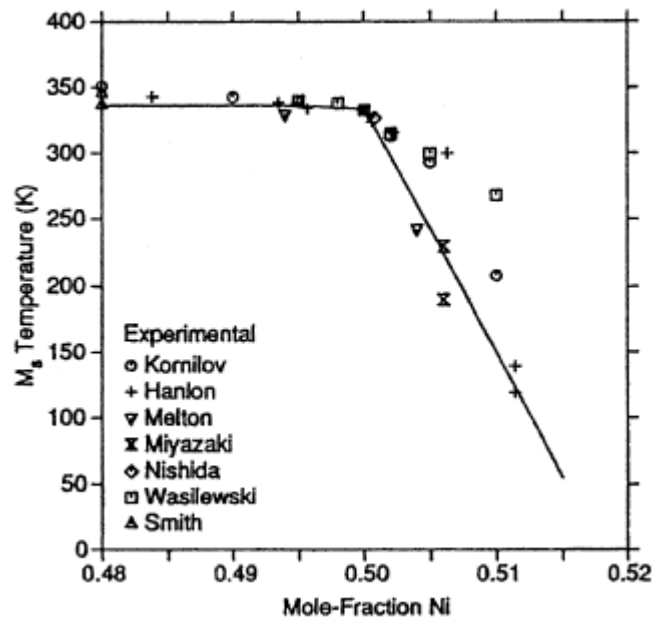


Figure 1.4 M_s temperature as a function of mole-fraction of Ni for binary NiTi alloys. Different symbols represent data from different authors. The solid line is obtained by thermodynamic calculations [16].

Ni_4Ti_3 precipitates strengthen the matrix by producing strain fields which improve shape memory recoverability [3]. Compared to near-equiatomic NiTi alloys, Ni-rich SMAs can reach high hardness values after aging heat treatments due to the precipitation hardening mechanism and increase the critical stress for slip.

In a previous work, a very high Ni content alloy, $\text{Ni}_{55}\text{Ti}_{45}$, was shown to demonstrate high strength and very high hardness (25-70 Rockwell C hardness) with low

thermal conductivity and low modulus [26]. Furnace cooling of $\text{Ni}_{55}\text{Ti}_{45}$, from single TiNi phase, resulted in low hardness, low yield strength, ultimate tensile strength, high ductility, high energy absorbing capacity or damping capacity, and about 5% shape memory effect. Its transformation temperatures can be increased above ambient by the heat treatment and temperature cool-down rate [27]. However, the reasons for the transformation temperature increases after furnace cooling have not been clearly explained. Note that this alloy does not show martensitic transformation down to -269°C .

Multi-stage martensitic transformation has been observed for low Ni-content Ni-rich NiTi alloys. There are several reasons responsible for this unusual behavior. According to Bataillard *et al.* [28], multi-stage martensitic transformation occurs due to small-scale stress inhomogeneity around Ni_4Ti_3 precipitates. Khalil-Allafi *et al.* [29] suggested that small-scale chemical inhomogeneities cause this behavior. Because the compositions of the regions which are close to Ni_4Ti_3 precipitates and the ones which are far away from these precipitates have different Ni-content, they transform separately. Another explanation by Khalil-Allafi *et al.* [23] and Dlouhy [30] for multi-stage transformation is the large-scale inhomogeneity of precipitation on grain boundaries and grain interiors. They suggest that Ni_4Ti_3 precipitates are placed at grain boundary regions and grain interiors are precipitates free regions. However, Fan *et al.* [25] explain that for low Ni content (50.6at.%Ni) Ni-rich NiTi SMAs, the nucleation rate of Ni_4Ti_3 is slow and the precipitation process is affected by the grain boundary. Since the precipitate nucleation rate near grain boundaries is higher than the grain interiors, there is heterogeneous precipitation. On the other hand, for high Ni content (51.5at.%Ni) SMAs, the nucleation rates near grain boundaries and the grain interiors are almost comparable. Thus, precipitation of Ni_4Ti_3 becomes homogenous throughout the microstructure [16, 25].

1.3 Motivation

Even though there are some studies investigating the effect of aging heat treatments on the microstructure and martensitic transformation temperatures of Ni-rich NiTi alloys with high Ni-content in the literature [22, 29, 31-36], there is an absence for comprehensive studies focusing also on the shape memory behavior including actuation

type response. In this work, the effects of additional aging treatments on the microstructural evolution, transformation temperatures and shape memory behavior of a Ni-rich NiTi SMA were investigated in the light of the following motivation;

1. High Ni-content Ni-rich NiTi SMAs have very low transformation temperatures.
2. Recent preliminary work shows that Ni_3Ti is detrimental for fatigue life [37].
3. Conventional methods (training) to produce TWSME in NiTi are costly and time consuming.

1.4 Objectives

Furnace-cooling results relatively high transformation temperatures (above ambient) because of slow cooling [27]. Additional aging to furnace-cooled material may increase transformation temperatures but it may affect the dimensional stability and shape memory properties. Ni_3Ti precipitates may eliminate by solutionizing the material. Meanwhile, there some studies in the literature showing that constrained aging results TWSME by creating oriented internal stress in the microstructure [15, 38-39]. I aim at undertaking a systematic study to address the following issues;

1. Furnace cooling results the transformation temperatures above ambient. However, can the transformation temperatures be increased more while keeping dimensional stability and transformation strain levels as high as possible?
2. To eliminate Ni_3Ti completely with controlled heat treatments but still have Ni_4Ti_3 precipitates, which are responsible for the dimensional stability, and increase transformation temperatures, above ambient, by decreasing Ni content of matrix but decrease transformation strain due to decreasing transforming volume fraction.
3. To investigate the effect of heat treatments on transformation strain (can the precipitate volume fraction be reduced while keeping the transformation temperature high?).
4. Selection of single variant Ni_4Ti_3 precipitates through aging under stress for the formation of oriented internal stress to eventually obtain TWSME and enhanced dimensional stability.

1.5 Approaches

To investigate and attain the mentioned objectives, the following approaches were determined as a road map for the represented study;

1. Optimize aging heat treatments based on the shape memory properties such as transformation temperatures and transformation strain for;
 - As-received (hot-rolled),
 - Solutionized (900°C-1hr-WQ),
 - Furnace-cooled (850°C/1hr-FC/12hr) materials.
2. Constraint aging under various stresses and temperature levels to select single variant precipitates and obtain dimensional stability.
3. Characterize systematically heat treated specimens to determine microstructural evolution, transformation temperatures and shape memory properties using differential scanning calorimetry (DSC), optical microscopy, scanning electron microscopy (SEM) and thermomechanical testing including isobaric heating-cooling experiments under various stress levels.

CHAPTER II

EXPERIMENTAL PROCEDURE

2.1 Sample Preparation

Thermo-mechanical stability, adjustable transformation temperatures by heat treatment and availability of hot forming of complex shapes make Ni-rich NiTi alloys desirable for actuator applications [4]. High Ni-content NiTi alloys such as Ni₅₅Ti₄₅ exhibited high strength and high hardness [4, 26, 40] but since these alloys shows the crack formation and propagation around Ni₃Ti precipitates [37], Ni₅₂Ti₄₈ alloys was chosen as a proper composition. A polycrystalline NiTi alloy with a nominal composition of 52 at.% Ni and 48 at.% Ti was prepared using vacuum induction melting. The sample was hot-rolled at 900°C and a 6.35 mm thick plate was obtained. Small dog-bone shaped tension specimens with gage dimensions of 8mm x 3 mm x 1.5 mm as shown in Figure 2.1 were cut using wire electrical discharge machining (EDM).

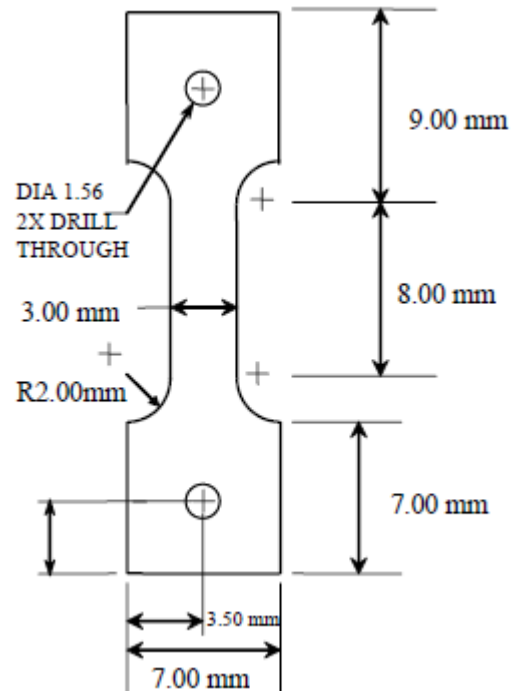


Figure 2.1 A schematic illustration of the tension sample dimensions [41].

One set of samples was solutionized at 850°C for 1 hour in vacuum the hot rolling process. Then the samples were controlled furnace cooled at a constant rate to room temperature in 12 hrs to form Ni-rich precipitates in high density to increase transformation temperatures by depleting Ni-content of the matrix. Since the cooling rate is very slow, cooling path should intersect different precipitate regions on the time-temperature-transformation diagram for this composition.

2.2 Determination of Aging Heat Treatment Conditions

In order to determine the best heat treatment conditions for high transformation temperatures and high hardness, to increase the critical stress for slip, the furnace-cooled samples were aged at different temperatures, 350-400-425-450-475-500-550-600°C, for different aging times, 0.5-1-5-24-48 hours. Vickers microhardness values and transformation temperatures were determined for the aged materials at NASA Glenn Research Center.

Figure 2.2 shows aging temperatures, aging times and Vickers Microhardness values as a 3-D graph for Ni₅₂Ti₄₈ SMA. It was observed that aging at 400°C for 48 hours results in the highest microhardness value. Hardness values rapidly drop off for aging above 400°C and the lowest hardness was obtained after aging at 600°C for 48 hours. Generally, for a constant aging temperature, hardness increased with increasing aging time except 600°C.

Figure 2.3 shows aging temperature, aging times, and martensitic transformation finish temperature (M_f) as a 3-D graph. Similar to the microhardness values, aging at 400°C for 48 hours result in the highest M_f temperature, and transformation temperatures rapidly drop off for aging above 450°C. Aging at 550°C for short aging times resulted in the lowest M_f temperatures.

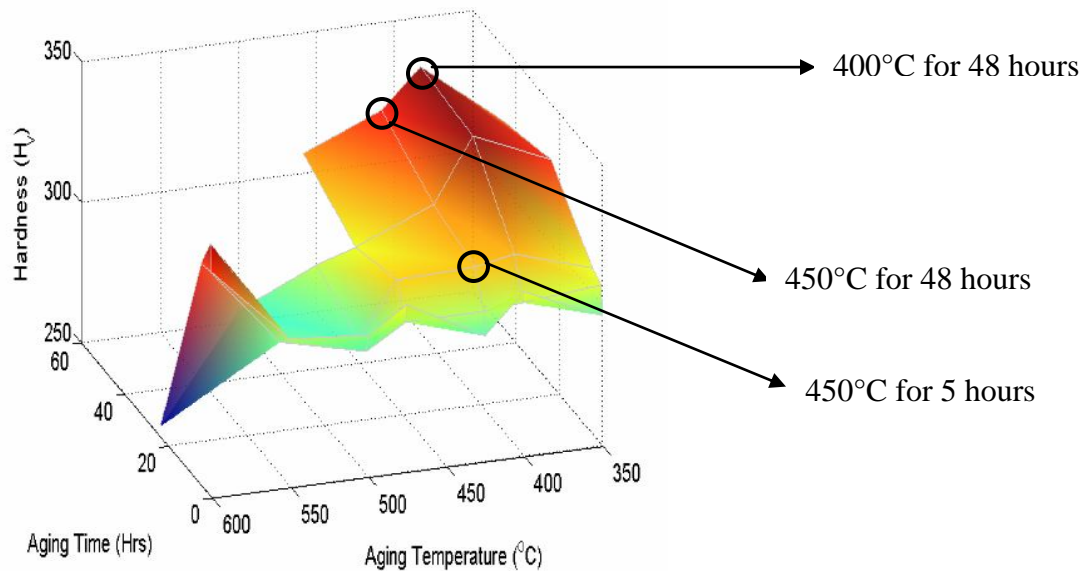


Figure 2.2 Time-temperature-vickers microhardness relationship for $\text{Ni}_{52}\text{Ti}_{48}$ materials furnace-cooled and aged at different temperatures ($350^{\circ}\text{C} - 600^{\circ}\text{C}$) for different aging times (30 mins.– 48 hrs).

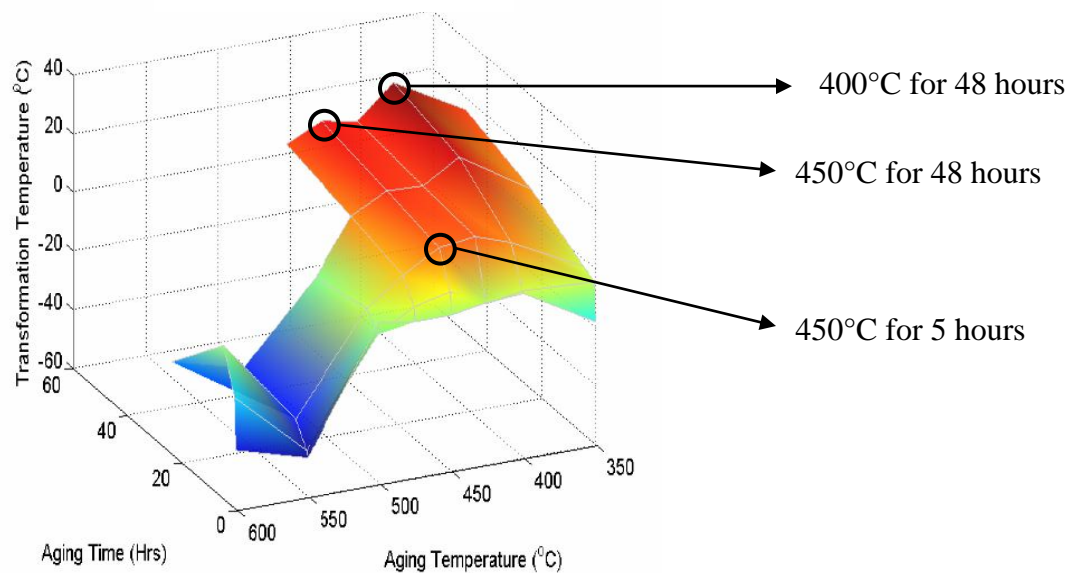


Figure 2.3 Time-temperature-martensite finish temperatures (M_f) relationship for $\text{Ni}_{52}\text{Ti}_{48}$ materials furnace-cooled and aged at different temperatures ($350^{\circ}\text{C} - 600^{\circ}\text{C}$) for different aging times (30 mins.– 48 hrs).

Finally, as shown in Figure 2.2 and 2.3, aging at 400°C and 450°C for 48 hours provides the highest, and aging at 450°C for 5 hours provides one of the lowest hardness values and martensitic transformation finish temperatures. In addition, since the furnace cooled condition was the prior condition for all aging treatments, it was chosen for further investigations in terms of transformation temperature, microstructure and shape memory properties. After these investigations, it was decided to focus on aging at 400°C and 450°C.

Table 2.1 shows the solution and aging treatment conditions for the Ni₅₂Ti₄₈ tension samples. Some of the samples were solution treated to dissolve the second phases created during casting and hot-rolling process. The solution heat treatment temperatures, 850°C and 900°C, were determined from the binary NiTi phase diagram. For this composition, since the solvus temperature is 812±22°C, 850°C and 900°C refers to single NiTi phase.

Table 2.1 Solution and aging heat treatment conditions for polycrystalline Ni₅₂Ti₄₈ samples. All samples were hot-rolled prior to these heat treatments. Cooling rates FC and WQ represent furnace-cooling for 12 hours and water-quenching, respectively.

Solution Heat Treatment			Aging Heat Treatment		
Temp.(°C)	Time(hrs)	Cooling Rate	Temp.(°C)	Time(hrs)	Stress(MPa)
-	-	-	-	-	-
-	-	-	450	5	-
850	1	FC	-	-	-
850	1	FC	450	5	-
850	1	FC	450	48	-
850	1	FC	400	48	-
900	1	WQ	450	5	-
-	-	-	450	5	200

2.3 Isobaric Cooling-Heating Experiments

Isobaric heating-cooling experiments were performed on a servo hydraulic MTS load frame at a heating-cooling rate of $10^{\circ}\text{C}/\text{min}$ under various tensile stresses. Figure 2.4 shows the parts of the servo hydraulic MTS load frame. The stress levels were increased incrementally from 0 to 300 MPa with 50 MPa and from 300 to 500 MPa with 100 MPa increments.

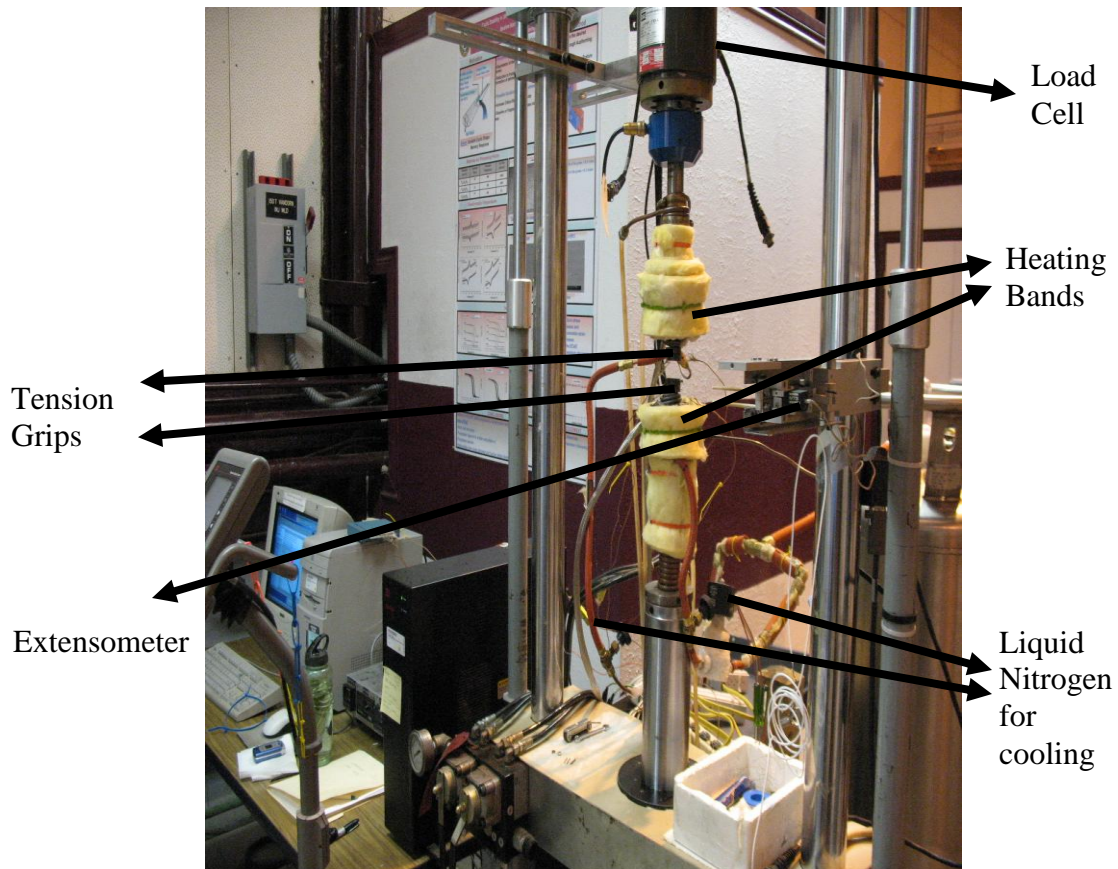


Figure 2.4 Servo hydraulic MTS load frame used for thermo-mechanical testing.

As shown in Figure 2.5, a high temperature extensometer, with a gage length of 12.7 mm, was attached to the sample to record the axial strain. A K-type thermocouple was attached to the middle of the sample gage section to measure the sample temperature.

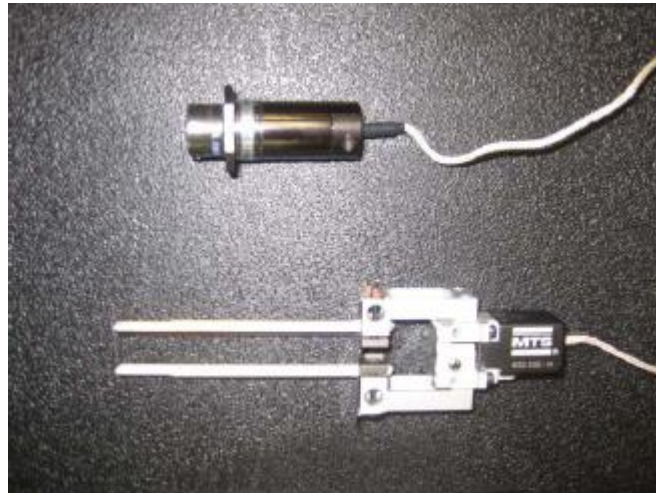


Figure 2.5 High temperature extensometer used to measure axial strain [41].

Shape memory characteristics such as transformation temperatures, recovered transformation and irrecoverable strain levels, and temperature hysteresis levels of the samples as a function of applied stress were determined from these experiments. Figure 2.6 demonstrates a representative strain vs. temperature curve to explain how these characteristics were determined from isobaric heating cooling experiments. Temperature hysteresis was determined from the middle of the strain vs. temperature curves. Recoverable and irrecoverable transformation strains were obtained at 30°C above austenite finish temperature.

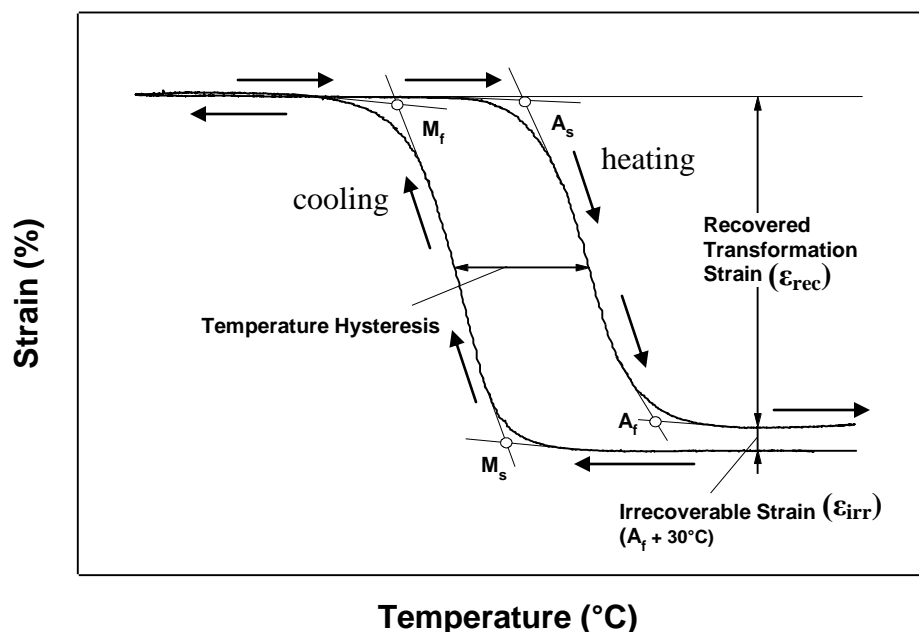


Figure 2.6 A schematic of strain vs. temperature response of a SMA showing how to determine the transformation temperatures, transformation thermal hysteresis, and the recovered transformation (ϵ_{rec}) and irrecoverable (ϵ_{irr}) strain values.

2.4. Isothermal Loading-Unloading Experiments

Isothermal loading-unloading experiments were also performed on the same test frame to verify and extend the stress vs. temperature phase diagrams for the stress-induced martensite. As shown in section 4.4, the sample was loaded in either 1% or 2% strain increments and unloaded, at various temperature levels starting from room temperature going up with 25°C increments until the specimens failed. The irrecoverable strain was obtained from the stress-strain results.

2.5 Optical, Scanning and Transmission Electron Microscopy

A digital Keyence VH-Z100 optical microscope was used to monitor the evolution of the precipitates after aging treatments provided that the precipitates are large enough. The samples were mechanically ground using SiC papers and polished with a mixture of 0.5 μm Al₂O₃ and distilled water at the last stage of polishing. For chemical etching, a solution of 5 vol.% Glycerol + 3 vol.% HNO₃ + 1 vol.% HF was used. A

Cameca SX50 scanning electron microscope (SEM) was used for microstructural and chemical analyses with the wavelength-dispersive spectrometer (WDS).

A JEOL JEM-2010 microscope operated at an accelerating voltage of 200 kV was used for transmission electron microscopy studies. TEM images were obtained from undeformed samples. Samples were electro-polished with a 20 vol.% Nitric Acid and 80vol.% Methanol solution at -10°C .

2.6 Differential Scanning Calorimetry

Transformation temperatures under stress-free condition were determined using a Perkin-Elmer Pyris I differential scanning calorimeter (DSC) at a heating-cooling rate of $10^{\circ}\text{C}/\text{min}$. DSC specimens were prepared as 5 mm diameter and 1 mm thick discs using wire EDM. Each DSC sample was initially cooled down to -90°C or -60°C and held 2 minutes before thermally cycling two times from min. to max. temperature depending on the sample.

2.7 X-ray Diffraction

X-ray diffraction (XRD) patterns of the specimens were collected in the 2θ range of 20 - 120° at room temperature using a Bruker-AXS D8 X-ray diffractometer with a CuK_{α} (1.5406 \AA) radiation. Crystal structures of transforming phases and precipitates were determined from these experiments.

2.8 Microhardness

Vickers microhardness testing was performed on the mounted and polished samples at NASA Glenn Research Center in accordance with the ASTM standard for metallic materials (ASTM Standard E 384 – 99, “Standard Test Method for Microindentation Hardness of Materials”). A Struers Duramin A300 Hardness Tester and a pyramid shaped (square) Vickers indenter with 500 gram force and 12 seconds dwell time was used. Approximately, 7-10 measurements were taken at random locations in order to yield a statistically significant mean hardness values.

CHAPTER III
EFFECT OF AGING HEAT TREATMENTS ON THE SHAPE
MEMORY CHARACTERISTICS OF FURNACE-COOLED Ni₅₂Ti₄₈
SMA

3.1 Differential Scanning Calorimetry Experiments

Figure 3.1 demonstrates how the transformation temperatures were determined from the DSC curves using the results for the furnace-cooled and aged at 450°C for 5 hrs then water-quenched sample. For this material which demonstrate multi-stage transformations, M_s^1 represents the martensitic transformation start temperature of some B2 parent phase regions. While these regions complete the transformation to either to R-phase or B19' martensite, the other parts of the material start the martensitic transformation at another temperature (M_s^2) upon further cooling. There is another martensitic transformation start temperature (M_s^3) with small heat flow in this particular sample. With heating from martensite phase, there are two distinct peaks for reverse transformation. For reverse transformation, when transformation temperatures can not be directly determined from these curves due to overlapping peaks, fictitious lines are constructed to complete the individual peaks. This helps to determine the first austenite finish temperature (A_f^1) in Figure 3.1. A_f^2 represents the second austenite finish temperature. As mentioned previously, a high density of precipitates causes inhomogeneous coherency stress fields throughout the microstructure. Because stressed and unstressed regions transform separately, forward and reverse transformation occur in multiple stages. Meanwhile, the regions which are close to precipitates and far away from the precipitates have different Ni-content and create chemical inhomogeneities in the microstructure. Since Ni-content of the matrix effects the transformation temperatures, different Ni-content regions transform at different temperatures.

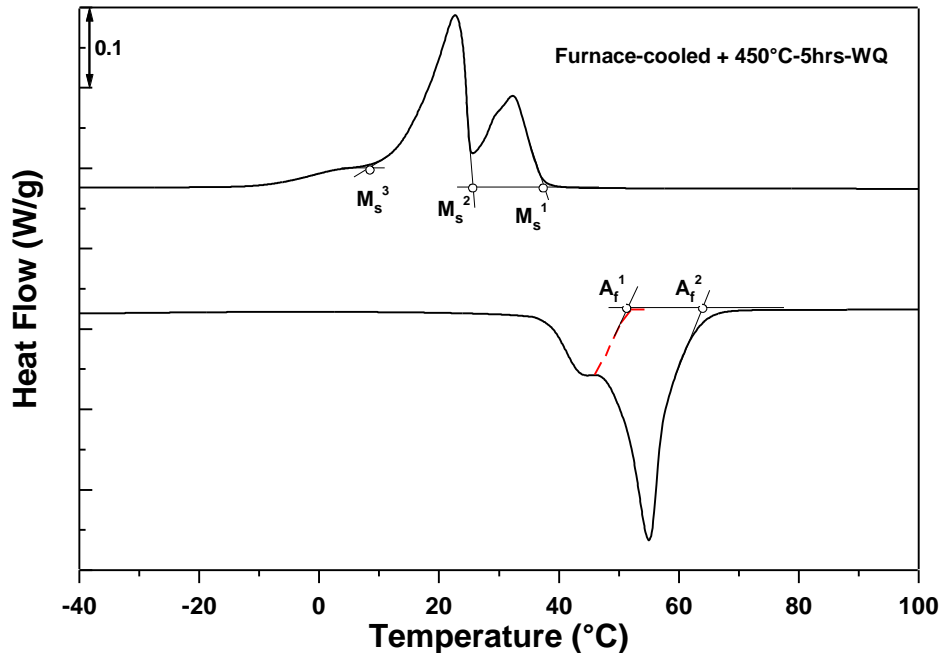


Figure 3.1 DSC response of the furnace-cooled Ni₅₂Ti₄₈ aged at 450°C for 5 hrs exhibiting multi-stage transformation.

Figure 3.2 shows the forward and reverse martensitic transformation temperatures of Ni₅₂Ti₄₈ solutionized at 850°C for 1 hr, subsequently furnace-cooled for 12 hours under stress-free conditions. Normally, no transformation can be seen in the solutionized condition because of the high Ni-content of the matrix. However, because the sample was cooled slowly during the furnace-cooling process, the transformation temperatures increase due to the formation of Ni-rich precipitates and finally depleting the Ni-content of the matrix. It is observed that during cooling from the B2 structured parent phase, the B2 – B19' martensitic transformation starts in multiple stages, but it is hard to discern these peaks from the plot. Therefore, we assume that the material transforms in a single stage with $M_s = 27^\circ\text{C}$ and $M_f = -13^\circ\text{C}$. Upon heating, the reverse transformation starts at 8°C (A_s) and finishes at 59°C (A_f). There is one more peak at about 40°C like in the forward transformation, but it is hard to differentiate it from the major transformation peak.

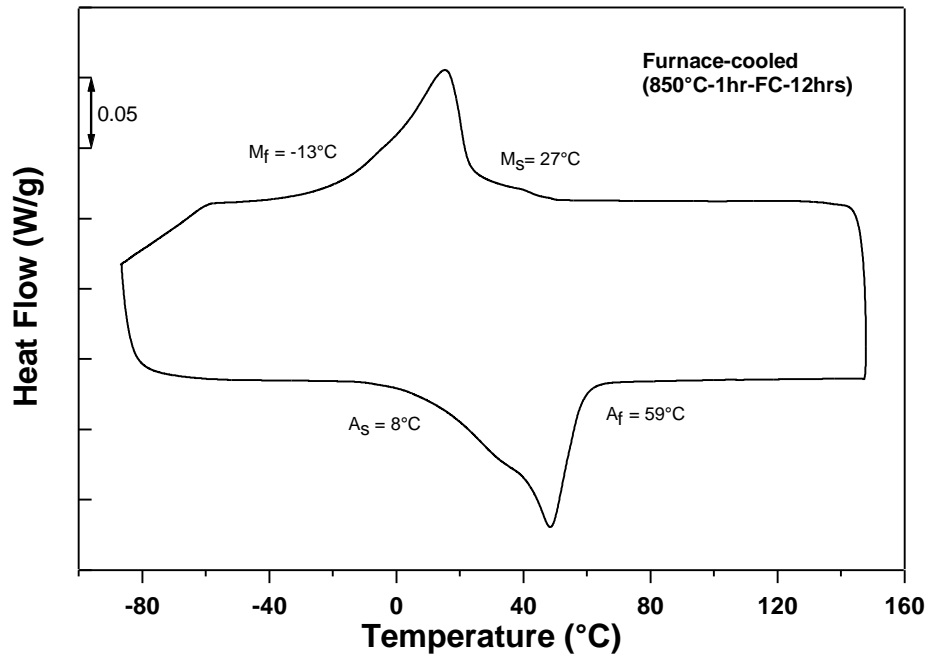
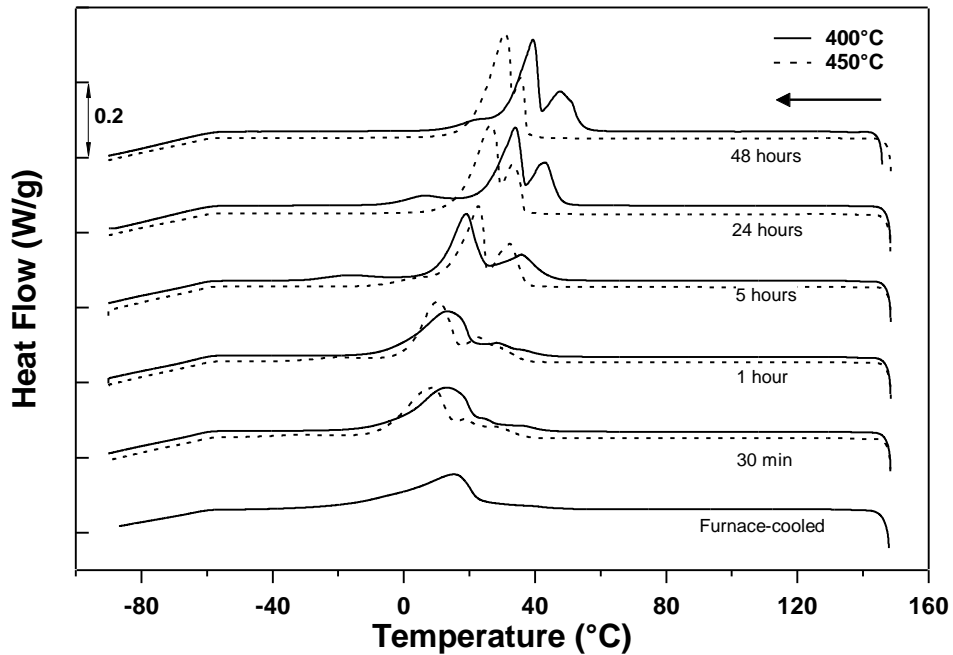
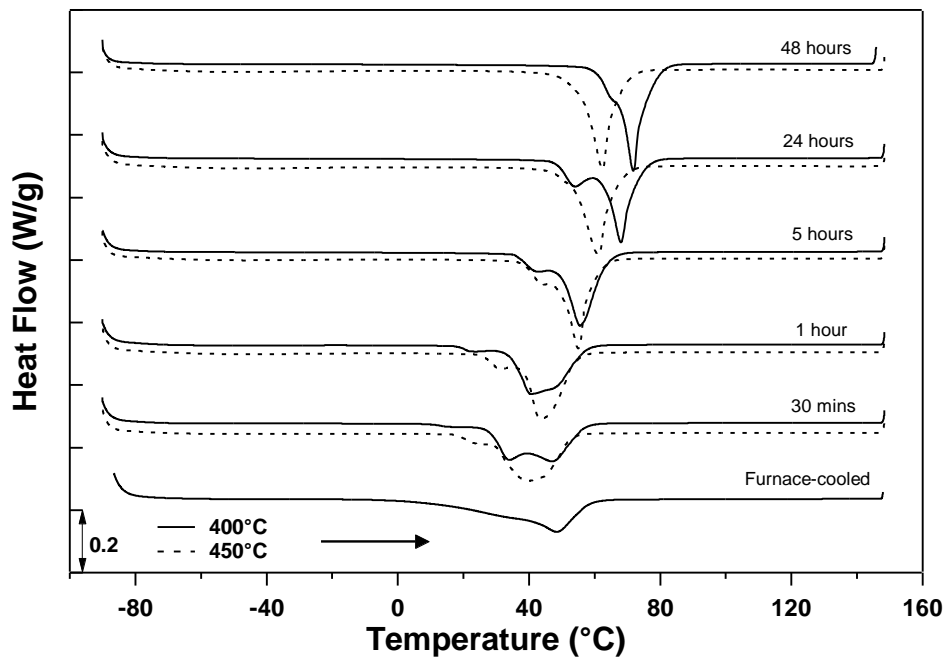


Figure 3.2 DSC response of the furnace-cooled $\text{Ni}_{52}\text{Ti}_{48}$.

Figures 3.3.a and b represent the stress free transformation behavior of the furnace-cooled sample, aged at 400°C and 450°C , during forward and reverse transformations, respectively. Solid lines indicate the transformation behavior of the material aged at 400°C ; dashed lines indicate the transformation behavior of the material aged at 450°C for different aging times. As mentioned previously, the furnace cooled material exhibits almost a single-stage transformation on both forward and reverse transformations. However, it is hard to determine the M_f and A_s temperatures for this material due to the lack of a sharp transformation peak. It is also observed that multi-stage transformations take place in the materials aged at 400°C and 450°C .



(a)

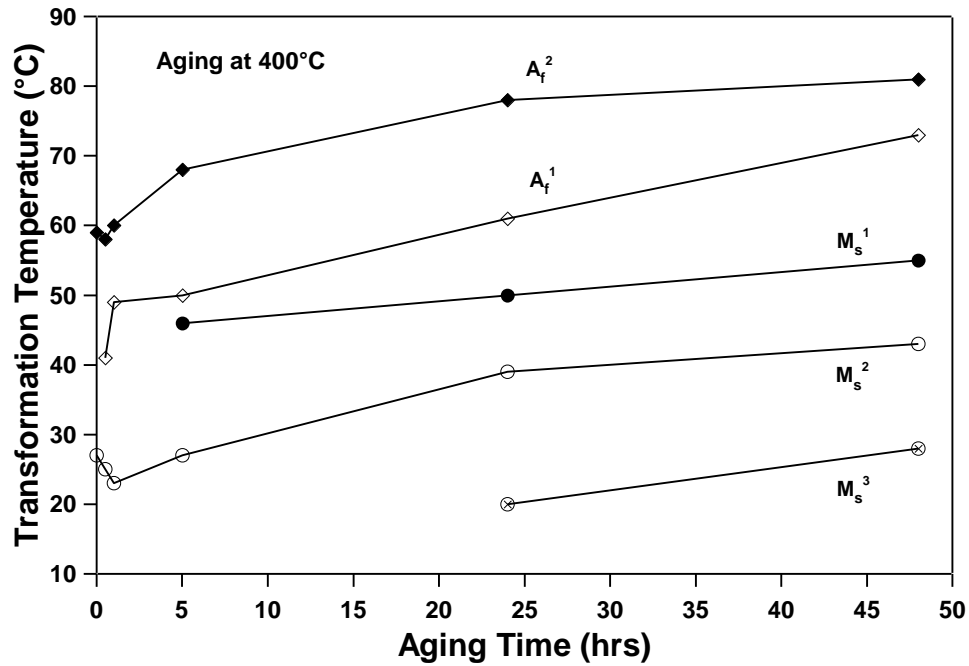


(b)

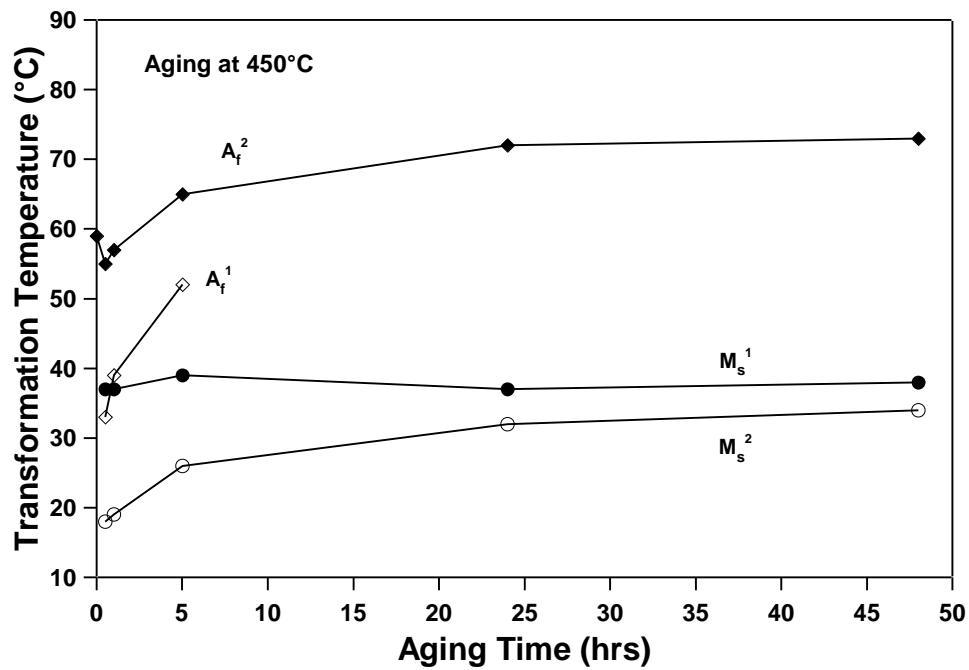
Figure 3.3 DSC responses showing the effect of aging at 400°C and 450°C for 30 mins., 1, 5, 24 and 48 hrs on the transformation temperatures of the furnace-cooled Ni₅₂Ti₄₈ samples during; (a) cooling and (b) heating.

Upon cooling from the parent phase (Figure 3.3.a), similar transformation behavior was observed after aging at 400°C and 450°C for 30 mins., 1, 5, 24 and 48 hours. However, the transformation occurs at higher temperatures after aging at 400°C compared to 450°C for longer aging times (24 and 48 hours), and the difference in transformation temperatures increases with increasing aging time. No obvious multi-stage transformation was detected for short aging times during cooling. On the other hand, it is clear that multi-stage martensitic transformation occurs for both intermediate and long aging times. It was observed in Figure 3.3.b that reverse transformation start and finish temperatures remain almost the same for short aging times at 400°C and 450°C. However, the transformation takes place at a higher temperature for longer aging times after aging at 400°C compared to 450°C. Another important point is that the first transformation peak disappears and single-stage transformation is observed after aging at 450°C for 24 and 48 hrs aging times. The heat flow intensity associated with the first peak also decreased with increasing aging times for aging at 400°C.

Figures 3.4.a and b show the variation of transformation temperatures ($M_s^{1,2,3}$ and $A_f^{1,2}$) after aging at 400°C and 450°C, respectively, for different aging times. The transformation temperatures remain almost constant or decrease for short aging times (≤ 1 hours) for both aging temperatures probably because of the formation of very small Ni_4Ti_3 precipitates, which increase the internal resistance against transformation. On the other hand, the transformation temperatures increase with increasing aging times above 1hr aging times for all cases. It is observed that the forward transformation occurs in three-stages for long aging times (24 and 48 hours) at 400°C. This one takes place in two-stages after aging at 450°C for the same aging times. Additionally, the reverse transformation occurs in two-stages after aging at 400°C for long aging times while single-stage transformation is observed after aging at 450°C for long aging times. As shown in Fig. 3.3, both forward and reverse transformations occur at higher temperatures for aging at 400°C than 450°C.



(a)



(b)

Figure 3.4 The change in transformation temperatures for the furnace-cooled $\text{Ni}_{52}\text{Ti}_{48}$ SMA aged at; (a) 400°C and (b) 450°C, for different aging times.

3.2 Microstructural Evolution

Figure 3.5 shows an optical micrograph and an SEM image of the initial furnace-cooled sample demonstrating an average grain size of about 100 μm and an interparticle distance of about 3 μm in the regions of nearly uniform precipitates. Since the cooling rate is slow, the cooling path intersects several precipitation regions on the time-temperature-transformation diagram [21], and Ni_4Ti_3 and Ni_3Ti precipitates are formed in high volume fraction. It was found from the EDS analysis that the composition of the matrix is $\text{Ni}_{50.9}\text{Ti}_{49.1}$. The below nominal Ni content of the matrix is due to the formation of the Ni-rich precipitates. There are high density of lenticular shaped Ni_4Ti_3 precipitates in four different orientations throughout the matrix, having a significant effect on the transformation behavior and shape memory behavior of the material. Ni_3Ti (white) precipitates occupy only a small volume fraction and are oriented along the rolling direction.

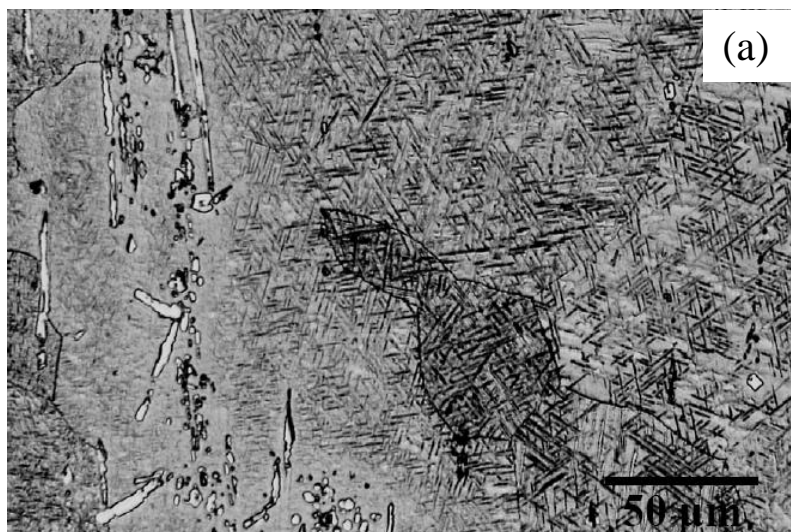


Figure 3.5 a) Optical micrograph, and b) SEM image of the furnace cooled $\text{Ni}_{52}\text{Ti}_{48}$ and chemical compositions of the matrix and precipitates obtained by EDS analysis.

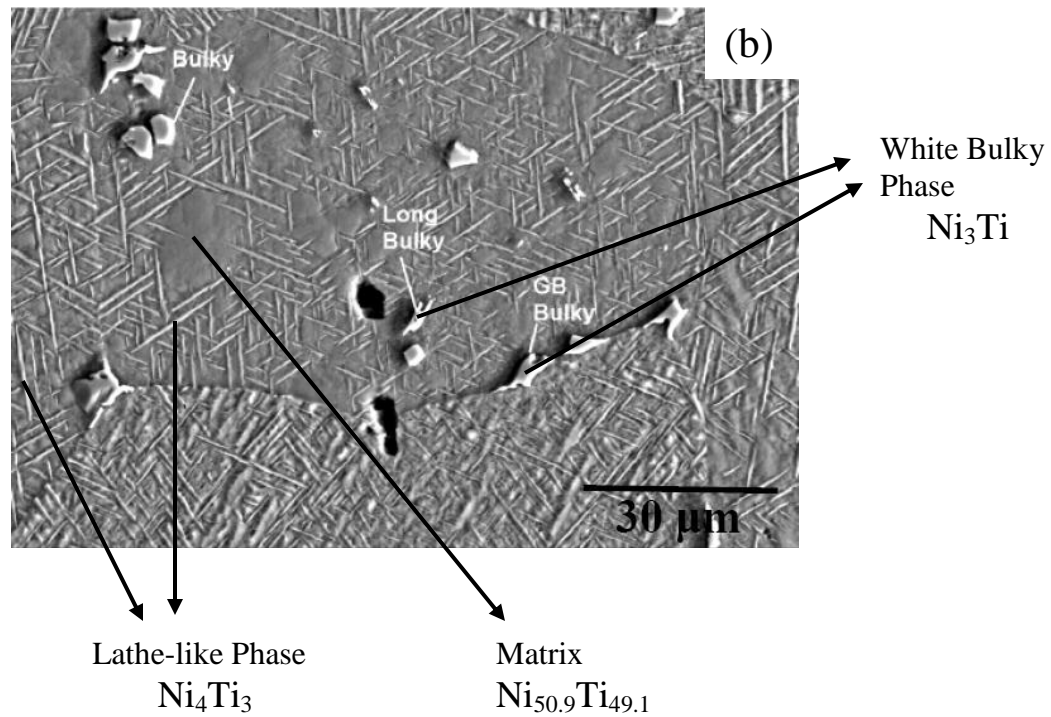


Figure 3.5 Continued.

Figure 3.6.a and b show the microstructures of furnace-cooled and aged at 400°C for 48 hrs material. It can be observed that the volume fraction of Ni_4Ti_3 precipitates increased from $20\pm 1\%$ in the furnace cooled case to $27\pm 1\%$ after aging at 400°C for 48 hrs. Increased volume fraction of precipitates decreases the Ni-content of the matrix leading to an increase in transformation temperatures. Finally, furnace-cooled and aged at 400°C for 48 hrs material has higher transformation temperatures than furnace-cooled material due to higher volume fraction of Ni_4Ti_3 precipitates.

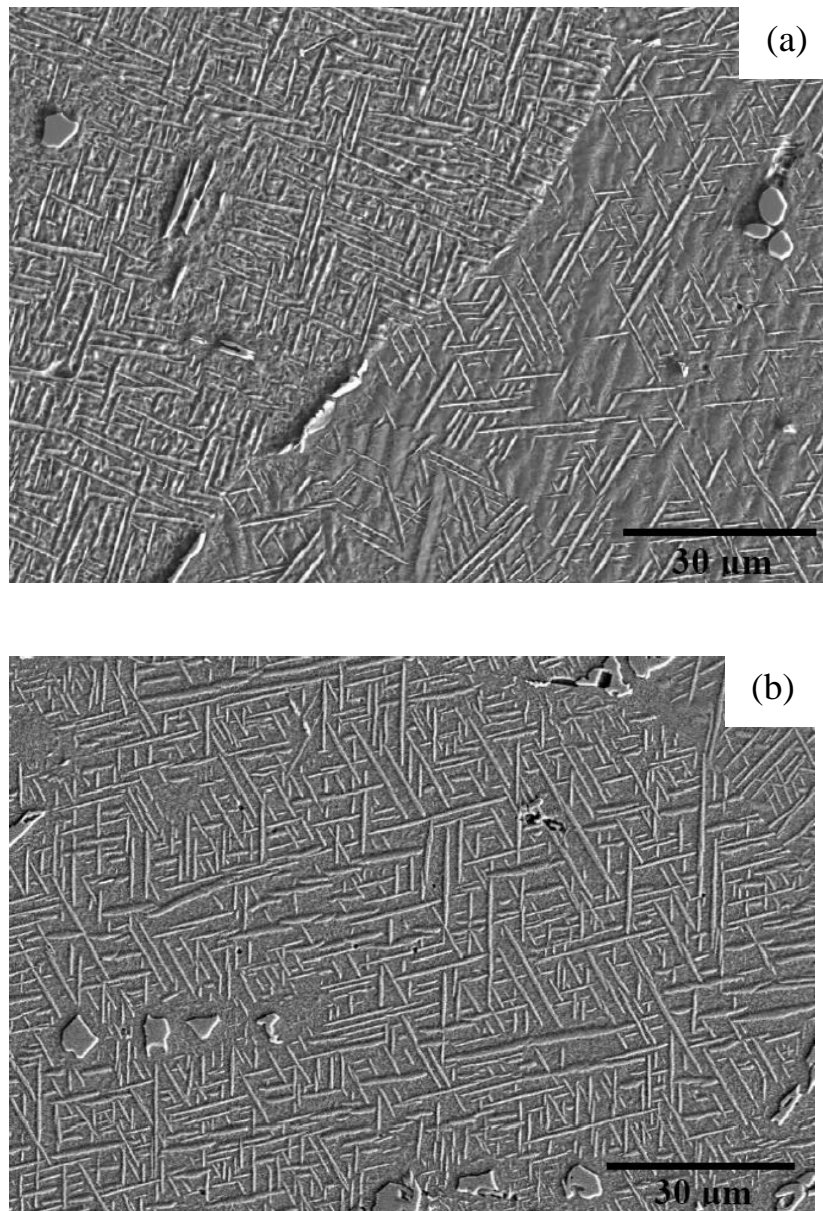


Figure 3.6 SEM images of (a) furnace-cooled and (b) furnace-cooled and aged at 400°C for 48 hrs $\text{Ni}_{52}\text{Ti}_{48}$.

Figure 3.7 shows SEM image of the furnace-cooled and aged at 450°C for 48 hrs material. It was also calculated that the volume fraction of Ni_4Ti_3 precipitates is about $27\pm 1\%$ after aging at 400°C for 48 hrs and $24\pm 1\%$ after aging at 450°C for 48 hrs. Due to the formation of higher volume fraction of Ni_4Ti_3 precipitates, the Ni content of the matrix is depleted more after aging at 400°C than at 450°C , which results in higher transformation temperatures.

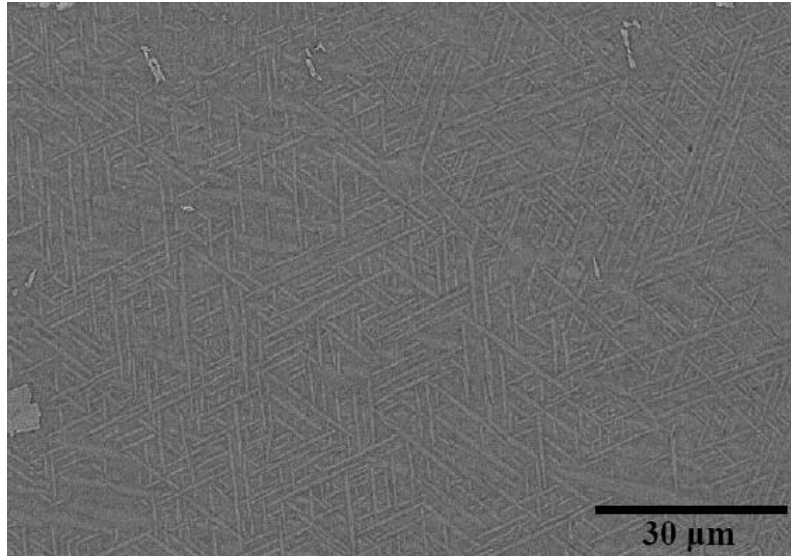
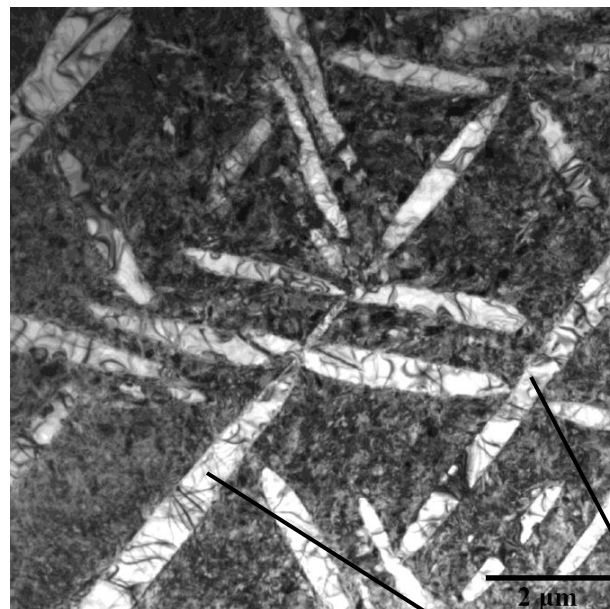


Figure 3.7 SEM image of the sample furnace-cooled and aged at 450°C for 48 hrs.

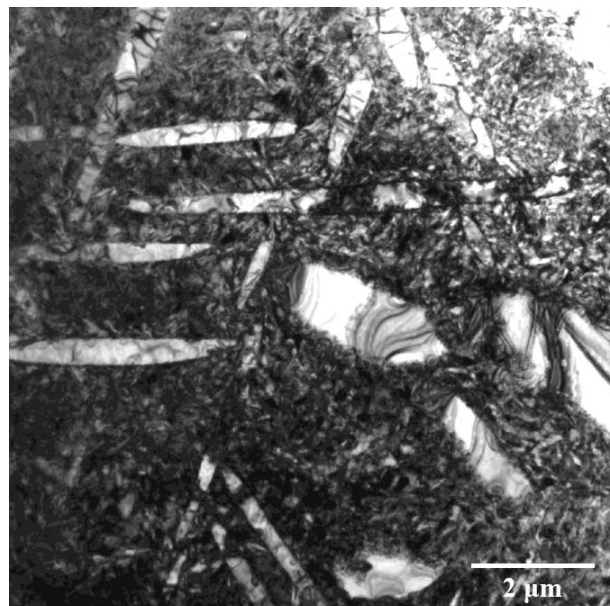
Figure 3.8 presents the bright and dark-field TEM images of the sample furnace-cooled and aged at 400°C for 48hrs recorded at room temperature, illustrating the general microstructure having big Ni_4Ti_3 precipitates. The volume fraction of Ni_4Ti_3 precipitates is pretty high which is about 27%. Lack of clear martensite variants or twins in between non-transforming precipitates indicate that there are very small precipitates in the matrix and due to their coherency stress fields, it is very difficult to distinguish martensite twins. In addition, martensite twins are likely to be very thin because of to accommodate transformation shear in between these small precipitates, martensite needs to have small twin sizes due to size effect as it is observed in nano-grain sizes in NiTi SMAs [42]. Cloudy regions around precipitates represent the matrix having dislocations. Since the precipitates are in high dense, they cause lots of defects in the structure and finally strengthen the materials.

Figure 3.8.d shows detectable martensite twins near the large Ni_4Ti_3 precipitate because of the Ni depletion near the precipitate. Such that new, much smaller, precipitates do not form near the large precipitates, they form away from them in the matrix.

TEM images were recorded at room temperature, so aged at 400°C for 48 hrs material has martensitic structure. Figure 3.8.e represents the twinned martensite structure close to the big Ni_4Ti_3 precipitate. Twinned structure can clearly be seen.

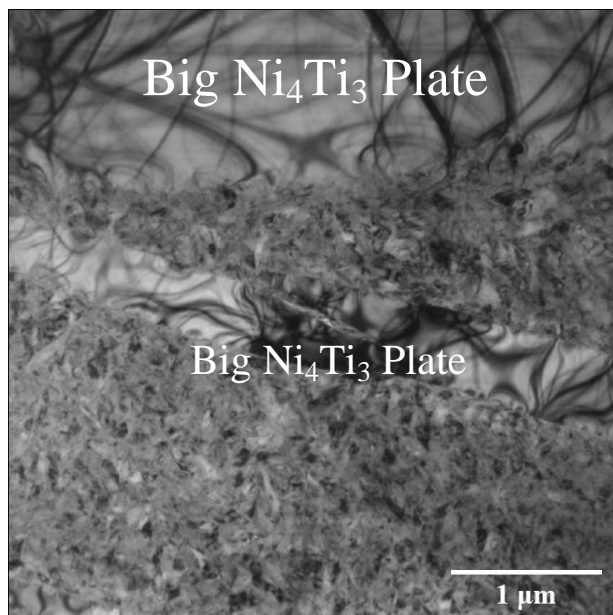


(a)

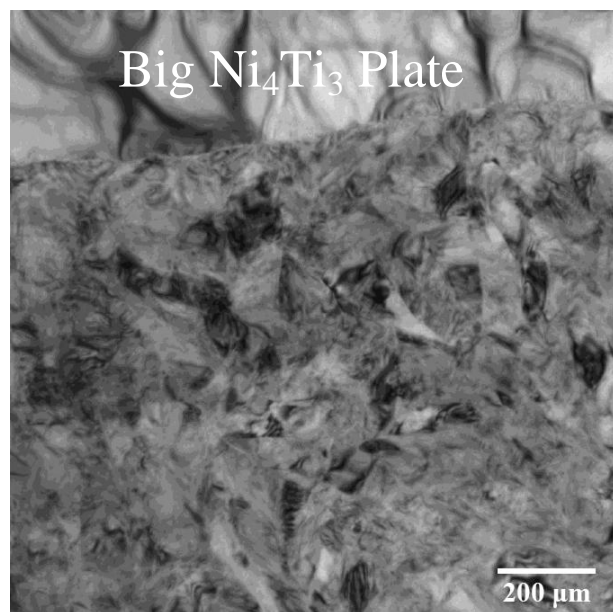
**Ni₄Ti₃
Precipitates**

(b)

Figure 3.8 Bright and dark-field TEM images of the sample furnace-cooled and aged at 400°C for 48 hrs at room temperature showing the big Ni₄Ti₃ precipitates and microstructure in details.

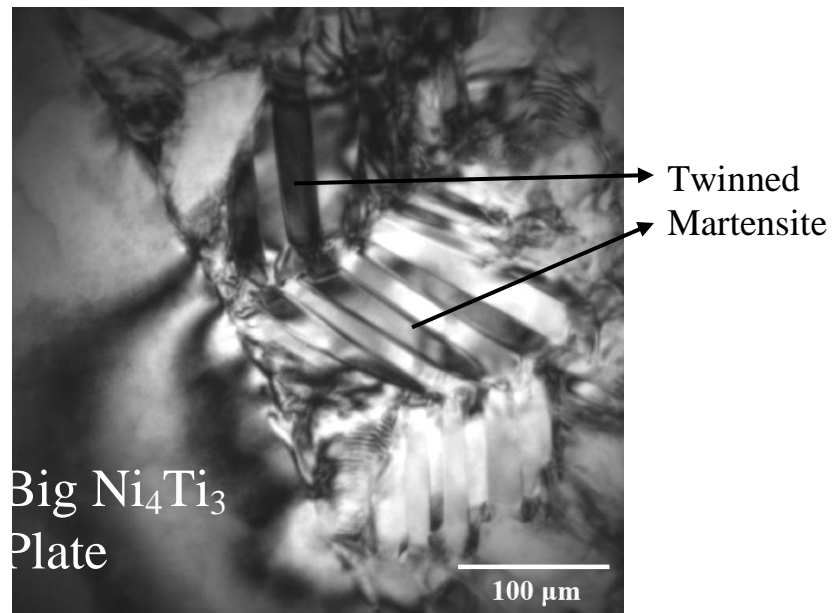


(c)



(d)

Figure 3.8 Continued.

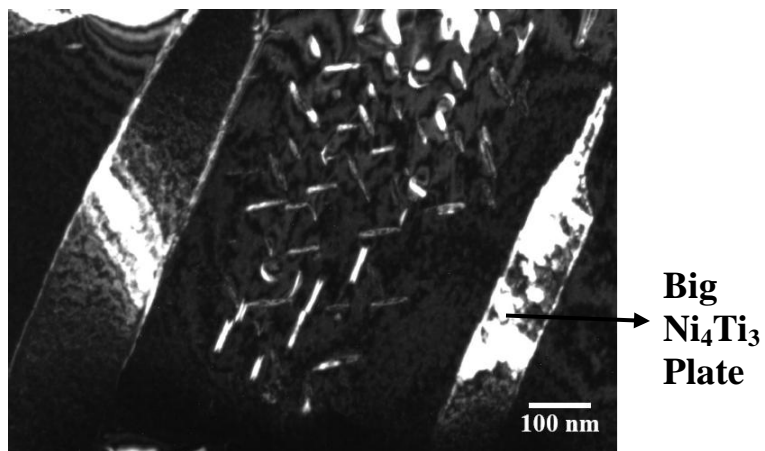


(e)

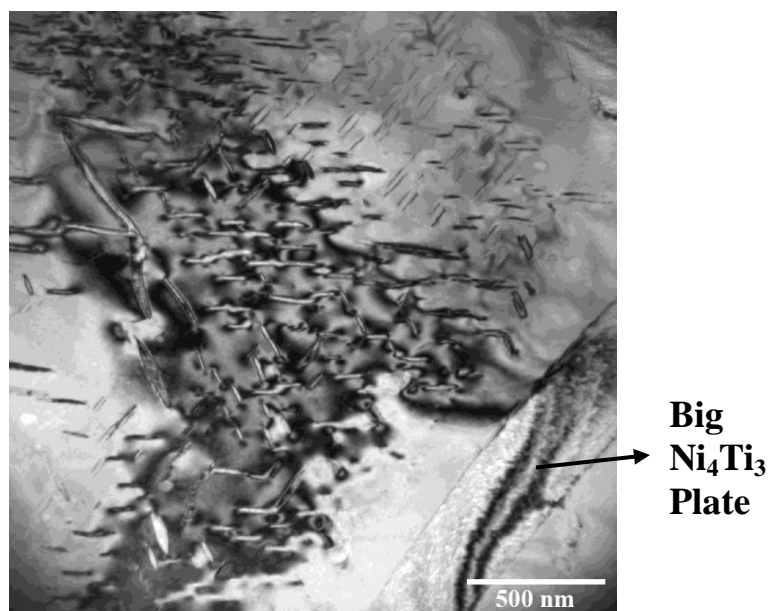
Figure 3.8 continued.

Meanwhile, some R-phase regions and small Ni_4Ti_3 precipitates in R-phase regions were observed additional to big Ni_4Ti_3 precipitates for the sample furnace-cooled and aged at 400°C for 48 hrs as shown in Figures 3.9. Average size of fine Ni_4Ti_3 precipitates is about 100 nm. As expected from previous TEM study, fine precipitates forms away from the big precipitates and explains the twinned martensite structure close to big precipitates.

Coarsening of existent Ni_4Ti_3 precipitates and formation of new, much small, ones explains the increase of transformation temperatures after aging at 400°C for 48 hrs due to increase of volume fraction of precipitates and finally Ni depletion of the matrix.

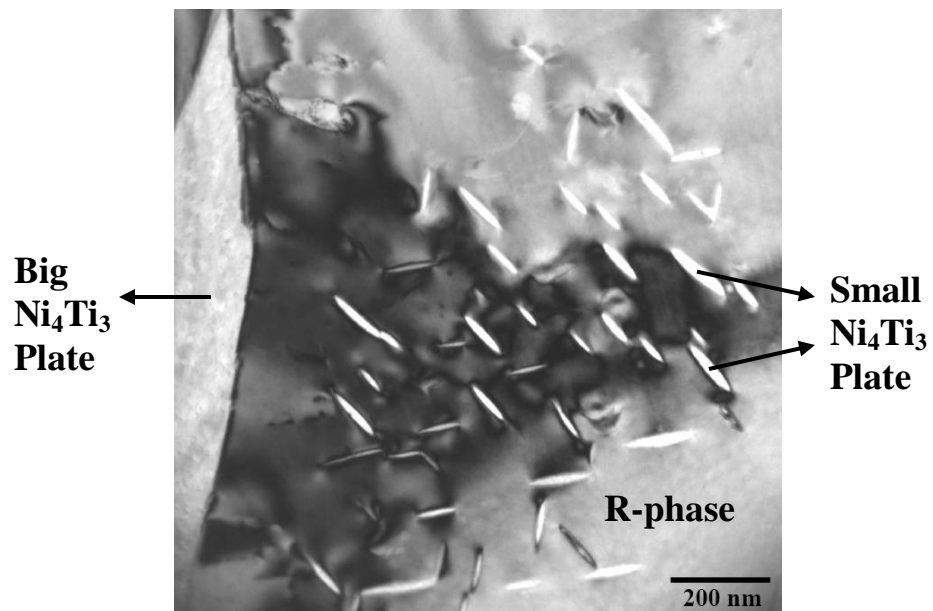


(a)

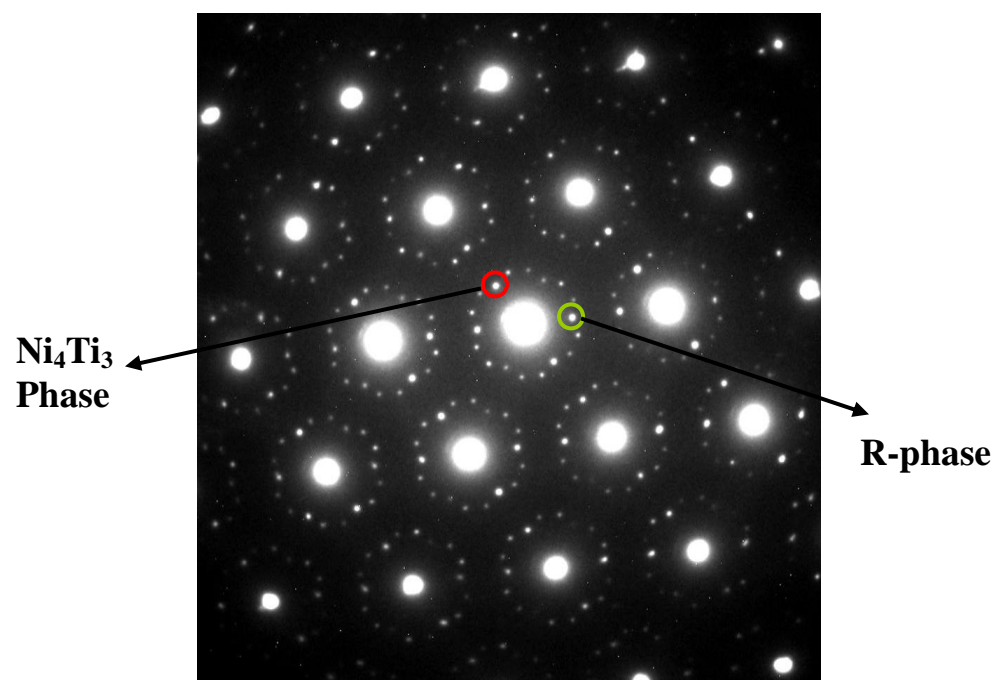


(b)

Figure 3.9 (a) Bright, (b) and (c) dark-field TEM images, and (d) electron diffraction pattern obtained from image (c) of the material furnace-cooled and aged at 400°C for 48 hrs showing big and small Ni₄Ti₃ precipitates and R-phase regions.



(c)



(d)

Figure 3.9 Continued.

Since some R-phase regions were observed in TEM analysis, new DSC experiments were needed to identify the multi-stage martensitic transformation which some of the peaks may belong to R-phase transformation instead of B19' transformation. Figure 3.10 shows the partial cooling-heating experiments of the material furnace-cooled and aged at 400°C for 48 hrs between different temperature ranges. When the material was cooled down before completing the second martensitic transformation peak, two-stage reversible transformation was observed. Due to the small temperature hysteresis, first peak corresponds to R-phase transformation while second peak represent B19' transformation from B2 parent phase. For the full cycle, first peak correspond to R-phase transformation and B19' martensitic transformation occurs in three-stage. First, the regions which close to big Ni_4Ti_3 precipitates transform due to low Ni content and seen in the graph as (1) peak. Then, the regions around small Ni_4Ti_3 precipitates transform in (2) peak. Finally, matrix regions which are far away from precipitates transform in (3) peak due to high Ni content. On the other hand, reversible transformation occurs from B19' to B2 in multi-stage due to inhomogeneities in the microstructure without R-phase transformation.

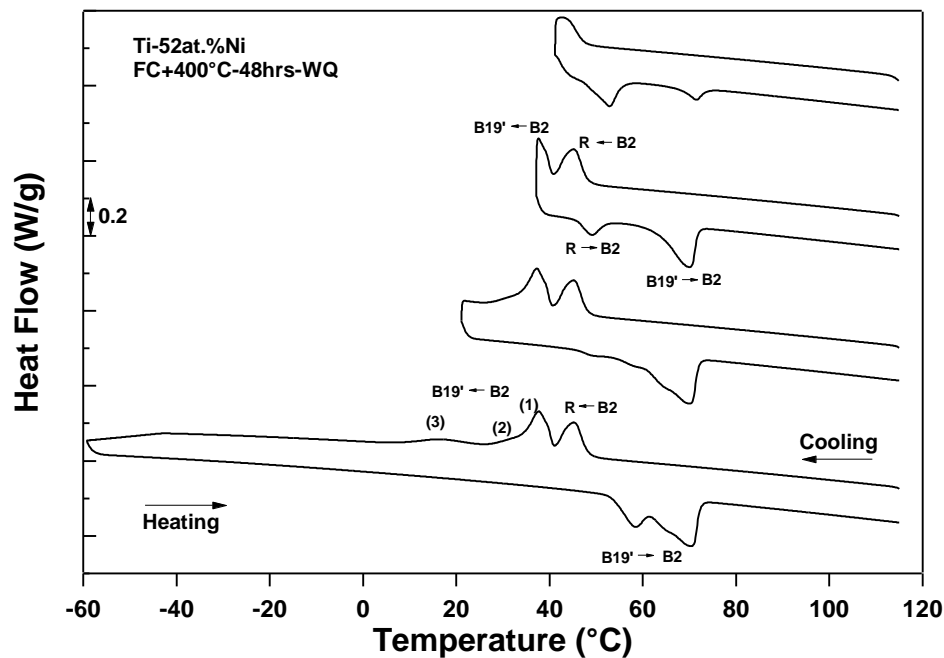


Figure 3.10 Partial cooling-heating experiments of the material furnace-cooled and aged at 400°C for 48 hrs.

Figure 3.11 shows the effect of aging time on the size of Ni_4Ti_3 precipitates. It is observed that Ni_4Ti_3 precipitates coarsen with increasing aging time. Precipitate growth behavior can be explained with the Ostwald ripening phenomenon [43]. According to this phenomenon, large precipitates have the least solubility and small precipitates have the highest solubility. This solubility difference creates a solute gradient between the small and large precipitates and finally small precipitates shrink and disappear as illustrated in Figure 3.12. On the other hand, the solute from small precipitates causes coarsening of medium and large precipitates [44]. Wagner [45] and Lifshitz et. al. [46] explain the kinetics of ripening in details in their studies.

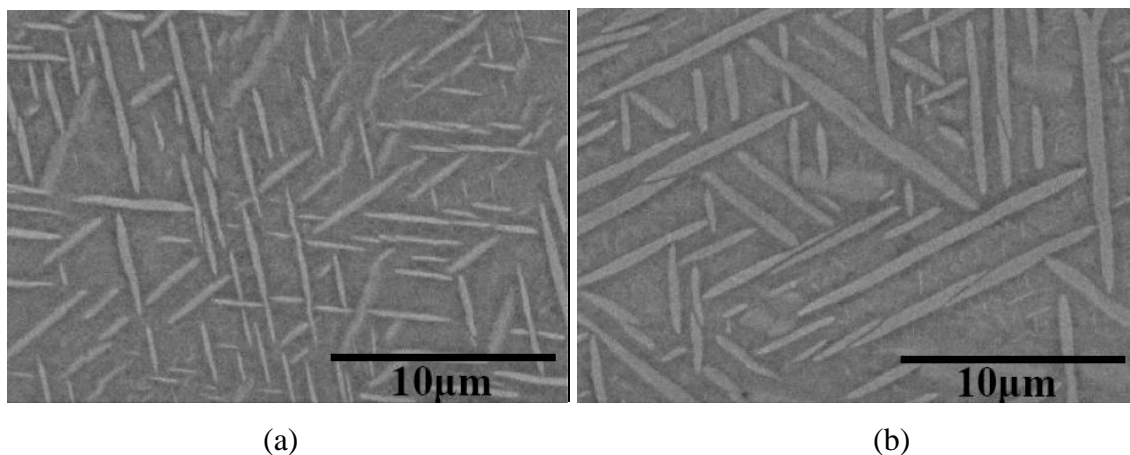


Figure 3.11 SEM images of the furnace-cooled and aged $\text{Ni}_{52}\text{Ti}_{48}$ at 450°C for; (a) 30 mins. and (b) 48 hrs.

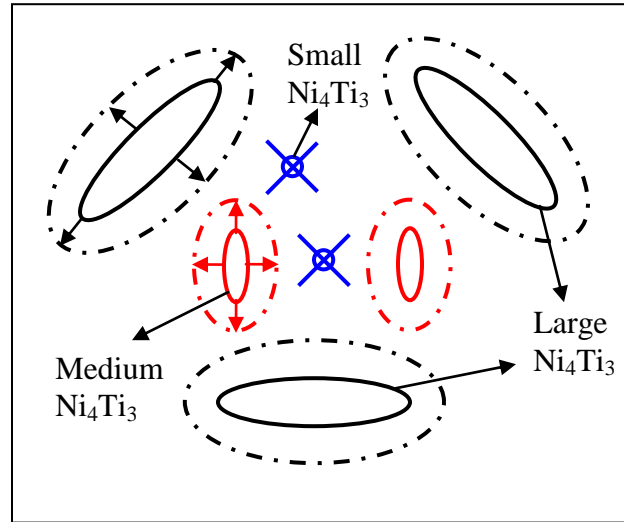
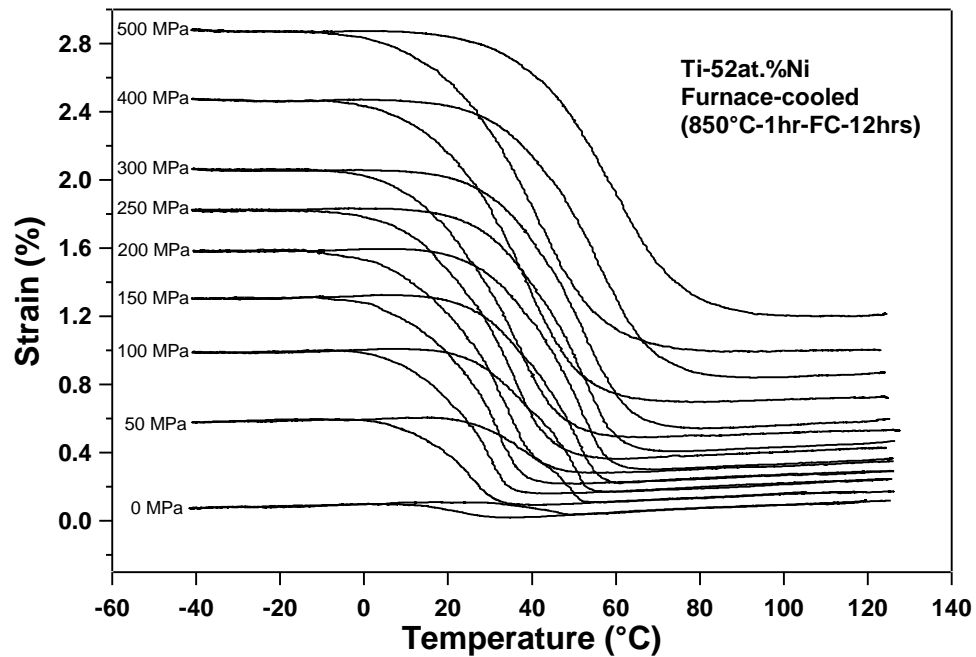


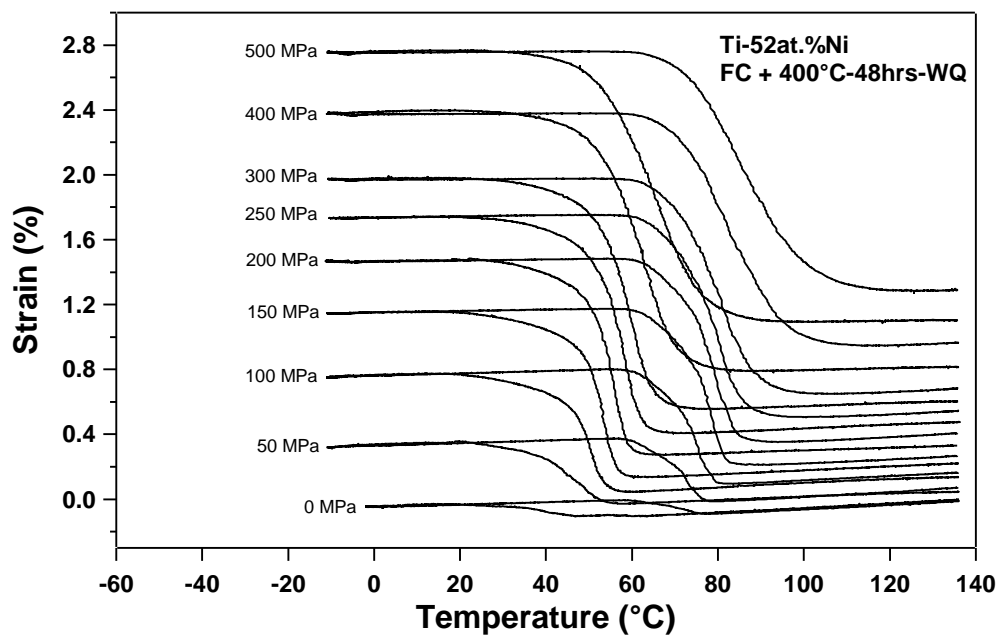
Figure 3.12 Schematic illustration of growth of Ni_4Ti_3 precipitates having different sizes after long aging times. Solid lines represent precipitate sizes before aging treatment; dashed lines represent precipitate sizes after long aging times. Large and intermediate precipitates coarsen at the expense of small precipitates after long aging times.

3.3 Isobaric Cooling-Heating Experiments

Figures 3.13.a and b show the strain vs. temperature curves for the $\text{Ni}_{52}\text{Ti}_{48}$ samples furnace cooled and furnace-cooled plus aged at 400°C for 48 hrs under different stress levels. It should be reiterated that aging at 400°C for 48 hrs material exhibits the highest increase for transformation temperatures. Both materials exhibit two way shape memory effect (TWSME) as evident from the small ϵ_{rec} under 0 MPa. This TWSME can be explained by the presence of dense Ni_4Ti_3 precipitates, which cause oriented internal stress resulting in the selection of more single variant martensite instead of self-accommodated martensite [38]. The onset of ϵ_{irr} is at 200 MPa and ϵ_{irr} increases steadily with increasing stress levels for the furnace cooled material. On the other hand, ϵ_{irr} is recorded at 100 MPa for the furnace cooled and aged at 400°C for 48 hours material.



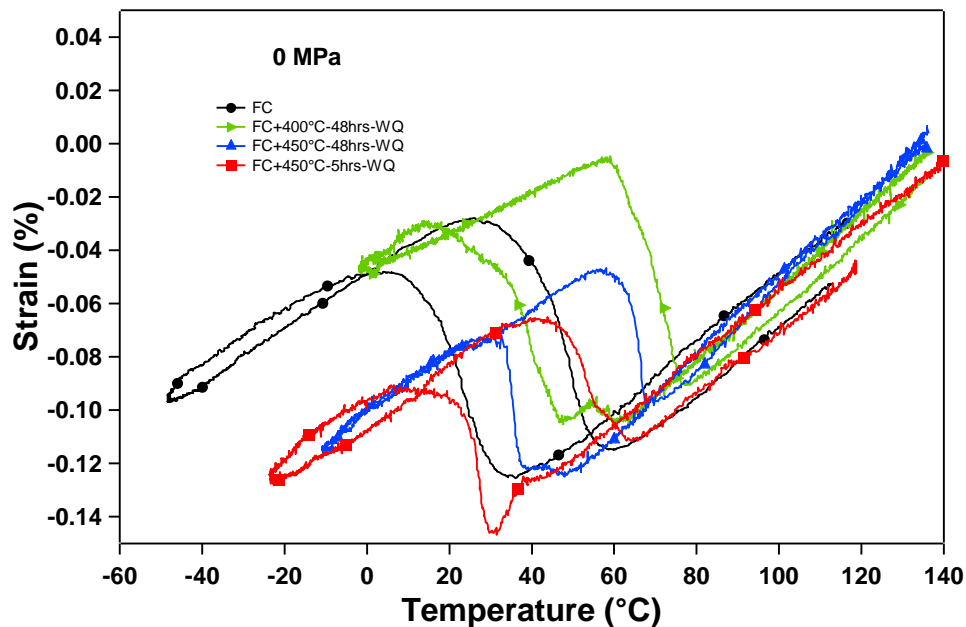
(a)



(b)

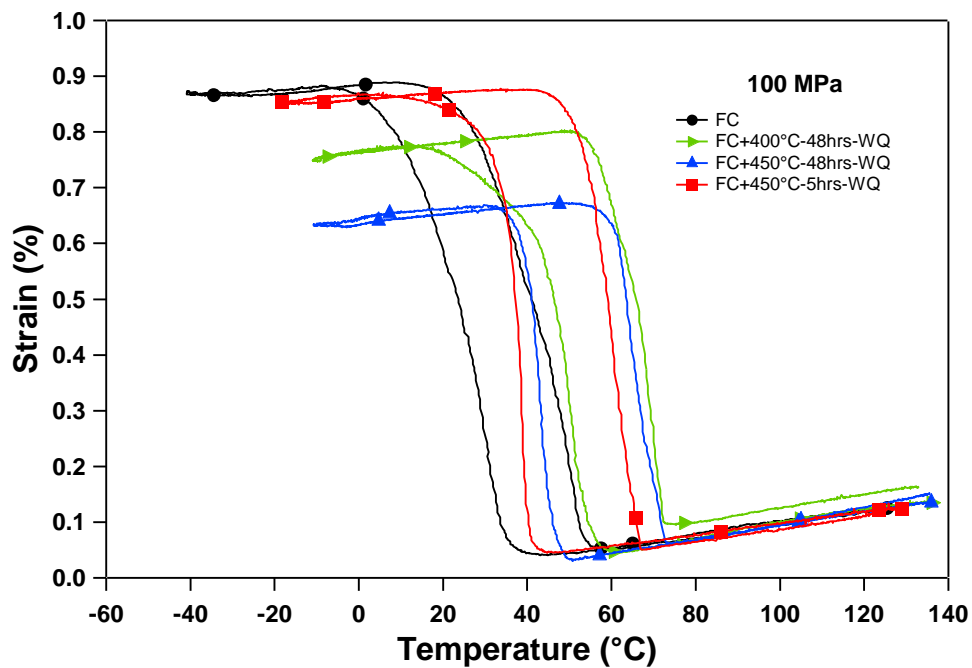
Figure 3.13 Strain vs. temperature response of the furnace-cooled $\text{Ni}_{52}\text{Ti}_{48}$; (a) before and (b) after aging at 400°C for 48 hrs under various constant stress levels during isobaric cooling-heating experiments.

Isobaric cooling-heating responses of the materials that are investigated were compared under selected applied stress levels to better understand the influence of aging on the shape memory behavior. Results are shown in Figures 3.14.a, b, c and d with stress levels as 0, 100, 200, and 400 MPa, respectively. Aged materials exhibit multi-stage martensitic transformation under 0 MPa stress due to chemical inhomogeneity and coherent stress fields around the precipitates. At 100 MPa, aging at 400°C for 48 hours results in a large ϵ_{irr} compared to the other conditions, and furnace cooled materials exhibit the highest ϵ_{rec} . All materials exhibit ϵ_{irr} under 200 MPa stress. It was observed that the furnace cooled material needs a large driving force, as evidenced by a shallower slope of the cooling curve, or larger $M_s - M_f$ difference to complete the martensitic transformation compared to the aged materials under 200 and 400 MPa.

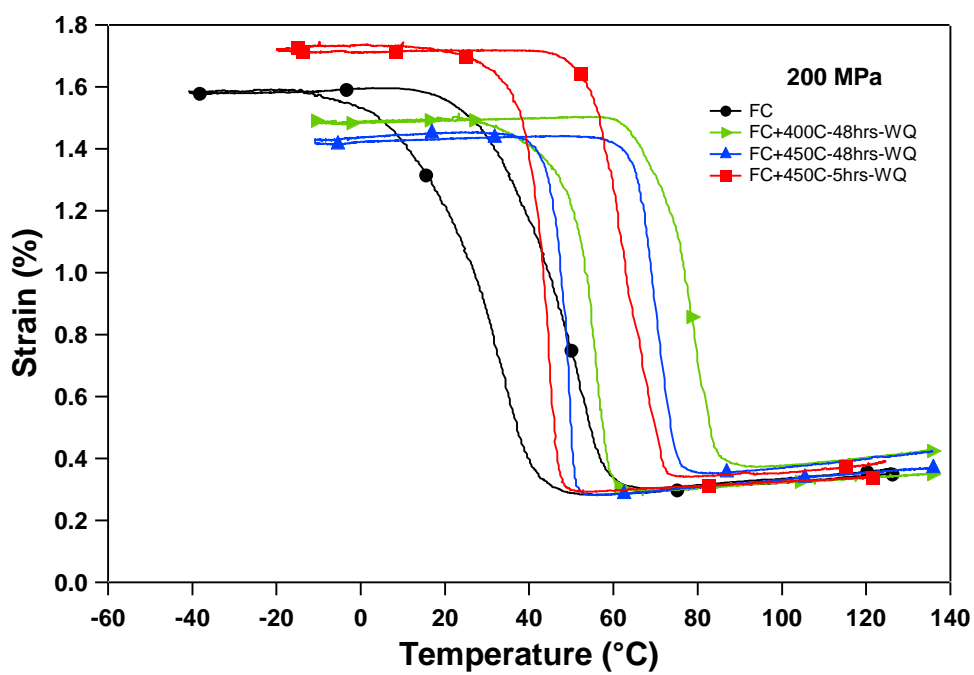


(a)

Figure 3.14 Comparison of strain vs. temperature curves of the furnace-cooled and aged $Ni_{52}Ti_{48}$ under various constant stress levels: (a) 0 MPa, (b) 100 MPa, (c) 200 MPa and (d) 400 MPa.



(b)



(c)

Figure 3.14 Continued.

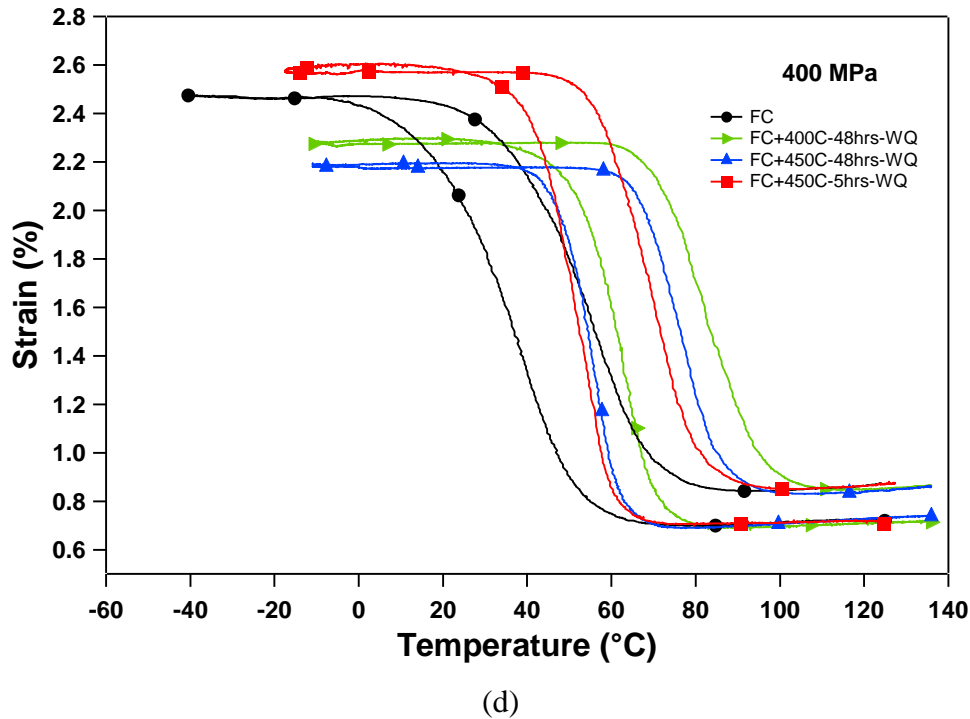


Figure 3.14 Continued.

Figures 3.15.a and b show the recovered transformation, ϵ_{rec} , and irrecoverable strain, ϵ_{irr} , levels, respectively, as a function of applied stress for the furnace cooled and aged materials. It is seen that ϵ_{rec} decreases and ϵ_{irr} increases after aging. The ϵ_{rec} values for all materials are very low as compared to the near-equatomic NiTi (4.6% under 200 MPa for $\text{Ni}_{50.1}\text{Ti}_{49.9}$ from our previous studies) due to a high volume fraction of precipitates (20%) in the matrix. Since the precipitates do not transform, transforming volume fraction decreases. It has been found that since the compound twinning, rather than predominant type II twinning, which is observed in low Ni-content NiTi alloys, is formed in the aged high Ni-content NiTi alloys, lower ϵ_{rec} is obtained in these alloys [47-49]. Another reason for low ϵ_{rec} is that since some of the precipitates are small in size, interparticle spacing between these precipitates is also small as seen in Section 3.2. When material transforms even under high stress levels, the small regions in between these small particles will have geometrically necessary twins in martensite since precipitates do not transform and it is difficult to detwin the twinned martensite forming in these small volumes. As can be seen in the TEM images in Figure 3.9, the distance between these small particles is on the order of 100 nm. It is also likely that some of the regions may not

even transform. Therefore, ϵ_{rec} decreases due to these non-transform or twinned small regions.

The furnace cooled material has the highest ϵ_{rec} and lowest ϵ_{irr} values, while it has the lowest transformation temperatures. There is no ϵ_{irr} until above 200 MPa stress for the furnace cooled material. Furnace cooling and aging at 450°C for 48 hrs result in the lowest recovered transformation strain.

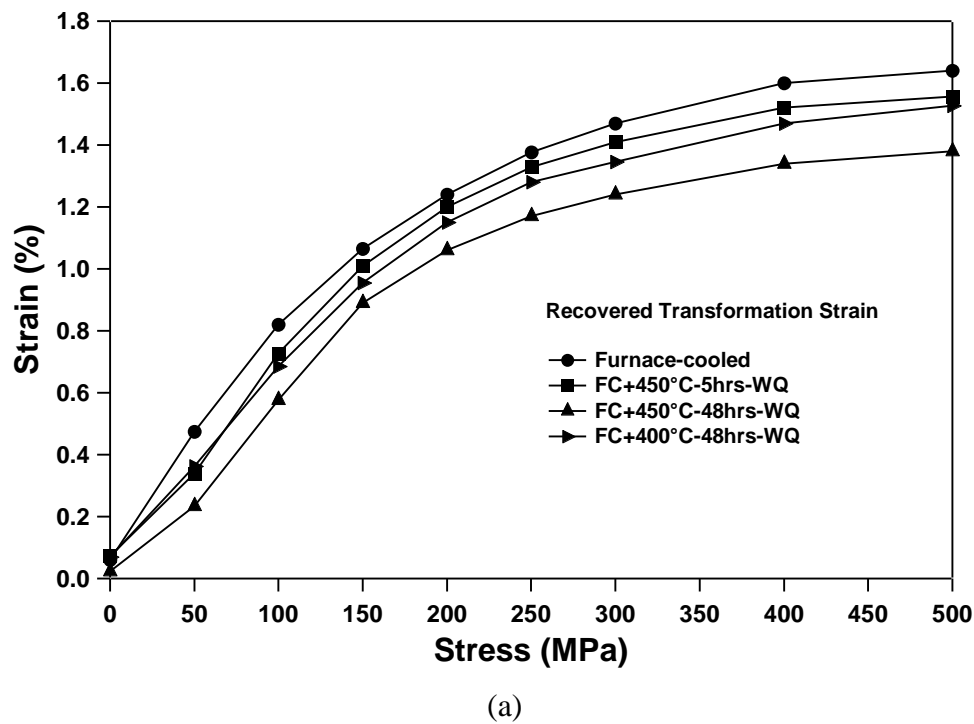


Figure 3.15 (a) Recovered transformation and (b) Irrecoverable strain responses of the furnace-cooled and aged $\text{Ni}_{52}\text{Ti}_{48}$ as a function of constant tensile stress levels.

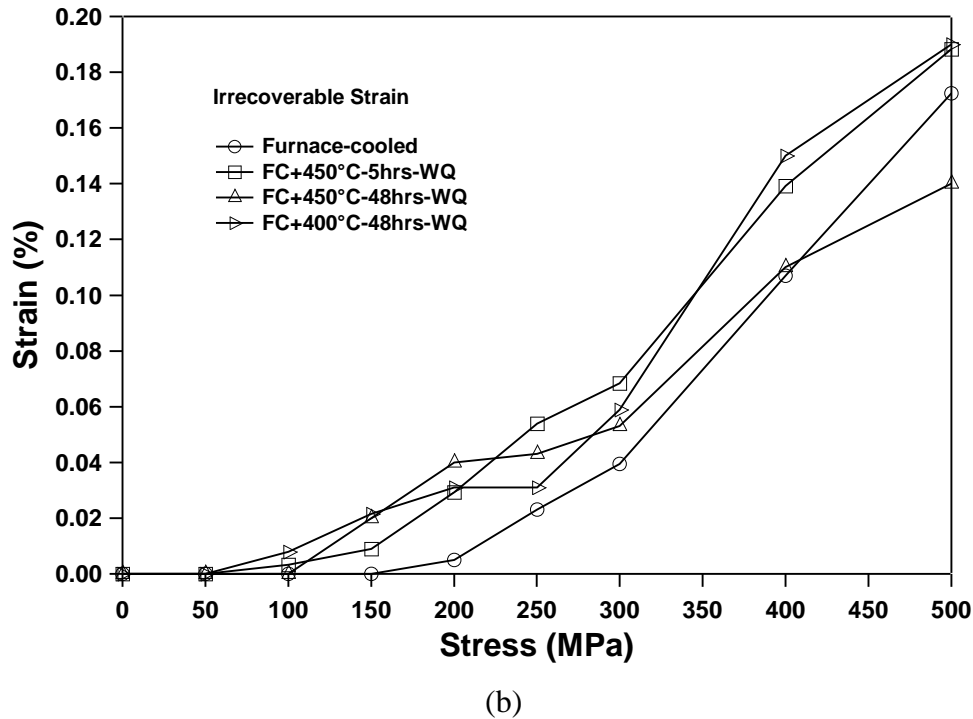


Figure 3.15 Continued.

Figure 3.16 shows temperature hysteresis as a function of applied stress for the furnace cooled and aged materials. As expected from the previous works, the temperature hysteresis first shrinks then small increase is observed with increasing external stress for the higher Ni alloys (>50.5at.%Ni) the present of precipitates [47]. Since the volume fraction of precipitates is very high, the material is stronger because of precipitation hardening. Elastic strains provide high elastic strain energy because of coherency stress fields around precipitates. Since the elastic stored energy increases with increasing external stress and promotes the reverse transformation, less chemical energy is needed to start and finish the reverse transformation [47]. Finally, temperature hysteresis decreases with increasing stress for the stress levels below 250 MPa. With further increase in external stress, stored elastic strain energy level decreases due to more severe plastic relaxation of transformation shear and volume change, and frictional resistance to phase boundary motion increases due to increase in dislocation density and hardening effect [47]. Consequently, temperature hysteresis increases with increasing stress for the stress levels 250 MPa.

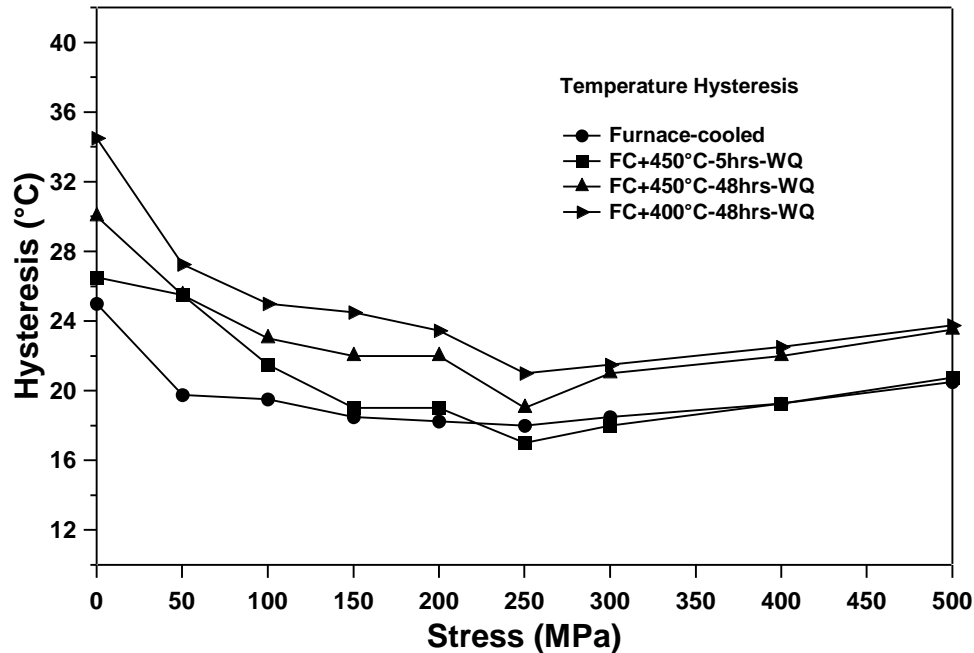


Figure 3.16 Temperature hysteresis responses of the furnace-cooled and aged $\text{Ni}_{52}\text{Ti}_{48}$ as a function of constant tensile stress levels.

The increase in transformation temperatures due to the formation of Ni-rich precipitates after long aging times was also observed in isobaric cooling-heating experiments. Overaging resulted in the loss of coherency of the precipitates negatively impacting the dimensional stability during thermal cycling. ϵ_{rec} decreased, ϵ_{irr} increased, temperature hysteresis increased, and they were less stable after long time aging compared to short time aging and non-aged materials.

Figure 3.17 demonstrates the critical stress values for the martensitic transformation as a function of temperature for all processing conditions investigated. Because the slopes of the curves for the points change below 150 MPa, the slopes are represented by dashed lines to better exhibit the two different behaviors. The slopes of the curves are almost the same for all materials with the highest for the material aged at 450°C for 5 hours, and the lowest for the material aged at 400°C for 48 hours. Aging at 450°C for 5 hours and 400°C for 48 hours result in two-stage martensitic transformation under 0 MPa stress and these two martensite start temperatures obtained from isobaric cooling-heating experiments (filled square and triangle) correlate with the temperatures obtained from DSC (unfilled symbols) results.

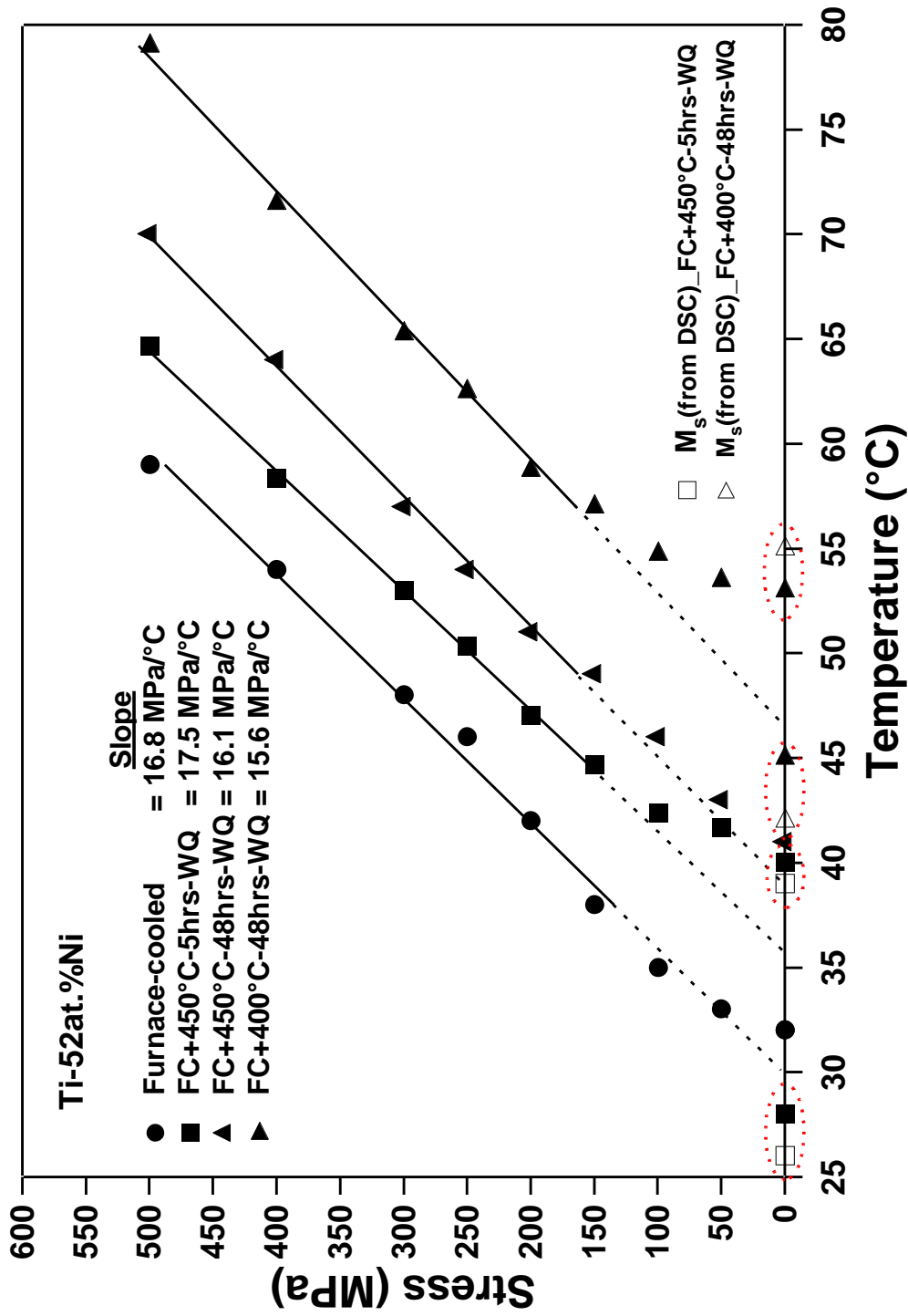


Figure 3.17 The effect of aging on the martensitic transformation start temperature, and stress induced martensitic transformation for the furnace-cooled and aged $Ni_{52}Ti_{48}$.

To better understand multi-stage martensitic transformation and the correlation between transformation temperatures determined from DSC and isobaric cooling-heating experiments, the results were plotted in the same graph in Figure 3.18. It was explained in the previous sections that multi-stage martensitic transformation was observed for some conditions of the furnace-cooled and aged materials. This kind of transformation was also observed during the isobaric cooling-heating experiments. It is clearly seen that martensitic transformation start temperatures correlates well with each other for the DSC and isobaric cooling heating experiments.

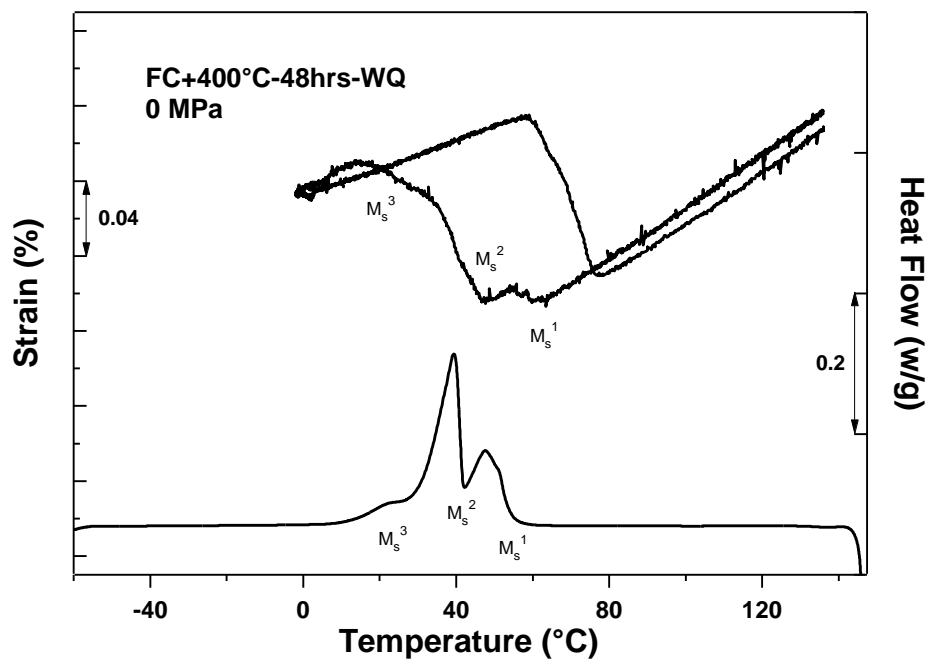


Figure 3.18 Martensitic transformation start temperatures of the furnace-cooled and aged at 400°C for 48 hrs sample from DSC and isobaric cooling-heating experiments under 0 MPa.

3.4 Summary

Microstructure, transformation temperatures and shape memory behaviors of furnace-cooled and aged $Ni_{52}Ti_{48}$ SMAs were investigated to characterize the shape memory properties.

Furnace-cooled results the transformation temperatures above ambient due to formation of Ni_4Ti_3 and Ni_3Ti precipitates. Multi-stage martensitic transformation occurs after aging the furnace-cooled $\text{Ni}_{52}\text{Ti}_{48}$ at 400°C and 450°C for different aging times because of chemical inhomogeneity in the microstructure and the stress distribution around precipitates. These transformation behaviors correlate with isobaric heating cooling experiments.

Aging at 400°C for 48 hrs results in the highest increase for the transformation temperatures of the furnace-cooled material due to the highest volume fraction of Ni_4Ti_3 precipitates since these precipitates decrease the Ni-content of the matrix. It was observed that existent precipitates coarsen and new, much small, ones form after aging.

Transformation temperatures increase with increasing aging time at a constant aging temperature due to coarsening of medium and large Ni_4Ti_3 precipitates and disappearing of small ones.

Since overaging results in a loss of coherency of the precipitates, dimensional stability during isobaric thermal cyclic is negatively impacted after long aging times.

CHAPTER IV

EFFECTS OF CONSTRAINED AND UNCONSTRAINED AGING ON THE SHAPE MEMORY CHARACTERISTICS OF Ni₅₂Ti₄₈ SMA

In this chapter, effects of aging heat treatment under stress free and constrained conditions on the shape memory characteristics of the as-received and solutionized materials were studied. As-received (hot-rolled) condition is the prior condition for all materials. The materials were held at 900°C for 1 hour in evacuated quartz tubes, and then quenched in ice water for solutionizing. Constrained aging heat treatments were performed in an MTS machine having heating chamber around the grip section to be able to heat the material to desirable temperature while the material is under stress. For stress free aging heat treatments, the materials were placed between four metal plates, each pin-hole section was placed between two metal plates to be able to create similar aging conditions with constrained aging like top and bottom grip holds the material from the pin-hole section. Since metal grips heat up during aging heat treatments, when the material was cooled under stress condition, it cools slower than normal air-cooling time. Therefore, the materials were replaced in furnace between four metal plates and held at desirable temperature and time, then taken out from the furnace with these plates and air-cooled in this condition. Aging temperatures and times were determined from the aging time, temperature versus Vicker microhardness and transformation temperatures experiments which were shown in the experimental procedure section.

4.1 Differential Scanning Calorimetry Experiments

Figure 4.1 shows the transformation temperatures under stress free conditions for the materials as-received and aged (at 450°C for 5 hours then air-cooled) conditions. The as-received material exhibits single-stage B2 ↔ B19' transformation during forward and reverse transformations. On the other hand, the aged material exhibits two-stage B2 → R → B19' transformations during forward transformation, and single-stage B19' → B2 transformation during reverse transformation. Aging at 450°C for 5 hours and air cooling

increases the transformation temperatures. Also, the transformation heat flow during transformation for the aged material is higher than that for the as-received material.

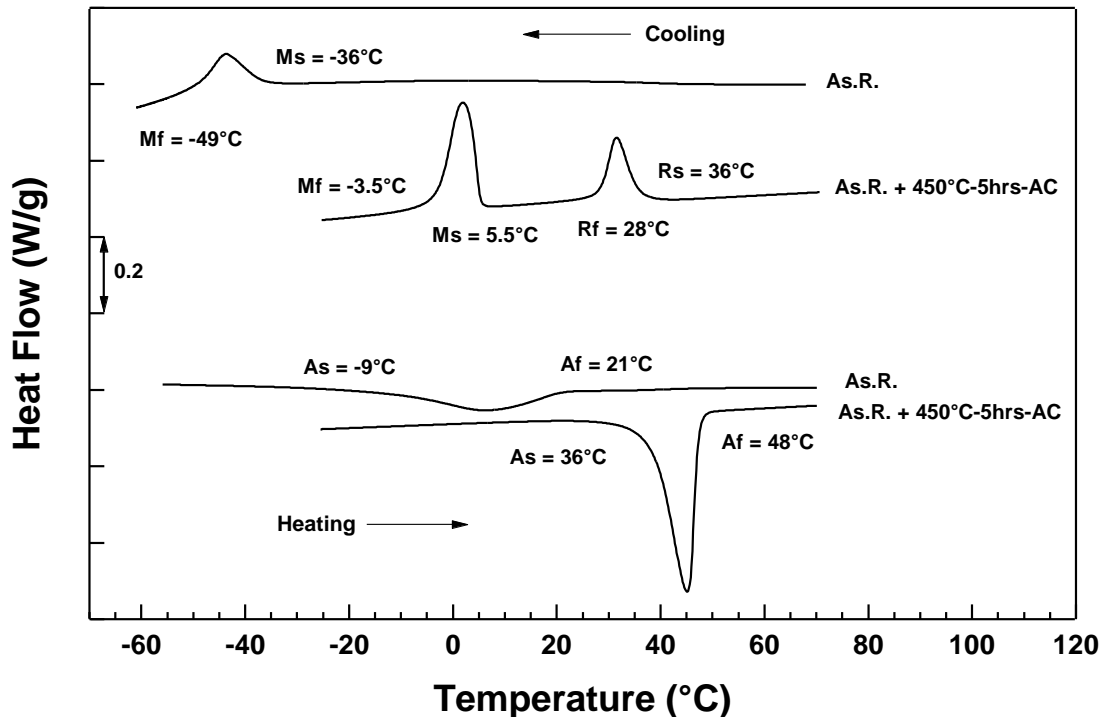


Figure 4.1 Transformation temperatures of the as-received and aged at 450°C for 5 hrs and air-cooled materials under stress free condition.

While martensite finish temperature is -49°C for the as-received material, it increases to -3.5°C after aging treatment. Austenite finish temperature also increases from 21°C to 48°C after aging heat treatment. Another important behavior is that the transformation peaks are more discernable after aging. Since all transformation temperatures increase in similar amounts, thermal hysteresis stays almost constant after aging.

As shown in Figure 1.4, transformation temperatures are strongly influenced by Ni concentration in Ni-rich compositions of NiTi [16]. 0.1 at.% decrease in Ni concentration causes almost 10°C increase in transformation temperatures. Basically, formation of Ni₄Ti₃ precipitates decreases the Ni-content of the NiTi matrix; as a

consequence martensitic transformation start temperature increases depending on aging time.

4.2 Microstructural Evolution

Since as-received (hot –rolled) condition is the prior condition for all materials, microstructure analysis was performed for this condition first. Optical microscopy (OM) and scanning electron microscopy (SEM) images were obtained from different parts of the sample surface to be able to determine the average grain size, interparticle distance, and precipitate volume fractions. WDS analysis was performed to determine chemical compositions of the precipitates which were seen throughout the microstructure.

Figure 4.2.a shows the optical micrograph of the as-received (hot-rolled) material demonstrating the average grain size of about $100\mu\text{m} \pm 5\mu\text{m}$. Precipitates were observed along the rolling direction. Figure 4.2.b shows the high density of Ni_4Ti_3 precipitates having lenticular shape. These coherent precipitates affect the martensitic transformation and shape memory behavior of the material by causing R-phase transformation and changing the Ni-content of the matrix [3, 16, 22-24]. Figure 4.2.c and d demonstrates white, gray and black precipitates for the as-received (hot-rolled) material. White Ni_3Ti precipitates are very rare in the microstructure for this material. Recent results have shown that Ni_3Ti precipitates decreases the fatigue life of the material [37]. Gray Ti_2Ni precipitates are also determined as $\text{Ti}_4\text{Ni}_2\text{O}$ phase in the literature [16]. Black regions in the middle of gray precipitates are TiO_2 and it is hard to eliminate these precipitates.

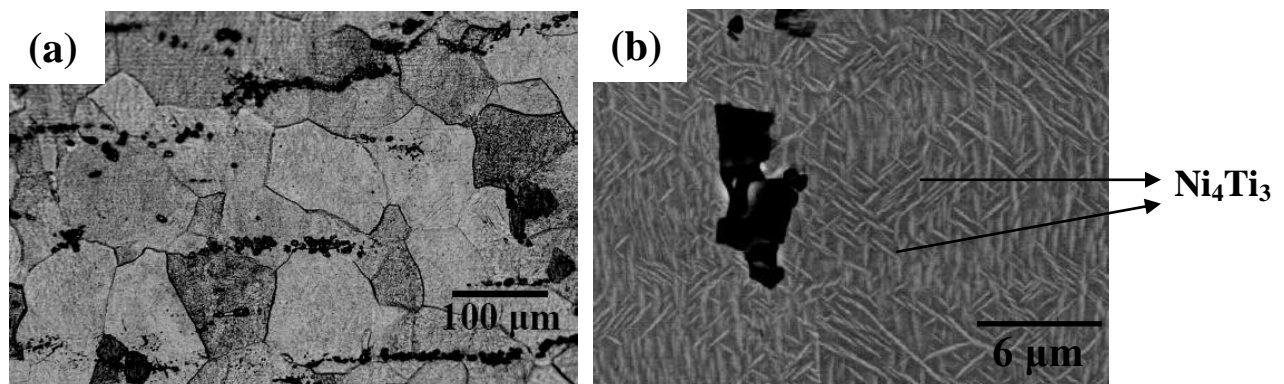


Figure 4.2 (a) Optical Microscopy, and SEM images of the as-received material showing; (b) lenticular, (c) matrix, gray and dark and (d) white precipitate compositions.

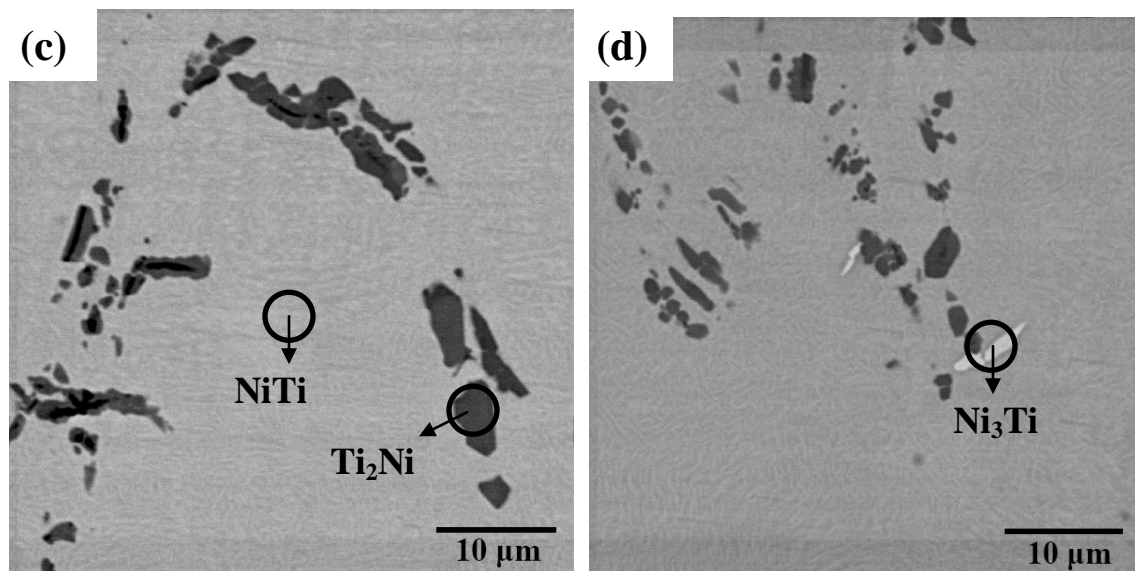


Figure 4.2 Continued.

Figures 4.3.a, b and c demonstrate SEM images of the material in as-received aged at 450°C for 5 hours and water-quenched condition. Average grain size is almost the same with the as-received condition. Clearly white, gray and black precipitates are kept in the microstructure and are aligned along the rolling direction. It was interestingly observed that the volume fraction of Ni₃Ti precipitates increases after aging. However, as seen in Figure 1.3 (TTT diagram of Ni₅₂Ti₄₈) of the introduction section, aging at 450°C for short aging time appears in the region of NiTi and Ni₄Ti₃ phases. Therefore, it was not clearly understood the effect of aging on the formation of Ni₃Ti. Meanwhile, it is hard to determine the exact volume fraction of Ni₄Ti₃ precipitates from (c) because of the low quality of the image. The volume fraction of Ni₄Ti₃ precipitates increases after aging as compared to the as-received material. Such increase can also be correlated with increasing transformation temperatures and R-phase transformation.

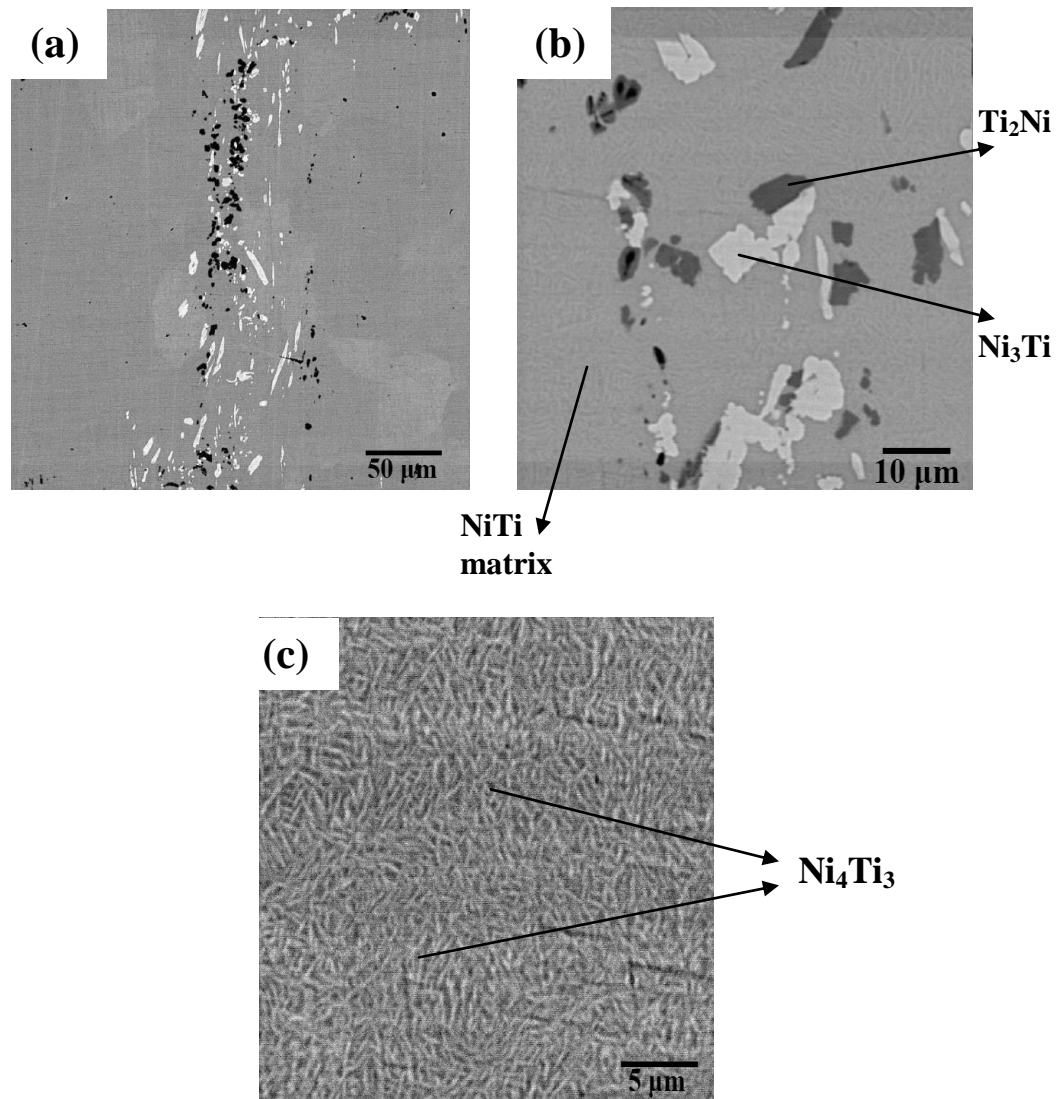


Figure 4.3 SEM images of the matrix and different precipitates including their types obtained by WDS analysis for the material in as-received, aged at 450°C for 5 hours, and then air-cooled condition.

4.3 Isobaric Cooling-Heating Experiments

Isobaric cooling-heating experiments were performed after different aging heat treatments to be able to characterize the transformation temperatures and shape memory behavior of the materials with increasing stress levels. In addition to the as-received and aged (at 450°C for 5 hours) samples, the samples solutionized (at 900°C for 1 hour then water-quenched) and aged at 450°C for 5 hours, and the sample as-received and aged at 450°C for 5 hours under 200 MPa tensile stress were also investigated to determine the effect of solutionizing and constrained aging on shape memory properties. Since the transformation temperatures are very low, isobaric heating-cooling experiments could not be performed on the solutionized material.

Figure 4.4 shows strain vs. temperature response of the as-received (hot-rolled) material under several constant stress levels. M_s temperature of the sample increase with increasing stress levels as expected. There is no R – phase transformation for this condition. The sample exhibits almost zero transformation strain under 0 MPa that means no two-way shape memory effect. Irrecoverable strain first appears at 400 MPa.

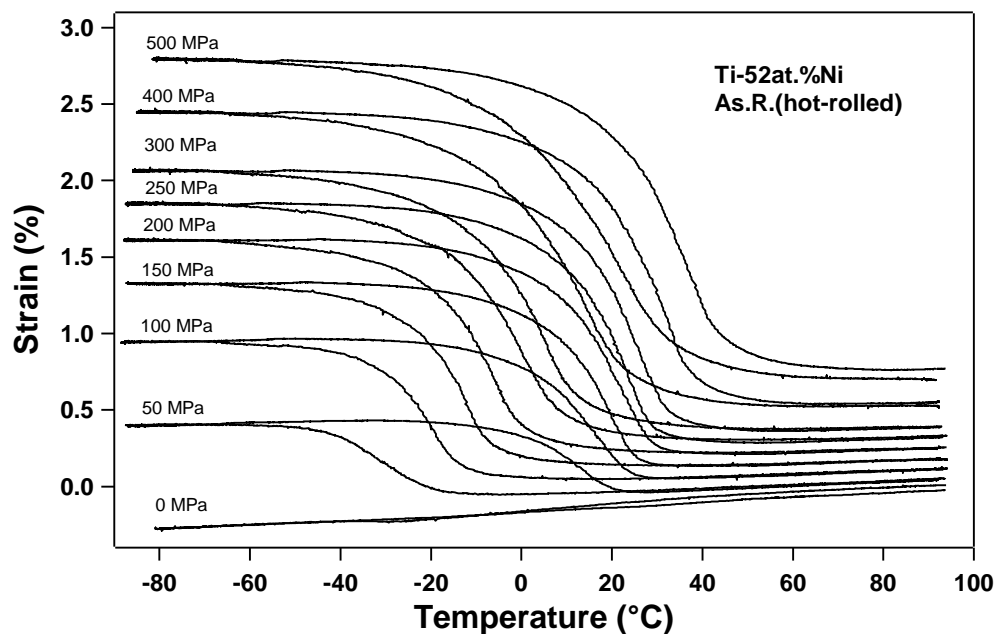


Figure 4.4 Strain vs. temperature response of the as-received (hot-rolled) $Ni_{52}Ti_{48}$ under various constant stress levels during isobaric heating-cooling experiments.

Figure 4.5 shows strain vs. temperature response of the as-received material in aged at 450°C for 5 hours and air-cooled condition under several constant stress levels. There is an R-phase transformation up to 250 MPa prior to B19' transformation. R-phase transformation temperatures also increase with increasing stress levels but they are more stable than the martensitic transformation ones. Since high density Ni_4Ti_3 precipitates cause internal stress in the microstructure, small negative recovered transformation strain was observed under 0 MPa. It is clearly seen that irrecoverable strain increases for aged sample compared to the as-received one.

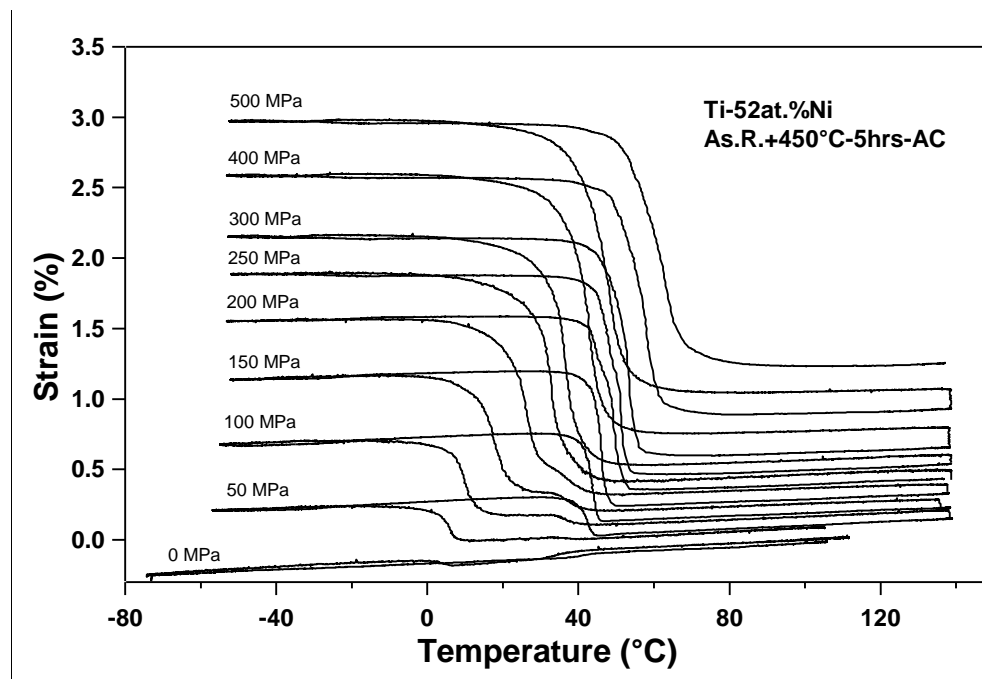


Figure 4.5 Strain vs. temperature response of the as-received, aged at 450°C for 5 hours, and air-cooled $\text{Ni}_{52}\text{Ti}_{48}$ under various constant stress levels during isobaric heating-cooling experiments.

Figure 4.6 shows strain vs. temperature curves of the material in solutionized (900°C for 1 hour then water-quenched), aged at 450°C for 5 hours, and air-cooled condition under several constant stress levels. The sample failed at 400 MPa during cooling. The transformation strain was seen in the negative direction under 0 MPa that indicates two-way shape memory effect due to R-phase transformation. Since the solutionized and aged material failed at 400 MPa, the data could be analyzed until 300

MPa. Isobaric heating-cooling tests are repeated several times for this material but the samples generally failed above 300 MPa. Wide temperature hysteresis was observed for this material compared to the other conditions.

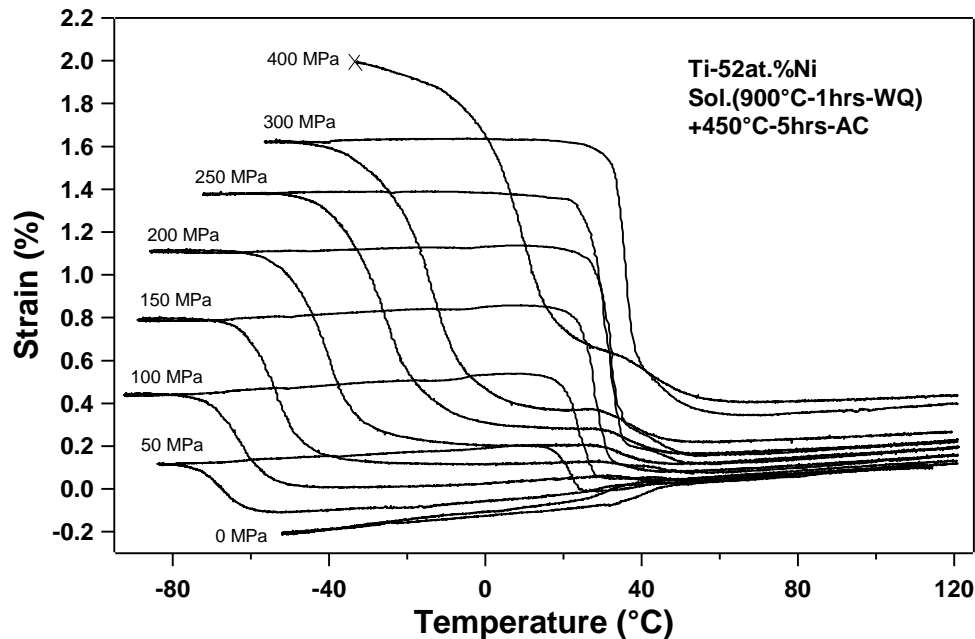


Figure 4.6 Strain vs. temperature response of the solutionized at 900°C for 1 hour, aged at 450°C for 5 hours, and air-cooled $\text{Ni}_{52}\text{Ti}_{48}$ under various constant stress levels during isobaric heating-cooling experiments.

It was found from previous studies that constrained aging of Ni-rich NiTi alloys at around 500°C results two-way shape memory effect (TWSME) [15, 50-51]. Figure 4.7 shows strain vs. temperature response under various constant stress levels of the sample aged at 450°C for 5 hours under 200 MPa. TWSME can be seen clearly from the curves under 0 MPa. Negative recovered transformation strain is associated with the $\text{B2} \rightarrow \text{R}$ -phase transformation. On the other hand, positive recovered transformation strain obtained by further cooling is associated with $\text{R} \rightarrow \text{B19}'$ transformation. When the specimen is aged under tensile stress, Ni_4Ti_3 precipitates are expected to aligned parallel to the applied stress direction and create directional internal stress in the microstructure [16, 38, 52]. Internal stress controls the R-phase transformation and creates compressive strain. When the applied stress exceeds the internal stress level which is created aligned

Ni_4Ti_3 precipitates, R-phase transformation creates positive recovered transformation strain.

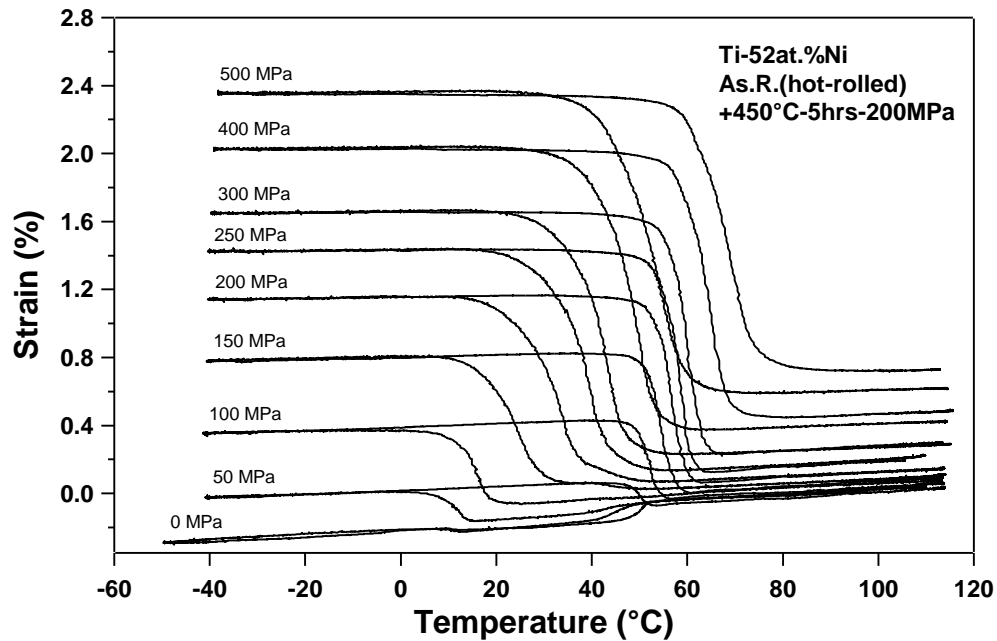
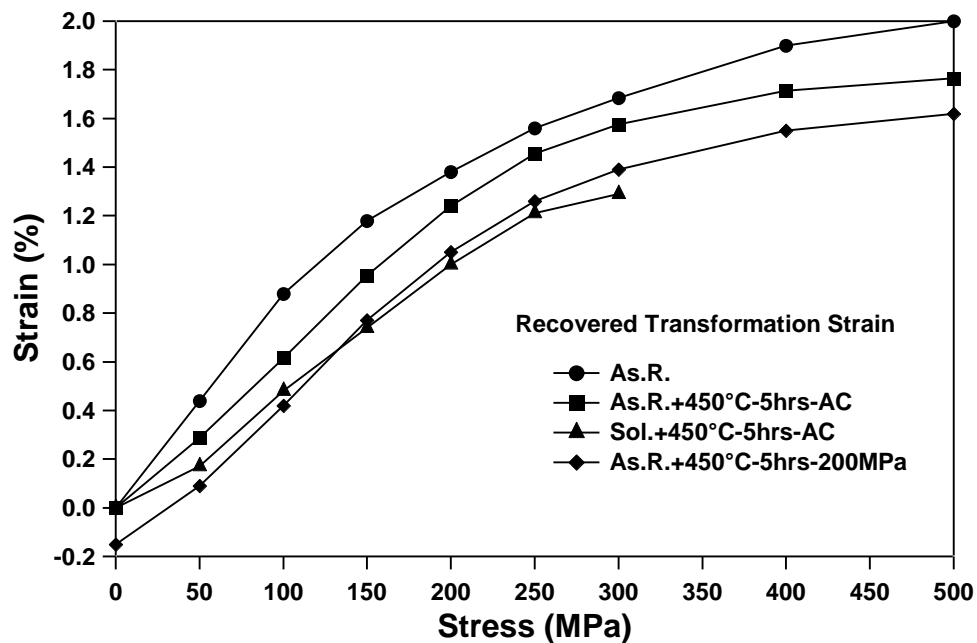
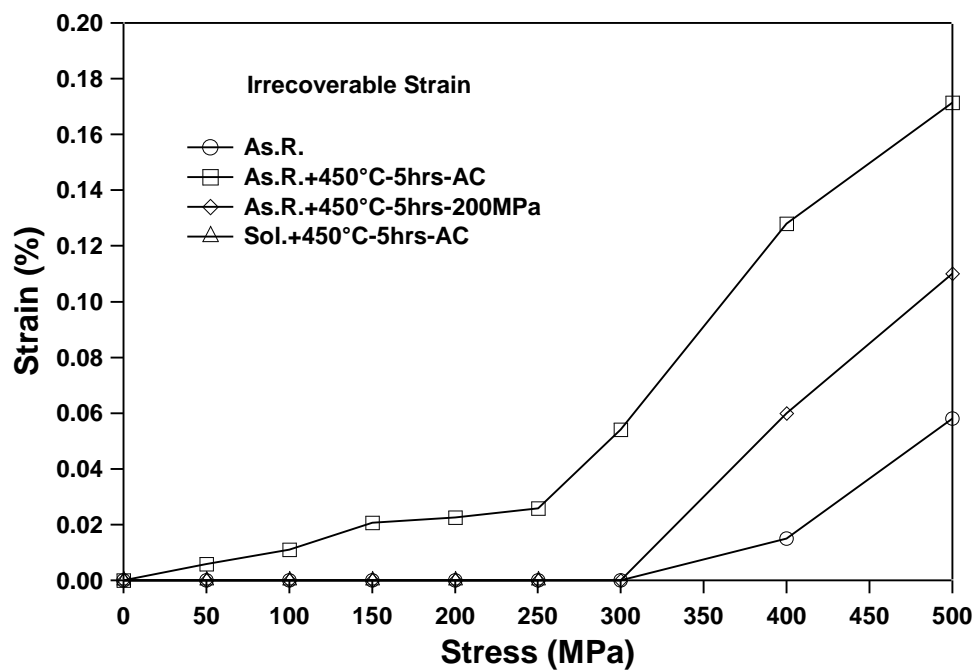


Figure 4.7 Strain vs. temperature response of the as-received and aged at 450°C for 5 hours under 200 MPa $\text{Ni}_{52}\text{Ti}_{48}$ under various constant stress levels during isobaric heating-cooling experiments.

Figure 4.8.a and b shows the recoverable transformation (ϵ_{rec}) and irrecoverable (ϵ_{irr}) strain levels, respectively, for as-received (hot-rolled), as-received and aged at 450°C for 5 hours then air-cooled, solutionized (at 900°C for 1 hour then water-quenched) and aged at 450°C for 5 hours then air-cooled, and as-received and aged at 450°C for 5 hours under 200 MPa samples as a function of constant tensile stress levels. It was clearly observed that as-received material demonstrates the highest recovered transformation and lowest irrecoverable strain as compared to the other conditions. The material in as-received and aged without stress condition displays recovered transformation strain levels close to the as-received material but it in results the highest irrecoverable strains.



(a)



(b)

Figure 4.8 (a) Recovered transformation and (b) irrecoverable strain responses of as-received, aged at 450°C for 5 hours, solutionized (at 900°C for 1 hour) and aged at 450°C for 5 hours, and as-received and aged at 450°C for 5 hours under 200 MPa $\text{Ni}_{52}\text{Ti}_{48}$ samples as a function of constant tensile stress levels.

Figure 4.9 shows temperature hysteresis of the as-received (hot-rolled), as-received and aged at 450°C for 5 hours then air-cooled, solutionized (at 900°C for 1 hour then water-quenched) and aged at 450°C for 5 hours then air-cooled, and as-received and aged at 450°C for 5 hours under 200 MPa samples as a function of applied stress. Compared to the other conditions investigated, wide temperature hysteresis was observed for the solutionized and aged sample. According to Hamilton et al. [47], since coherent precipitates lose coherency upon further heat treatment and thus, growth frictional resistance to interfacial motion and stored elastic strain energy dissipation increase. As a consequence, wide temperature hysteresis occurs.

For all conditions, temperature hysteresis decreases with increasing stress and almost stabilizes above 250 MPa except solutionized and aged sample that the data above 250 MPa could not be obtained because of the sample failure. Since the reasons for decreasing hysteresis with increasing stress levels was explained in the previous section, it was not repeated in this section.

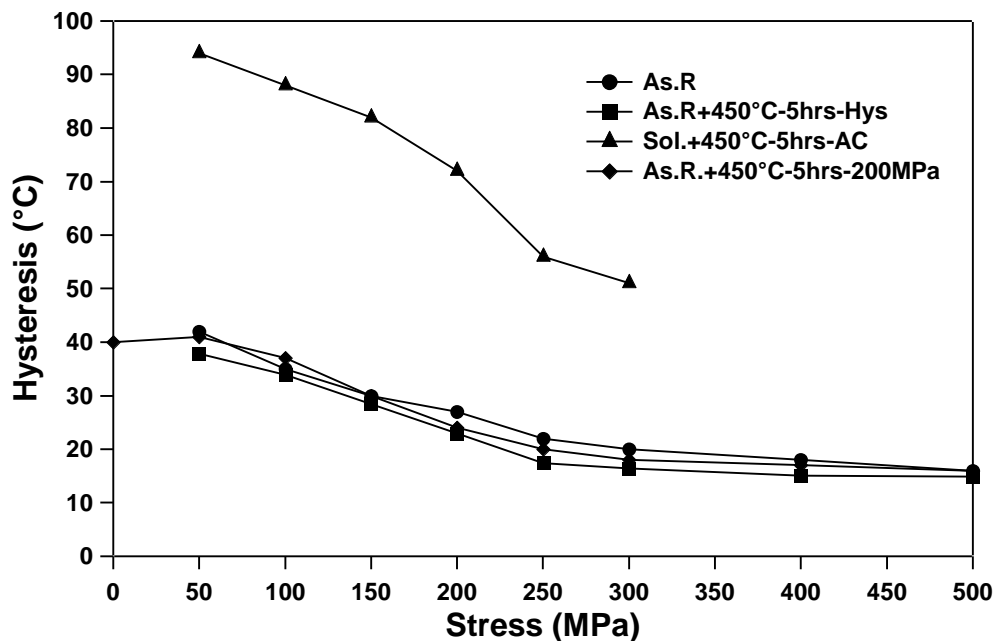


Figure 4.9 Thermal hysteresis responses of the as-received, aged at 450°C for 5 hours, solutionized (at 900°C for 1 hour) and aged at 450°C for 5 hours, and as-received and aged at 450°C for 5 hours under 200 MPa $\text{Ni}_{52}\text{Ti}_{48}$ samples as a function of constant tensile stress levels.

Figure 4.10 shows the effect of aging with or without stress on the martensitic transformation start temperature for as-received and solutionized material. It is well known that critical stress for martensitic transformation increases with increasing temperature because of Clausius – Clapeyron relation. The slope of solutionized and aged material is lower than those for the other conditions which means that martensitic transformation start temperature increases more with increasing stress levels as compared to the other conditions. It is clear that as-received and aged under stress sample results in the highest martensite start temperature for all stress levels. Aging of as-received material under stress or without stress results the similar martensite start temperature behavior with increasing stress levels.

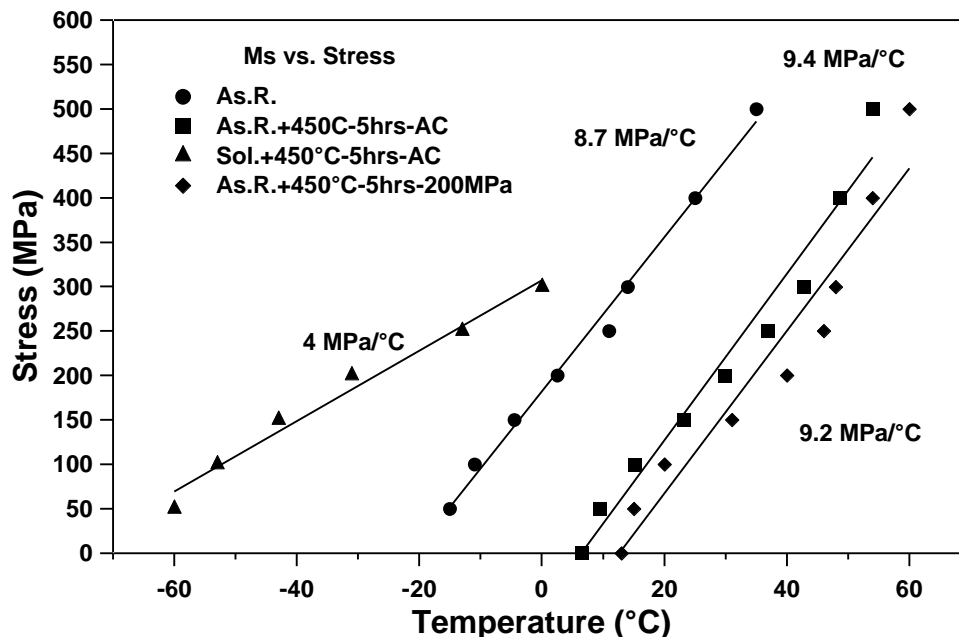


Figure 4.10 The effect of aging with or without stress on the martensitic transformation start temperatures for the as-received and solutionized material.

4.4 Isothermal Loading-Unloading Experiments

To obtain critical stresses for martensitic transformation and finally complete the phase diagram of as-received material, isothermal loading-unloading experiments were performed in austenite at different temperatures. Figure 4.11 shows the isothermal loading-unloading experiments of the as-received material at different temperatures. The

critical stress for stress induced martensitic transformation was measured at 0.2% offset strain from the apparent elastic modulus of austenite on the stress vs. strain curves. The sample was first heated to about 50°C, which is above A_f temperature, then cooled to room temperature for the first cycle. Since the room temperature is above M_s temperature, the microstructure was fully austenite. The sample was loaded until 1% strain and unloaded, then again loaded until 2% strain to obtain critical stress for stress induced martensite and irrecoverable strain levels at different temperatures. Irrecoverable strain was first observed when the material was loaded-unloaded until 1% strain at 75°C which was 0.04%. The sample failed at 126°C while it was loaded to 2% strain.

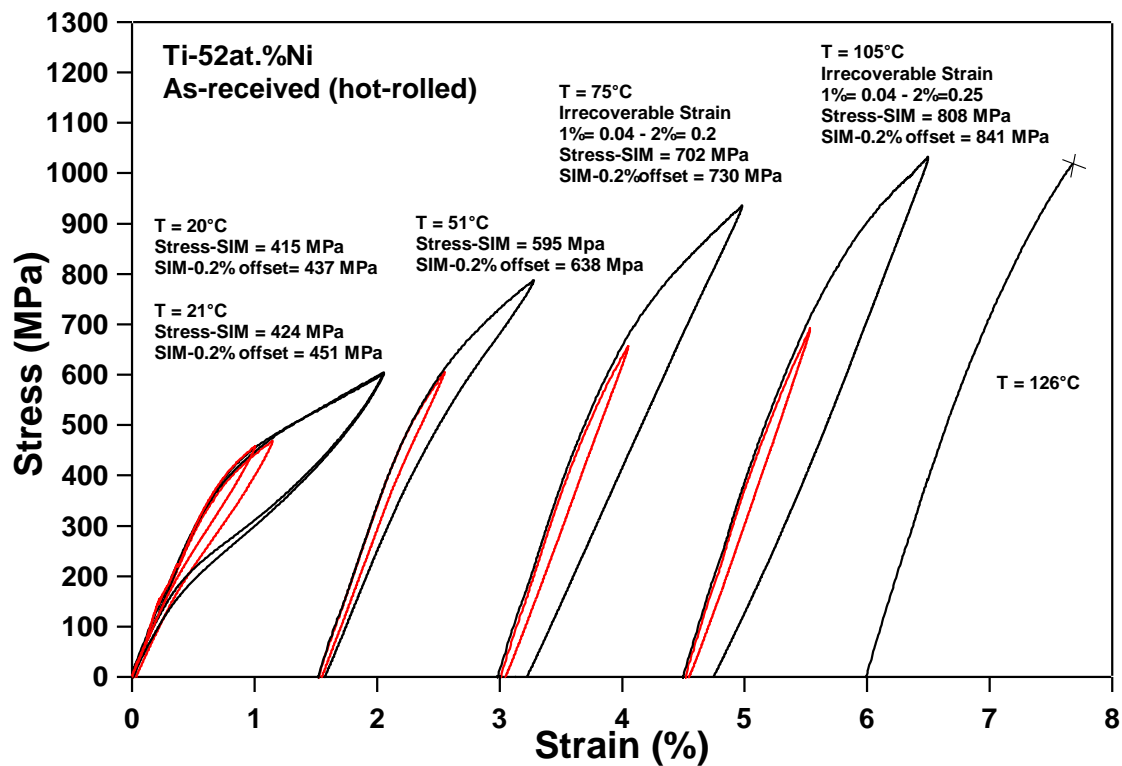


Figure 4.11 Isothermal loading-unloading experiments of the as-received $Ni_{52}Ti_{48}$ at different temperatures.

The linear relationship between stress and temperature to induce martensitic transformation can be represented using Clausius-Clapeyron equation [3, 49];

$$\frac{d\sigma}{dT} = -\frac{\Delta H}{T_0 \varepsilon_{tr}}$$

where ε_{tr} is transformation strain, ΔH is enthalpy change of the transforming body and T_0 is the chemical equilibrium temperature of the transformation. Figure 4.12 shows the stress vs. temperature relationship for stress-induced martensitic transformation of as-received (hot-rolled) sample and the slopes of $M_{s,f}$ and $A_{s,f}$ curves. That the critical stress curve for stress induced martensitic transformation obtained from the isothermal loading-unloading experiments correlates well with the M_s curve obtained from the isobaric heating-cooling experiments. The transformation temperatures at 0 MPa was obtained from DSC.

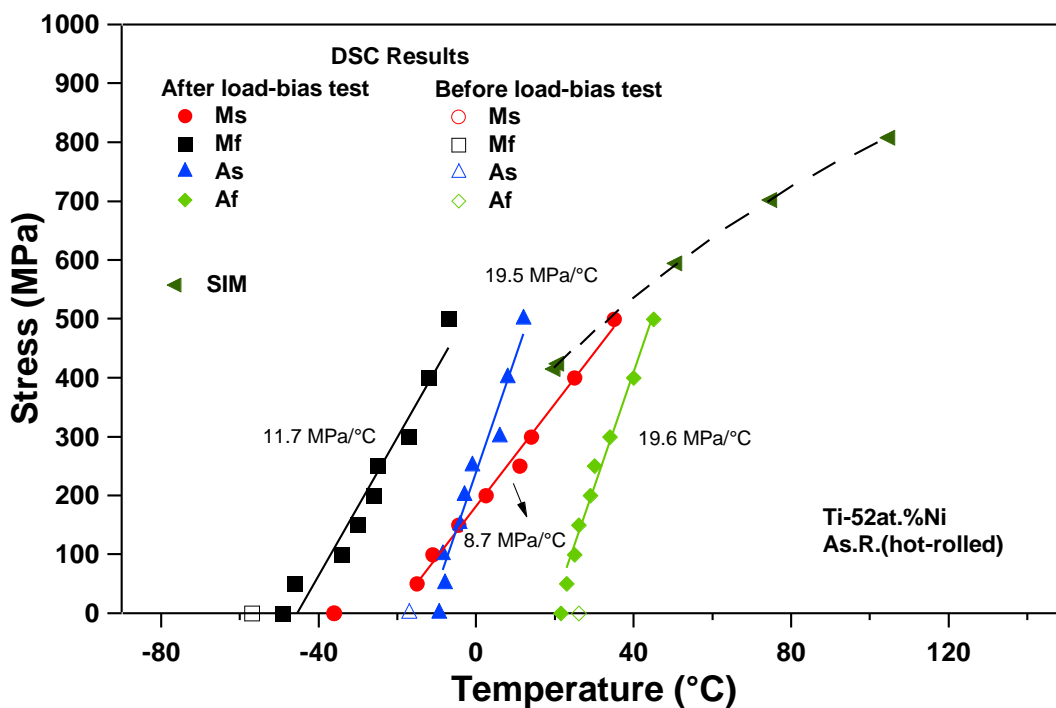


Figure 4.12 Effect of temperature on the critical stress for stress-induced martensitic transformation of as-received $Ni_{52}Ti_{48}$.

4.5 Texture Analysis

In polycrystalline materials, when the orientations of the crystal axes are distributed randomly for different grains, the material behaves in an isotropic manner. On the other hand, most of the physical and mechanical properties depend on the crystallographic orientations as shown in several single crystalline studies [11, 47-48,

53]. Polycrystalline NiTi demonstrates preferred orientation of grains when thermomechanically processed. Preferred orientation of grains or texture dictates transformation strain levels in SMA [11, 13, 47, 53].

To better understand the reasons for low transformation strains in the present alloys and to reveal whether there might be other reasons in addition to high volume of non-transforming precipitates, texture effect was also studied. Figure 4.13 shows the pole figures for the as-received material in the austenite state at room temperature for 3 different crystallographic poles. Directions 1 and 2 represent rolling direction and transverse direction, respectively. (110), (200) and (211) poles were determined by XRD analysis of the material. The poles exhibit very weak intensity in both directions, therefore, texture should not be one of the main factors responsible for low transformation strains in the present study.

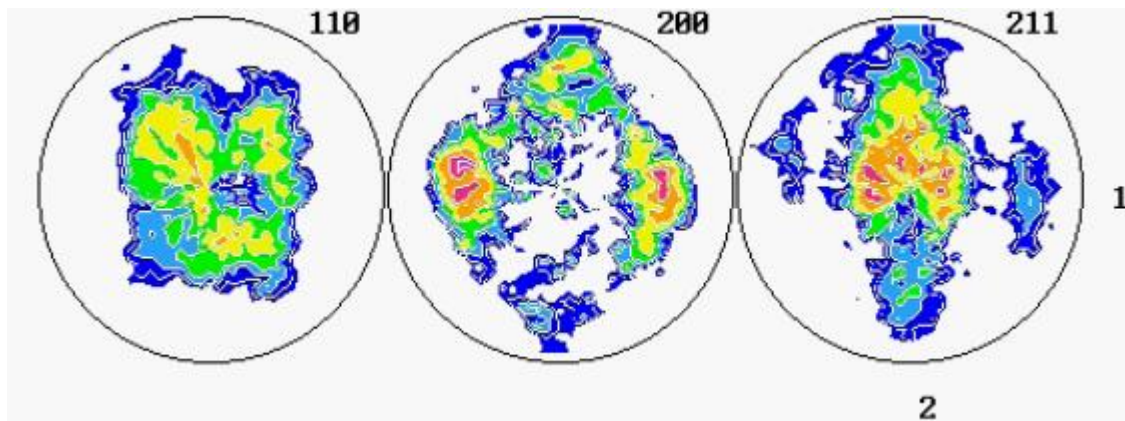


Figure 4.13 Pole figures for the as-received material in the austenite state at room temperature.

Tension direction in the samples tested so far was parallel to the transverse direction for the as-received sample, results of which are shown in Section 4.3. Therefore, a new as-received tension sample that rolling direction is parallel to tension direction was tested to compare the transformation strains with the other samples. Figure 4.14 shows the isobaric heating-cooling curves for this new sample. It was observed that

both samples exhibit almost the same shape memory behavior, supporting the previous conclusion that the texture is not a critical factor here.

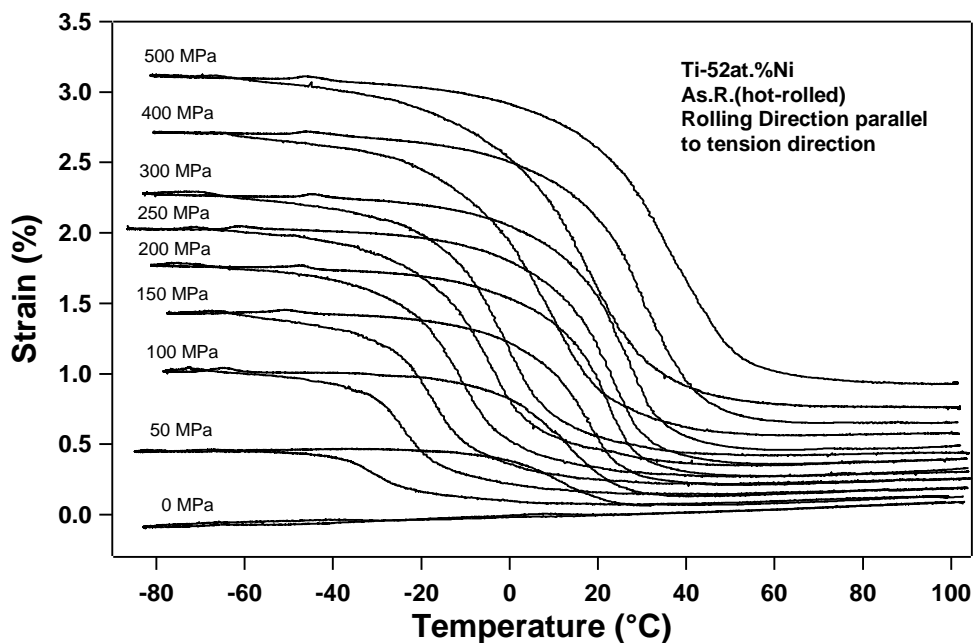


Figure 4.14 Strain vs. temperature response of the as-received $\text{Ni}_{52}\text{Ti}_{48}$ under various constant stress levels during isobaric heating-cooling experiments. The rolling direction is parallel to the tension direction.

Figure 4.15 shows the recovered transformation and irrecoverable strain comparison of the as-received materials cut along two different directions from the hot-rolled plate. Sample 2 exhibited higher ϵ_{rec} and ϵ_{irr} than sample 1 but the difference is small. Therefore, it can be concluded that transformation strain does not depend on the direction. In other words, the material does not have a strong texture.

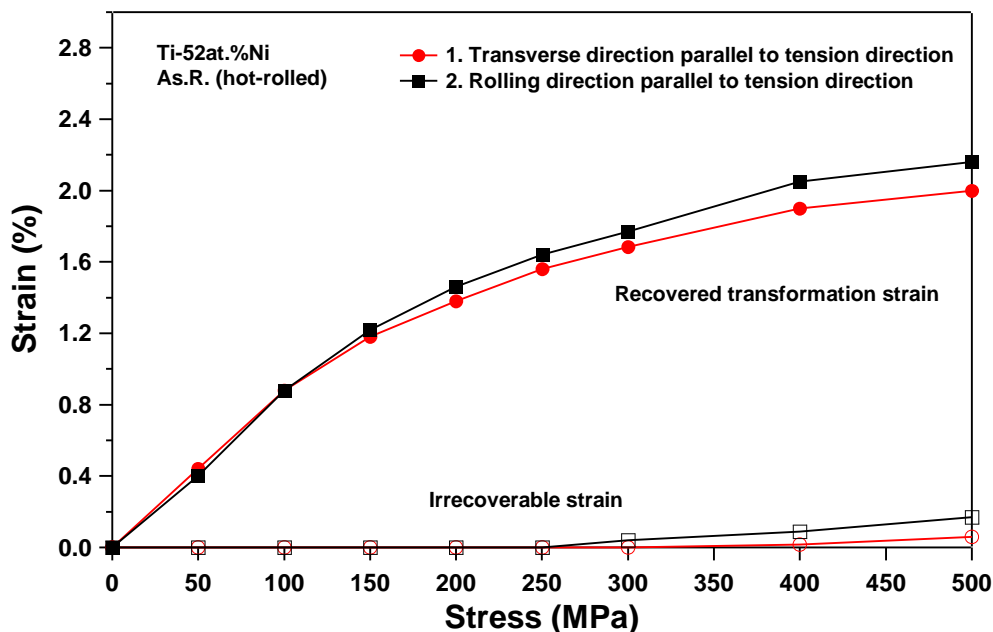


Figure 4.15 Recovered transformation and irrecoverable strain responses of the as-received $\text{Ni}_{52}\text{Ti}_{48}$ samples, cut along different directions, as a function of constant tensile stress levels.

4.6 Summary

As-received (hot-rolled), aged at 450° for 5 hours and air-cooled, solutionized (at 900°C for 1 hr and water-quenched), aged at 450°C for 5 hrs under 200 MPa materials were investigated to characterize the shape memory properties. The as-received material results the highest ϵ_{rec} and lowest ϵ_{irr} for different stress levels but transformation temperatures are lower than as-received and aged materials. Aging of the as-received material results R-phase transformation prior to B19'. Constrained aging of the as-received material results TWSME with R-phase transformation due to oriented internal stress created by oriented Ni_4Ti_3 precipitates. Solutionized and aged material results wide hysteresis due to losing coherency of coherent precipitates, frictional resistance to internal motion and increasing stored elastic strain energy dissipation.

Also, isothermal loading-unloading experiments were performed for the as-received material to complete phase diagram. Critical stress curve for the stress induced martensitic transformation correlates well with M_s curve.

Texture should not be one of the main factors responsible for low ϵ_{rec} .

CHAPTER V

ELIMINATION OF Ni₃Ti PRECIPITATES

5.1 Influence of Ni₃Ti Precipitates

Recently, Bertacchini et al. [37] found that the crack nucleation and crack growth through the thickness were observed in and around Ni₃Ti precipitates in Ni-rich NiTi SMA actuators upon cyclic loading. Since Ni₃Ti precipitates do not transform, large strain incompatibilities are created between transforming matrix and these precipitates during repeated phase transformation. Also, it was found that Ni₃Ti precipitates are harder and more brittle than NiTi matrix. As a consequence, Ni₃Ti precipitates dominate the fatigue failure of these alloys.

It was shown in the previous chapter that the as-received (hot-rolled) material has Ni₃Ti precipitates in the microstructure. Figure 5.1 shows the room temperature XRD results of the as-received sample. As expected from the optical microscopy and SEM images, XRD measurement presents B2 matrix with Ni₄Ti₃ and Ni₃Ti precipitates.

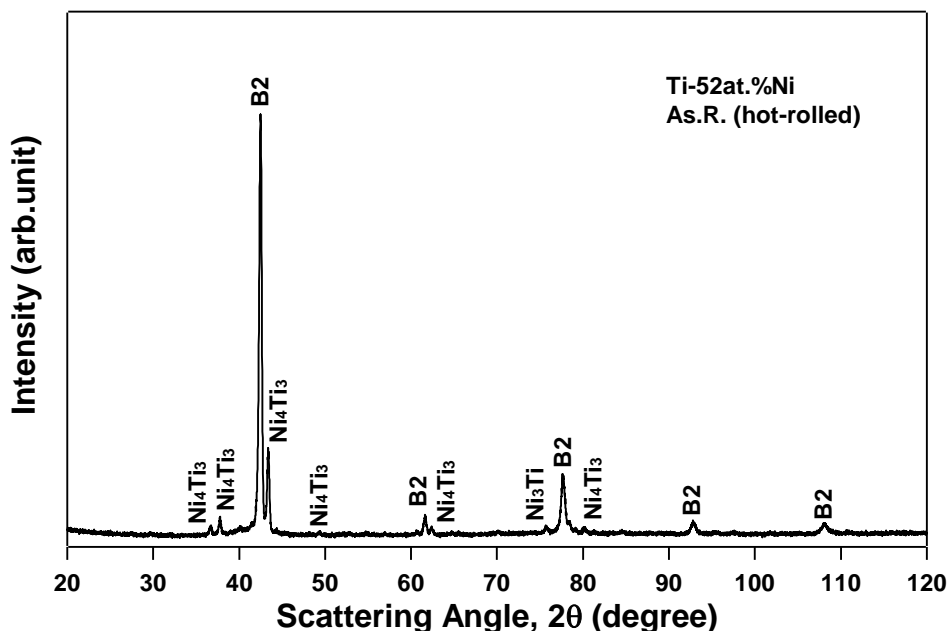


Figure 5.1 Room temperature XRD result of the as-received sample; identification of B2 matrix, Ni₄Ti₃ and Ni₃Ti precipitates.

5.2 Solutionizing (at 900°C for 1 hr)

To be able to eliminate these precipitates, the material was solutionized at 900°C for 1 hour in an evacuated quartz-tube, and water-quenched. Figure 5.2 shows the optical microscopy and SEM images of the solutionized sample. The average grain size is about $110 \pm 5 \mu\text{m}$ and precipitates are along the rolling direction. WDS analysis showed that white precipitates are Ni_3Ti and still existing in the microstructure in small amounts. Ni_4Ti_3 precipitates are mostly dissolved. Ti_2Ni precipitates could not be eliminated because of oxygen stabilization.

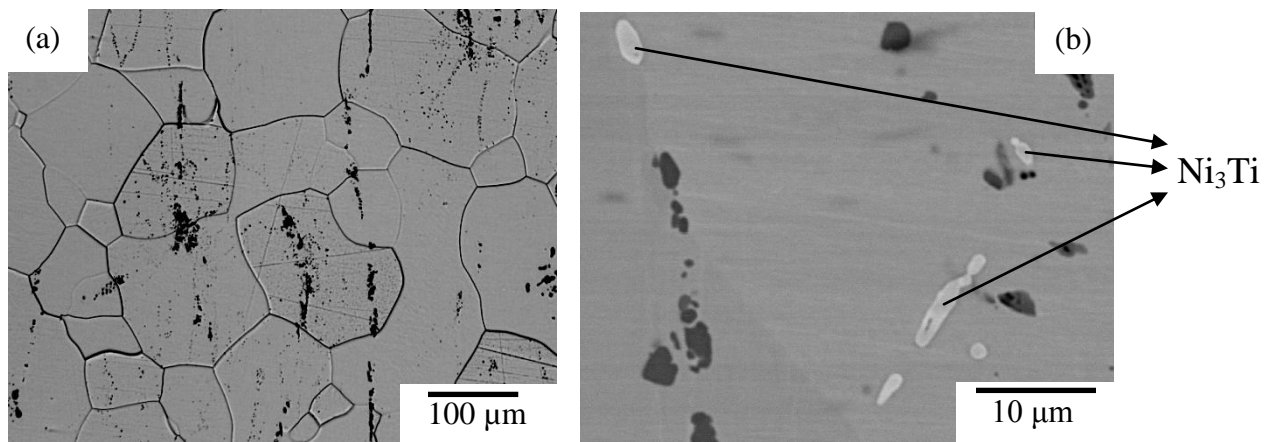


Figure 5.2 (a) Optical microscopy and (b) SEM images of the $\text{Ni}_{52}\text{Ti}_{48}$ sample solutionized at 900°C for 1 hr.

Figure 5.3 shows the room temperature the XRD result of the sample solutionized at 900°C for 1 hr, and water-quenched. As expected from the microstructural analysis, Ni_3Ti precipitates still exist in the microstructure. Therefore, it was decided that solutionizing temperature be increased to 24 hrs to be able to eliminate Ni_3Ti precipitates completely.

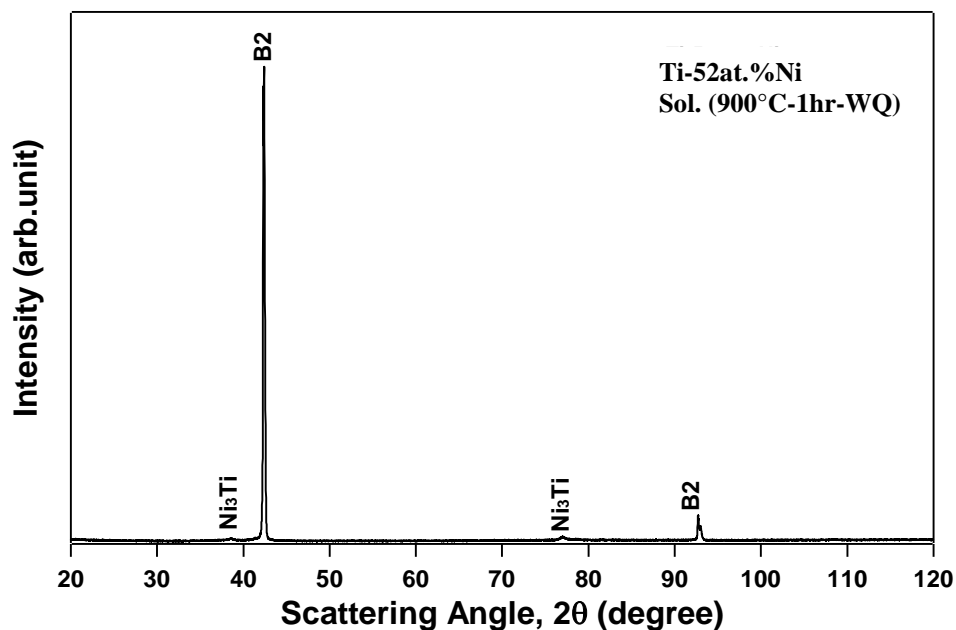


Figure 5.3 Room temperature XRD result of the $\text{Ni}_{52}\text{Ti}_{48}$ sample solutionized at 900°C for 1 hr.

5.3 Solutionizing (at 900°C for 24 hrs)

Figure 5.4 shows the SEM images of solutionized at 900°C for 24 hrs then water-quenched sample. The average grain size is about $110 \pm 5 \mu\text{m}$. Ni_3Ti precipitates were completely eliminated after 24 hours solutionizing. Ti_2Ni precipitates still exist in the microstructure. Since these precipitates include oxygen, it is hard to eliminate these precipitates. As shown in Figure 5.4.c, strange surface relief was observed, the reason of which is not clear at this point.

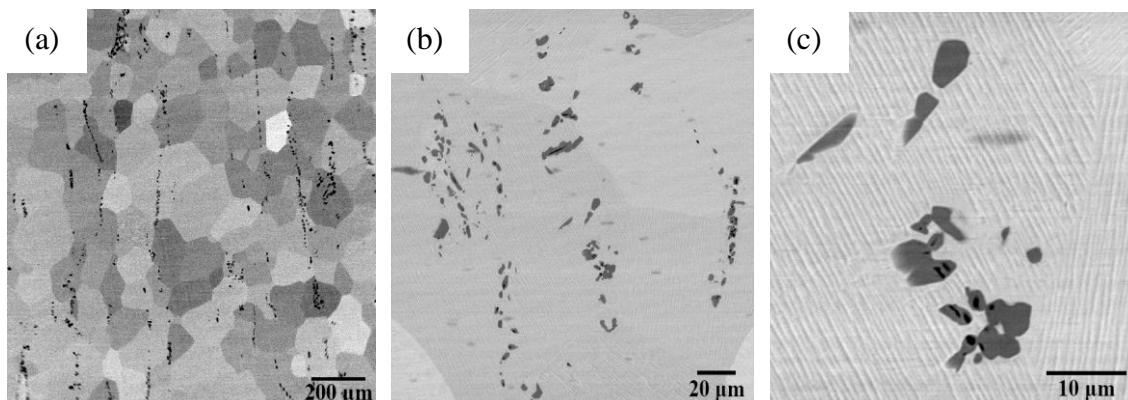


Figure 5.4 SEM images of the sample solutionized at 900° C for 24 hrs at different magnifications.

Figure 5.5 shows the room temperature XRD result of the sample solutionized at 900° C for 24 hours and water-quenched. It was confirmed by XRD measurement that Ni_3Ti precipitate were completely eliminated after 24 hours solutionizing.

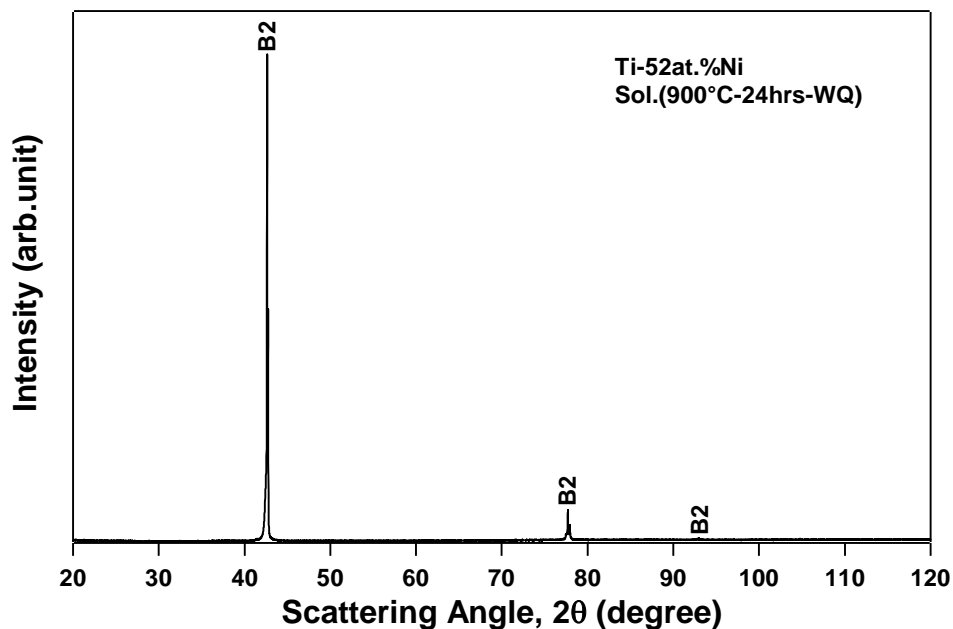


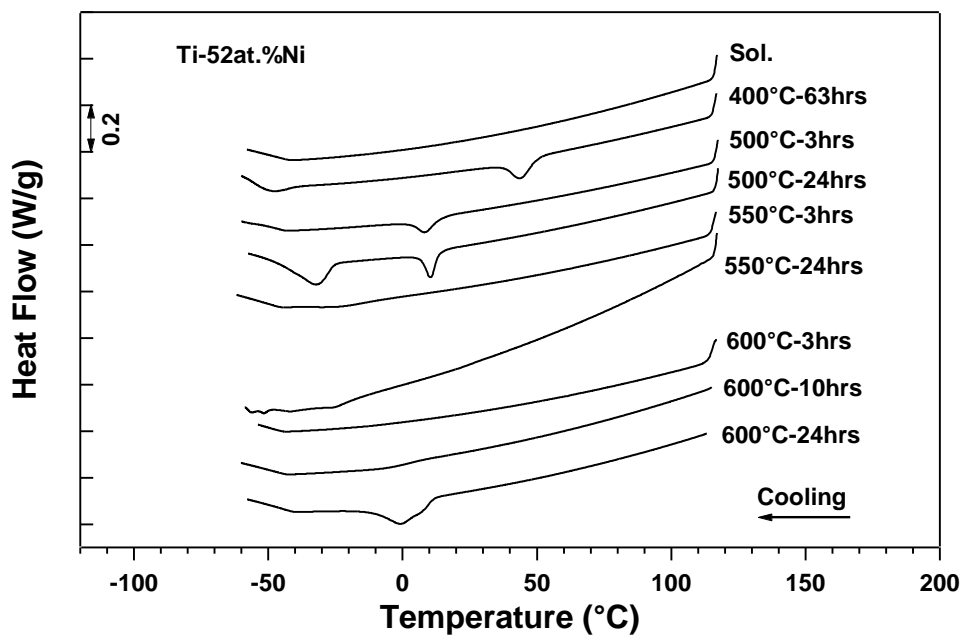
Figure 5.5 Room temperature XRD result of the sample solutionized at 900° C for 24 hrs.

5.4 The Effects of Aging Heat Treatments to Solutionized Materials

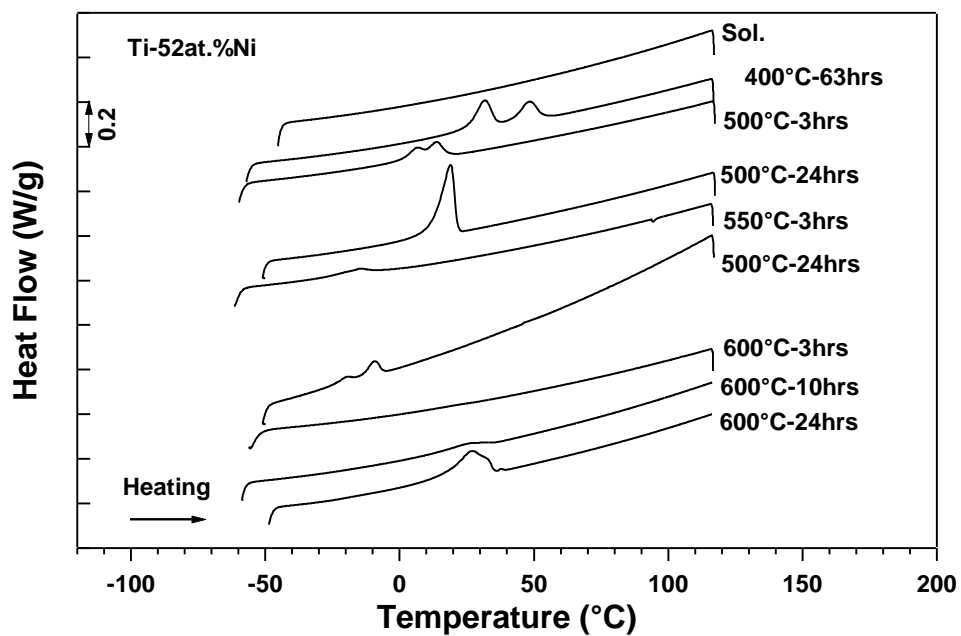
Since Ni_3Ti and Ni_4Ti_3 precipitates were dissolved in solution after the solutionizing heat treatment, Ni-content of the matrix is very high and so the transformation temperatures are very low after 24 hours solutionizing treatment. Therefore, additional aging heat treatments were applied at intermediate aging temperatures to form Ni_4Ti_3 precipitates and deplete the Ni-content of the matrix. 400, 500, 550 and 600°C as aging temperatures and 3, 10 and 24 hours as aging times were selected utilizing the time-temperature-transformation diagram of $\text{Ni}_{52}\text{Ti}_{48}$ material [21].

Figure 5.6 shows the DSC responses of the samples solutionized for 24 hours and aged at different temperatures. Since the transformation temperatures of solutionized sample are very low, it could not be determined from the DSC experiments. The transformation temperatures can be increased by changing the composition or forming coherent precipitates through aging heat treatments. With long aging times, incoherent Ni-rich precipitates form and deplete the Ni-content of the matrix, and as a result, increase transformation temperatures. With short aging times, coherent precipitates form and transformation temperatures increase.

Longer aging times increased the transformation temperatures more than short aging times. Aging at 400°C for 63 hours results in the highest increase. Aging at 600°C for 24 hours also increases the transformation temperatures around ambient but not as high as 400°C for 63 hours aging.



(a)



(b)

Figure 5.6 DSC responses showing the effect of aging heat treatment at 400, 500, 550 and 600°C for 3, 10 and 24 hrs on the transformation temperatures of the $\text{Ni}_{52}\text{Ti}_{48}$ samples solutionized at 900°C for 24 hrs.

CHAPTER VI

CONCLUSION AND FUTURE RECOMMENDATION

6.1 Conclusion

Microstructures, transformation temperatures and shape memory properties of the as-received (hot-rolled) and aged, furnace-cooled and aged, and solutionized and aged $\text{Ni}_{52}\text{Ti}_{48}$ samples were investigated to increase transformation temperature and improve shape memory behaviors. The materials were solutionized for different times to eliminate Ni_3Ti precipitates, which are responsible for the fatigue failure, and aged to form Ni_4Ti_3 precipitates to increase transformation temperatures above ambient.

Among all aging conditions investigated, aging at 400°C for 48 hours resulted in the highest transformation temperatures due to the combination of Ni_3Ti and high density of Ni_4Ti_3 precipitates. This behavior correlates with their high volume fraction of Ni-rich precipitates which is about 27%.

Multi-stage martensitic transformation occurs after aging the furnace-cooled $\text{Ni}_{52}\text{Ti}_{48}$ at 400°C and 450°C for different aging times because of chemical inhomogeneity in the microstructure and the stress distribution around the precipitates. The multi-stage transformation temperatures correlate well with the results from the isobaric heating cooling experiments.

Transformation temperatures increase with increasing aging time at a constant aging temperature because Ni_4Ti_3 precipitates coarsen according to the Ostwald ripening mechanism. Since overaging results in a loss of coherency of the precipitates, dimensional stability during isobaric thermal cycling is negatively impacted after long aging times.

As-hot rolled material has the highest recovered transformation and lowest irrecoverable strain levels for different constant stress levels, but its transformation temperatures are very low. Aging at 450°C for 5 hours followed by air-cooling resulted in R-phase transformation during the forward transformation due to the formation of additional Ni_4Ti_3 precipitates which should be small and coherent. Constrained aging of

as-received material results in two-way shape memory effect due to the oriented Ni_4Ti_3 precipitates creating oriented internal stress in the microstructure.

After solution treatment at 900°C for 24 hours, Ni_3Ti precipitates were eliminated completely. However, since the transformation temperatures are very low due to the high Ni-content of matrix, additional aging heat treatments are needed to form high density of Ni_4Ti_3 , or additional Ni_3Ti precipitates with controlled aging to finally increase transformation temperatures above ambient by depleting Ni-content of matrix.

In the sight of the present study, furnace-cooling and aging at 400°C and 450°C increase transformation temperatures above ambient due to forming Ni_4Ti_3 and Ni_3Ti precipitates in high density. On the other hand, the stability of shape memory properties, which is very important for the application, was negatively affected after long aging times due to losing coherency of coherent precipitates. Fatigue life upon cyclic loading can be improved by eliminating Ni_3Ti precipitates completely with solutionizing at 900°C for 24 hrs. TWSME and dimensional stability, which are important for actuator applications, can be improved by forming oriented Ni_4Ti_3 precipitates with constrained aging after solutionizing.

6.2 Future Recommendation

- Solutionizing at 1000°C for 1 hr rather than at 900°C for 24 hrs should be used to eliminate Ni_3Ti material to improve the fatigue response of material.
- Constrained aging at 400°C and 450°C for different aging times under different stress levels on the solutionized material should be performed to obtain oriented Ni_4Ti_3 precipitates to improve TWSME and increase transformation temperatures.
- Multi-stage aging heat treatments should be applied to solutionized samples to increase transformation temperatures above ambient while accomplishing dimensional stability for actuator-type application. High temperature aging like 500°C or 600°C for short aging times to form small Ni_4Ti_3 in high density, then low temperature aging for long aging times to coarsen these precipitates.
- Fatigue experiments should be performed to solutionized material to analyze the effect of elimination of the Ni_3Ti precipitates to the fatigue response.

REFERENCES

- [1] Chang LC, Read TA. *Trans. AIME* 1951;189:47.
- [2] Buehler WJ, Gilfrich JW, Wiley RC. *Journal of Applied Physics* 1963;34:1475.
- [3] Otsuka K, Wayman CM. *Shape Memory Materials*. London: Cambridge University Press, 1998.
- [4] Mabe JH, Ruggeri R, Calkins FT. *Characterization of Nickel-rich NiTiNol Alloys for Actuator Development. The International Conference on Shape Memory and Superelastic Technologies*. Pacific Grove, CA, 2006.
- [5] Funakubo H. *Shape Memory Alloys*. Amsterdam: Gordon and Breach Science Publishers, 1987.
- [6] Miyazaki S, Otsuka K. *ISIJ Int.* 1989;29:353.
- [7] Karaman I, Karaca HE, Basaran B, Lagoudas DC, Chumlyakov YI, Maier HJ. *Scr. Mater.* 2006;55:403.
- [8] Karaca HE, Karaman I, Basaran B, Chumlyakov YJ, Maier HJ. *Acta Materialia* 2006;54:233.
- [9] Tadaki T, Otsuka K, Shimizu K. *Annu. Rev. Mater. Sci.* 1988;18:25.
- [10] Duerig TW, Melton KN, Stockel D, Wayman CM. *Engineering Aspects of Shape Memory Alloys*. London: Butterworth-Heinemann, 1990.
- [11] Miyazaki S, Kimura S, Takei F, Miura T, Otsuka K, Suzuki Y. *Scripta Metallurgica* 1983;17:1057.
- [12] Miyazaki S, Otsuka K, Wayman CM. *Acta Metallurgica* 1989;37:1873.
- [13] Takei F, Miura T, Miyazaki S, Kimura S, Otsuka K, Suzuki Y. *Scripta Metallurgica* 1983;17:987.
- [14] Sehitoglu H, Hamilton R, Canadinc D, Zhang XY, Gall K, Karaman I, Chumlyakov Y, Maier HJ. *Metall. Mater. Trans. A-Phys. Metall. Mater. Sci.* 2003;34:5.
- [15] Nishida M, Honma T. *Scripta Metallurgica* 1984;18:1293.
- [16] Otsuka K, Ren X. *Prog. Mater. Sci.* 2005;50:511.
- [17] Miyazaki S, Otsuka K, Suzuki Y. *Scripta Metallurgica* 1981;15:287.

- [18] Miyazaki S, Imai T, Igo Y, Otsuka K. *Metallurgical Transactions a-Physical Metallurgy and Materials Science* 1986;17:115.
- [19] Miyazaki S, Igo Y, Otsuka K. *Acta Metallurgica* 1986;34:2045.
- [20] Eckelmeyer KH. *Scripta Metallurgica* 1976;10:667.
- [21] Nishida M, Wayman C, Honma T. *Metallurgical and Materials Transactions A* 1986;17:1505.
- [22] Gall K, Sehitoglu H, Chumlyakov YI, Zuev YL, Karaman I. *Scr. Mater.* 1998;39:699.
- [23] Khalil-Allafi J, Dlouhy A, Eggeler G. *Acta Materialia* 2002;50:4255.
- [24] Bojda O, Eggeler G, Dlouhy A. *Scr. Mater.* 2005;53:99.
- [25] Fan GL, Chen W, Yang S, Zhu JH, Ren XB, Otsuka K. *Acta Materialia* 2004;52:4351.
- [26] Adharapurapu RR, Vecchio KS. *Exp. Mech.* 2007;47:365.
- [27] Julien, Gerald. Shape Memory Parts of 60 Nitinol. U.S. Patent 7,005,018, Nitinol Technologies, Inc., Edgewood, WA, Feb. 28, 2006.
- [28] Bataillard L, Bidaux JE, Gotthard R. *Philos. Mag. A-Phys. Condens. Matter Struct. Defect Mech. Prop.* 1998;78:327.
- [29] Khalil-Allafi J, Ren X, Eggeler G. *Acta Materialia* 2002;50:793.
- [30] Dlouhy A, Khalil-Allafi J, Eggeler G. *Philos. Mag.* 2003;83:339.
- [31] Kim JI, Miyazaki S. *Metall. Mater. Trans. A-Phys. Metall. Mater. Sci.* 2005;36A:3301.
- [32] Kim JI, Miyazaki S. *Acta Materialia* 2005;53:4545.
- [33] Liu YN, Yang H, Voigt A. *Mater. Sci. Eng. A-Struct. Mater. Prop. Microstruct. Process.* 2003;360:350.
- [34] Jiang F, Liu Y, Yang H, Li L, Zheng Y. *Acta Materialia* 2009;57:4773.
- [35] Zheng Y, Jiang F, Li L, Yang H, Liu Y. *Acta Materialia* 2008;56:736.
- [36] J.I. Kim THN, Y.J. Lee, S. Miyazaki. *Functional Materials Letters* 2008;1:209.
- [37] Bertacchini OW. *Doctoral Dissertation. College Station: Texas A&M University, 2009.*
- [38] Fukuda T, Deguchi A, Kakeshita T, Saburi T. *Mater. Trans. JIM* 1997;38:514.
- [39] Kim HC, Yoo YI, Lee JJ. *Sens. Actuator A-Phys.* 2008;148:437.

- [40] Hartl DJ, Lagoudas DC, Calkins FT, Mabe JH. *Smart Mater. Struct.* 2010;19.
- [41] Kockar B. Doctoral Dissertation. College Station: Texas A&M University, 2007.
- [42] Kockar B, Karaman I, Kim JI, Chumlyakov YI, Sharp J, Yu CJ. *Acta Materialia* 2008;56:3630.
- [43] Ostwald W. *Zeitschrift Fur Physikalische Chemie--Stoichiometrie Und Verwandtschaftslehre* 1900;34:495.
- [44] Cahn RW, Haasen P. *Physical Metallurgy, Volume II.* Amsterdam: Elsevier 1996.
- [45] Wagner C. *Z.Electrochem* 1961;65:581.
- [46] Lifshitz IM, Slyozov VV. *J. Phys. Chem. Solids* 1961;19:35.
- [47] Hamilton RF, Sehitoglu H, Chumlyakov Y, Maier HJ. *Acta Materialia* 2004;52:3383.
- [48] Sehitoglu H, Jun J, Zhang X, Karaman I, Chumlyakov Y, Maier HJ, Gall K. *Acta Materialia* 2001;49:3609.
- [49] Liu Y, McCormick PG. *Acta Metall. Mater.* 1994;42:2401.
- [50] Nishida M, Wayman CM, Honma T. *Scripta Metallurgica* 1984;18:1389.
- [51] Nishida M, Honma T. *Scripta Metallurgica* 1984;18:1299.
- [52] Tadaki T, Nakata Y, Shimizu K, Otsuka K. *Transactions of the Japan Institute of Metals* 1986;27:731.
- [53] Matsumoto O, Miyazaki S, Otsuka K, Tamura H. *Acta Metallurgica* 1987;35:2137.

VITA

Erhan Akin, son of Yasar Akin and Melike Akin and younger brother of Emrah Akin, was born in Sakarya, Turkey. He went to the Navigational Vocational High School, and then Navigational Vocational College at Istanbul Technical University. After graduating in August 2002, he continued his education and graduated from Kocaeli University, Department of Mechanical Engineering, in June 2006. He earned a scholarship from Turkish Petroleum International Company which covers a master's degree education in the USA. In Fall 2008, he enrolled in Texas A&M University to pursue a master's degree in the Department of Mechanical Engineering. He completed his research and received a Master of Science majoring in Mechanical Engineering in August 2010. During his study, he was an author of one conference publication. Following graduation, he will go back to Turkey to perform research for Turkish Petroleum International Company and pursue a management position in the company.

His permanent address is:

Koprubasi Mahallesi

Degirmensirti Sokak, No:36,

Hendek, Sakarya 54300,

TURKEY

Email: erhanakin82@gmail.com